

Cambridge Books Online

<http://ebooks.cambridge.org/>



Microstructural Design of Fiber Composites

Tsu-Wei Chou

Book DOI: <http://dx.doi.org/10.1017/CBO9780511600272>

Online ISBN: 9780511600272

Hardback ISBN: 9780521354820

Paperback ISBN: 9780521019651

Chapter

3 - Strength of continuous-fiber composites pp. 80-168

Chapter DOI: <http://dx.doi.org/10.1017/CBO9780511600272.004>

Cambridge University Press

## 3 Strength of continuous-fiber composites

### 3.1 Introduction

Fiber-reinforced composites are a valuable class of engineering materials because they can exhibit both high stiffness and strength simultaneously, in contrast to more homogeneous materials which are generally brittle and defect sensitive. In fiber composites, the inherent lack of toughness of the reinforcing fiber, or its sensitivity to microstructural defects, is overcome by the local redundancy of the composite structure, so that its strength may be utilized effectively. Individual fibers are relatively weakly coupled by the matrix so that failure of one fiber does not generally precipitate immediate failure of the composite as a whole, allowing high strength and stiffness to be achieved in the fiber direction.

The tensile failure of a fiber-reinforced material is a complex process which involves an accumulation of microstructural damage. Unlike homogeneous brittle materials, fiber composites do not contain a population of observable pre-existing defects, one of which ultimately precipitates failure. Instead, an accumulation of fiber or matrix fractures develops as the material is loaded and this constitutes a 'critical defect' in a macroscopic view of the fracture. Fracture mechanics may successfully account for the strength of single fibers, but it is inadequate to extend its application to unidirectional fiber composites when the overall behavior is dominated by the probability of defects in fibers propagating under the stress concentrations surrounding previous fiber fractures as well as the probability of defects in the matrix which are responsible for the multiplication of transverse cracks. Consequently, the statistical process of damage development in composites needs to be emphasized (Manders, Bader and Chou 1982).

The development of a rigorous analysis of fracture, considering all the sequences of fiber and matrix fractures which result in fracture of the composite, is a formidable task, and for this reason the strength of composites with realistic dimensions is much less well understood than their elastic properties.

This chapter treats the strength of continuous fiber composites with a combination of statistical and fracture mechanics approaches. The statistical analysis of unidirectional composites is better de-

veloped than that for cross-ply laminates. No comprehensive statistical methodology is available at this time for treating the strength and failure of composites from the fiber and bundle level up to composite laminates. Thus, the fracture mechanics approach to laminate failure is necessary.

In this chapter, the classical approximation of the rule-of-mixtures is adopted as a starting point for composite axial strength. This approximation is substantially altered due to stress concentrations induced at fiber breakages. The statistical variations of fiber and bundle strengths are then discussed. The knowledge of the stress redistribution at fiber breaks is then incorporated into the statistical strength analysis of unidirectional fiber composites. Next, the strength analysis is extended to the case of cross-ply laminates which serve as model systems for laminate composites. Finally, an attempt is made to shed some light on the failure of laminated composites in general where both inter- and intralaminar failures play key roles in the failure modes. A method of analysis based upon the fracture mechanics approach is introduced. Section 3.4.6.2 is contributed by S. L. Phoenix, and Sections 3.4.7.4 and 3.4.8 are contributed by A. S. D. Wang.

Another approach to the strength and damage of fiber composites is based upon the overall properties degradation. The strength behavior can be modeled by regarding the composite with damage as a continuum with changing microstructure. A phenomenological theory of constitutive behavior then provides relationships between the severity of damage and the overall stiffness properties of a composite (Reifsnider, Henneke, Stinchcomb and Duke 1983; Talreja, 1985, 1986, 1987, 1989).

Strength theories dealing with short-fiber and hybrid composites are discussed in Chapters 4 and 5, respectively.

### 3.2 Rule-of-mixtures

The classical approximation of unidirectional continuous-fiber composite strength takes the form of the rule-of-mixtures. By assuming equal strain in the fiber and matrix phases, the stress in the composite under uniaxial loading can be expressed as (see Kelly and Nicholson 1971 and Vinson and Chou 1975)

$$\sigma_c = \sigma_f V_f + \sigma_m (1 - V_f) \quad (3.1a)$$

where  $\sigma$  and  $V_f$  denote, respectively, stress and fiber volume fraction. The subscripts c, f and m are for composite, fiber and

matrix, respectively. Then, the ultimate composite strength is

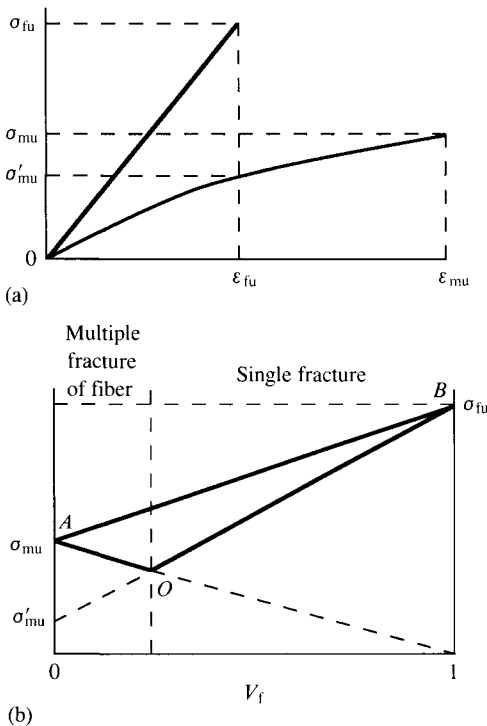
$$\sigma_{cu} = \sigma_{fu}V_f + \sigma_{mu}(1 - V_f) \tag{3.1b}$$

Here, the subscript u denotes ultimate strength. Equation (3.1b) is valid provided that both the fiber and matrix have the same ultimate strain.

Equation (3.1b) is not sufficient in determining the strength of continuous-fiber composites. Aveston, Cooper and Kelly (1971) have discussed the strength of composites based upon the transfer of load at the fiber/matrix interface and the mode of failure. For the case of brittle fiber-reinforced ductile matrix, the matrix ultimate strain is often higher than that of the fiber (Fig. 3.1a); then *single fractures* of the composite occur when

$$\sigma_{fu}V_f + \sigma'_{mu}(1 - V_f) > \sigma_{mu}(1 - V_f) \tag{3.1c}$$

Fig. 3.1. (a) Stress–strain relation of a brittle fiber/ductile matrix composite. (b) Composite strength vs. fiber volume fraction for brittle fiber/ductile matrix composites. (c) Stress–strain relation of a ductile fiber/brittle matrix composite. (d) Composite strength vs. fiber volume fraction for ductile fiber/brittle matrix composites.



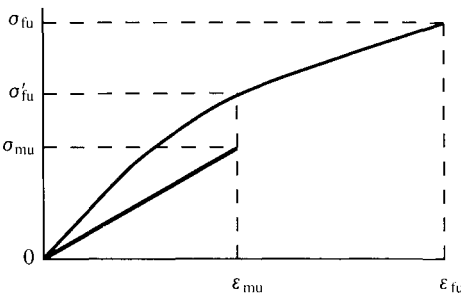
where  $\sigma'_{mu}$  is the stress in the matrix when the fibers fail. The matrix is unable to withstand the additional load transferred to it due to the fiber fracture, and thus single fracture prevails at sufficiently high fiber volume fractions. At low fiber fractions,

$$\sigma_{fu} V_f + \sigma'_{mu}(1 - V_f) < \sigma_{mu}(1 - V_f) \tag{3.1d}$$

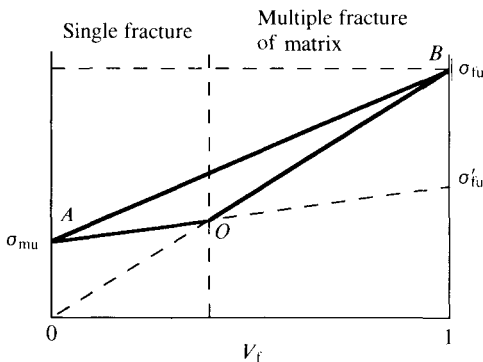
and the load is essentially born by the matrix material. The failure of the composite is characterized by *multiple fractures* of the fibers into shorter and shorter segments as the strain on the matrix increases (Fig. 3.1b). Experimental data on the ultimate strength of unidirectional fiber composites usually fall within the triangular region of Fig. 3.1b specified by the solid line segments.

Provided the failure strain of the matrix is sufficiently large, the fibers are fractured into lengths between  $x$  and  $2x$ . Assuming a constant fiber–matrix interfacial shear stress  $\tau$ , the fiber fracture

Fig. 3.1. (cont.).



(c)



(d)

spacing is determined from a simple force balance

$$x = \frac{\sigma_{fu} r}{2\tau} \quad (3.2)$$

where  $r$  denotes fiber radius.

The above analysis does not fully account for the fact that the strength of a fiber is a statistical quantity which results from flaws being randomly distributed along the length, as is discussed later. One result is that the strength depends on the fiber length, and thus is not really a fixed quantity  $\sigma_{fu}$ . Using the accepted Poisson/Weibull model, Henstenburg and Phoenix (1989) have developed a modified version of Eq. (3.2) which includes a factor connected to the variability in fiber strength. The revised formula typically produces values which are 15 to 20% larger. Also, these authors have delved further into the nature of the statistical distribution for fragment length, and experimental examples can be found in Netravali, Henstenburg, Phoenix and Schwartz (1989).

For the case of ductile fiber-reinforced brittle matrix composites, multiple fracture of the matrix occurs when the fiber ultimate strain,  $\epsilon_{fu}$ , is higher than that of the matrix,  $\epsilon_{mu}$  (Fig. 3.1c). The condition of multiple fracture, according to Aveston, Cooper and Kelly (1971), is

$$\sigma'_{fu} V_f + \sigma_{mu}(1 - V_f) < \sigma_{fu} V_f \quad (3.3)$$

Here,  $\sigma'_{fu}$  is the stress in the fiber at the failure strain of the matrix. A single fracture of the composite occurs if the fibers cannot withstand the increase in loading due to the matrix failure (Fig. 3.1d).

The spacing between two adjacent matrix cracks can again be determined from a simple force balance, and the separation distance is between  $x'$  and  $2x'$

$$x' = \frac{1 - V_f}{V_f} \frac{\sigma_{mu} r}{2\tau} \quad (3.4)$$

In deriving Eq. (3.4), it is understood that the number of fibers per unit area transverse to the fiber direction is given by  $V_f/\pi r^2$ .

Composites containing ductile fibers in a ductile matrix have shown work-hardening behavior. Mileiko (1969) has theorized that the instability or necking of the matrix can be suppressed due to the constraint of the matrix, and the ultimate strain of the composite, in this case, is shown to lie in between the ultimate strains of the fiber and matrix materials.

### 3.3 Stress concentrations due to fiber breakages

Fiber breakages in a continuous-fiber composite can occur at fabrication or during the early stage of loading. Stress redistribution takes place in the vicinity of a fiber breakage because load can no longer be transferred along the fiber in a continuous manner. The resulting stress concentrations in the neighboring fibers are detrimental to the strength of continuous-fiber composites. In the following, the shear-lag analysis is introduced to examine both the static and dynamic stress concentrations in unidirectional continuous-fiber composites.

#### 3.3.1 *Static case*

The problem of static stress concentration in composites has been treated by the shear-lag method (see Hedgepeth 1961; Hedgepeth and Van Dyke 1967; Fichter 1969, 1970; Van Dyke and Hedgepeth 1969; Zweben 1974; Fukuda and Kawata 1976a, 1980; Goree and Gross 1979, 1980; Hikami and Chou 1990), elasticity theory (see Burgel, Perry and Scheider 1970; Takao, Taya and Chou 1981), and numerical methods (see Carrara and McGarry 1968; Chen 1971).

Among these approaches, the shear-lag method, which is based upon simplified assumptions, often provides good physical insights of rather complex problems. The shear-lag method was first adopted by Hedgepeth (1961) to treat multi-filament failure problems of unidirectional composites. The technique also has been extended to include the effects of plasticity of the matrix (Hedgepeth and Van Dyke 1967; Goree and Gross 1979; Hikami and Chou 1984a), and the condition of interfacial debonding (Van Dyke and Hedgepeth 1969). The major assumptions of this method are that: (1) the fibers sustain only the axial loads, and (2) matrix between fibers transmits only the shear force.

In the following the single filament failure model of Fukuda and Kawata (1976a) is reproduced first to demonstrate the fundamentals of this method, and the nature of stress redistribution in unidirectional composites. Next, the work of Hikami and Chou (1990) is introduced for the explicit solutions of multi-filament failure problems.

##### 3.3.1.1 *Single filament failure*

Figure 3.2 shows the model of analysis by Fukuda and Kawata (1976a) which contains three parallel fibers with the middle one being broken. This model can also be considered as the

two-dimensional representation of a laminate with a broken middle layer. Because of symmetry, only half of the model needs to be considered and the fibers are denoted as  $n = 1$  and 2. The equilibrium of forces in the fibers in the free-body diagram of Fig. 3.3 gives

$$\frac{1}{2} \frac{dP_1}{dx} + \tau_1 = 0 \tag{3.5}$$

$$\frac{dP_2}{dx} - \tau_1 = 0 \tag{3.6}$$

Fig. 3.2. A three-fiber composite model for shear-lag analysis.

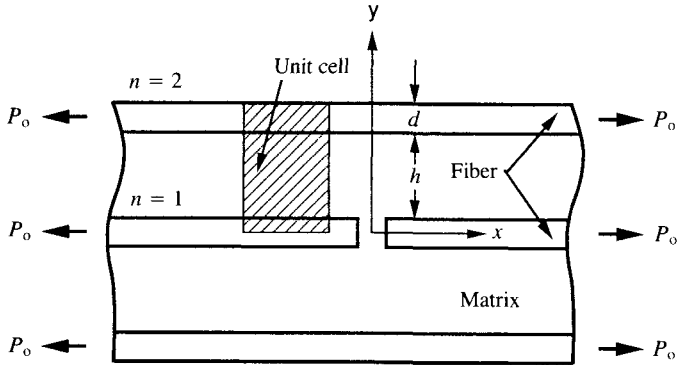
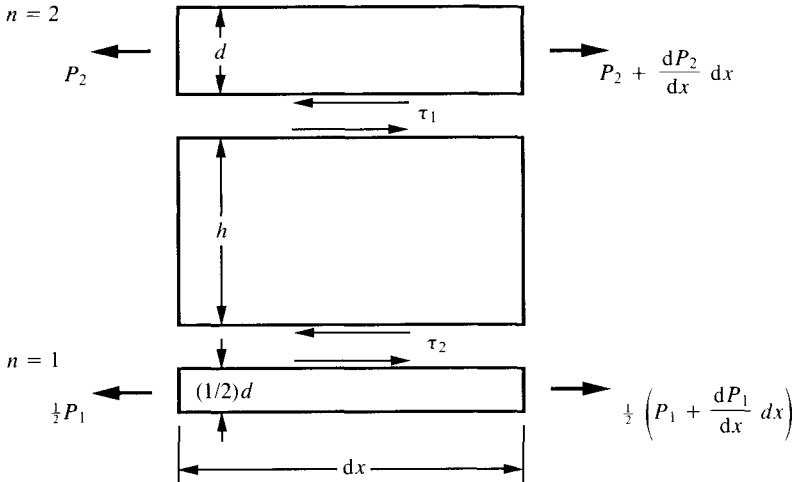


Fig. 3.3. Free-body diagrams for the 'unit cell' of the composite shown in Fig. 3.2.



where  $P_1$  and  $P_2$  denote fiber axial force per unit thickness, and  $\tau_1$  is the matrix shear stress. Let the displacement of the  $n$ th fiber be denoted as  $u_n$ . Then,

$$P_n(x) = Ed \frac{du_n(x)}{dx} \quad n = 1, 2 \quad (3.7)$$

$$\tau_1(x) = \frac{G}{h} (u_2(x) - u_1(x)) \quad (3.8)$$

where  $E$  is the Young's modulus of the fibers;  $G$  is the effective shear modulus of the matrix;  $h$  is the effective fiber spacing;  $d$  is the fiber width; and the lamina is of unit thickness.

Using Eqs. (3.7) and (3.8), and the following non-dimensional parameters

$$\xi = x/d \quad (3.9)$$

$$\alpha = Eh/Gd \quad (3.10)$$

Equations (3.5) and (3.6) become

$$\frac{1}{2}\alpha \frac{d^2 u_1}{d\xi^2} + u_2 - u_1 = 0 \quad (3.11)$$

$$\alpha \frac{d^2 u_2}{d\xi^2} + u_1 - u_2 = 0 \quad (3.12)$$

From Eq. (3.11),  $u_2$  can be expressed by  $u_1$  and its derivatives as follows:

$$u_2 = u_1 - \frac{1}{2}\alpha \frac{d^2 u_1}{d\xi^2} \quad (3.13)$$

Substitution of Eq. (3.13) into Eq. (3.12) yields

$$\frac{d^4 u_1}{d\xi^4} - \frac{3}{\alpha} \frac{d^2 u_1}{d\xi^2} = 0 \quad (3.14)$$

The general solution of Eq. (3.14) is

$$u_1 = A + B\xi + Ce^{\lambda\xi} + De^{-\lambda\xi} \quad (3.15)$$

where  $\lambda = \sqrt{3/\alpha}$  and  $A$ ,  $B$ ,  $C$  and  $D$  are integration constants. Substituting Eq. (3.15) into Eq. (3.13), the general solution of  $u_2$  is obtained as

$$u_2 = A + B\xi - \frac{1}{2}Ce^{\lambda\xi} - \frac{1}{2}De^{-\lambda\xi} \quad (3.16)$$

$A$ ,  $B$ ,  $C$  and  $D$  in Eqs. (3.15) and (3.16) can be determined from Eq. (3.7) and the following boundary conditions:

$$(u_2)_{\xi=0} = 0, \quad (P_1)_{\xi=0} = 0, \quad (P_1)_{\xi=\infty} = P_o \quad (3.17)$$

Finally, the fiber displacements and axial loads are obtained

$$u_1 = \frac{P_o}{E} \left( \frac{1}{2\lambda} + \xi + \frac{1}{\lambda} e^{-\lambda\xi} \right) \quad (3.18)$$

$$u_2 = \frac{P_o}{E} \left( \frac{1}{2\lambda} + \xi - \frac{1}{2\lambda} e^{-\lambda\xi} \right)$$

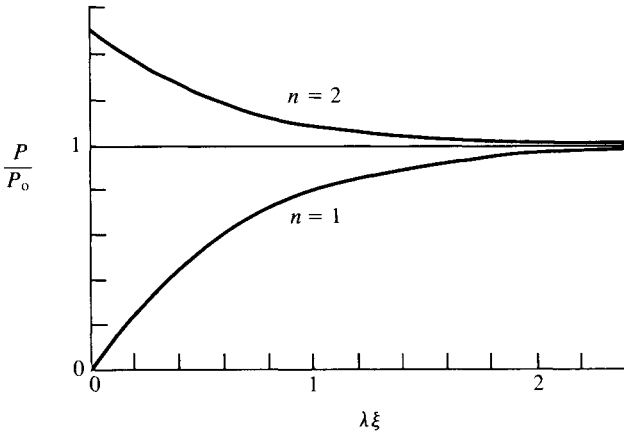
$$\begin{aligned} P_1 &= P_o(1 - e^{-\lambda\xi}) \\ P_2 &= P_o(1 + \frac{1}{2}e^{-\lambda\xi}) \end{aligned} \quad (3.19)$$

Values of  $P_1$  and  $P_2$  in Eq. (3.19) are shown in Fig. 3.4. The stress concentration factor of this model,  $(P_2/P_o)_{\xi=0}$ , is 1.5. According to Eq. (3.19), the distributions of fiber displacements and axial loads are functions of the material constant  $\lambda$ . However, the stress concentration factor is independent of  $\lambda$ . The above treatment has been extended to composites containing a finite number of fibers with any number of adjacent fiber breakages on the same transverse plane.

3.3.1.2 *Multi-filament failure*

Hikami and Chou (1984b, 1990) have examined the two-dimensional multi-filament failure problem of unidirectional fiber

Fig. 3.4. Variations of fiber axial forces.



composites, focussing specifically on the stress concentration factors of fibers adjacent to the cracks. The physical problems are analyzed by the two-dimensional shear-lag method under two loading conditions: (A) uniform tensile force applied to all fibers at infinity (Fig. 3.5), and (B) concentrated force dipole applied at a particular fiber,  $n = b - a$ , on the crack plane (Fig. 3.7).

These analyses are unique in that the general solution of the governing equations of the elastic field has been obtained in explicit forms in terms of the Legendre polynomials for the loading condition (A). Based upon this solution, closed form expressions of stress concentration factors in all fibers have been derived. These analyses also provide rigorous proofs of both Hedgepeth and Van Dyke's inspection (1967) on the general form of the tensile stress concentration factor at the tip of a crack and Fichter's inspection (1969) on the general form of the shear stress concentration factor for the loading condition (A). Since there exists a reciprocal relation between the influence function matrices for the loading conditions (A) and (B), the solution for the condition (B) can be readily derived from the solution for the condition (A).

The analysis considers a two-dimensional unidirectional continuous-fiber composite containing a slit notch in the transverse direction, as shown in Fig. 3.5. The fiber direction is taken along the  $x$  axis. The broken fibers are denoted as  $n = 1, 2, 3, \dots, b$ , starting from the left tip of the notch with  $b$  being the total number of fibers in the notch.

Under the assumption of shear-lag analysis, the matrix material transfers only shear force,  $\bar{\tau}_n(x)$ , per unit fiber length between two adjacent fibers. Thus  $\bar{\tau}_n(x)$  is related to the difference of displacements  $u_n(x)$  in the fiber direction as

$$\bar{\tau}_n(x) = \frac{G}{h} \{u_{n+1}(x) - u_n(x)\} \quad (3.20)$$

where  $G$  is the effective shear modulus of the matrix, and  $h$  is the effective fiber spacing. The tensile force  $P_n(x)$  per unit thickness in the  $n$ th fiber is related to the displacement by

$$P_n(x) = Ed \frac{du_n(x)}{dx} \quad (3.21)$$

where  $d$  is the width of the fiber. The equilibrium of forces in the  $x$  direction gives

$$\frac{dP_n}{dx} + \bar{\tau}_n - \bar{\tau}_{n-1} = 0 \quad (3.22)$$

The non-dimensionalized axial force, displacement and coordinate are given, respectively, by:

$$\begin{aligned}
 F_n(\xi) &= P_n(x)/P_o \\
 U_n(\xi) &= u_n(x)\sqrt{(EdG/hP_o^2)} \\
 \xi &= \sqrt{(G/Edh)}x
 \end{aligned}
 \tag{3.23}$$

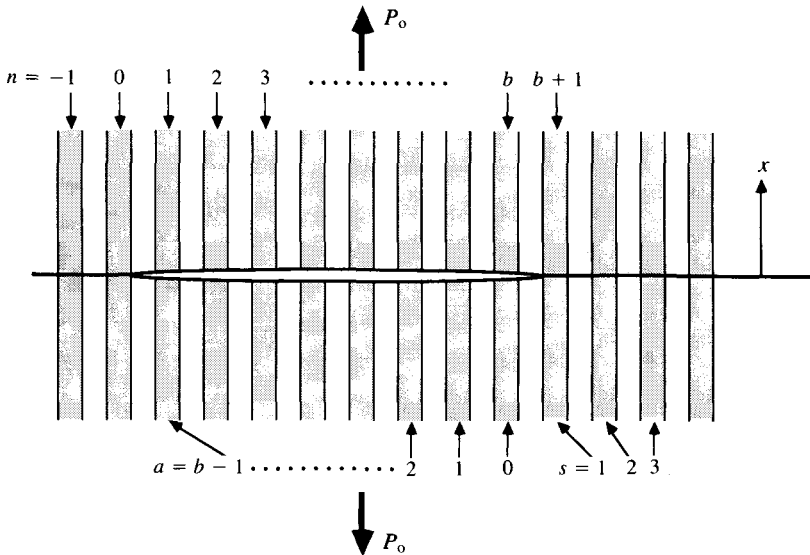
Then, the equilibrium equation (3.22) can be written as

$$\frac{d^2U_n(\xi)}{d\xi^2} = 2U_n(\xi) - U_{n+1}(\xi) - U_{n-1}(\xi)
 \tag{3.24}$$

The boundary conditions are:

$$\begin{aligned}
 F_n(0) &= 0 & (1 \leq n \leq b) \\
 U_n(0) &= 0 & (n \leq 0, n \geq b + 1) \\
 F_n(\pm\infty) &= 1 & (\text{all } n)
 \end{aligned}
 \tag{3.25}$$

Fig. 3.5. Model of a multi-filament crack in a unidirectional composite under uniform force at infinity (After Hikami and Chou 1990.)



for loading condition (A), and

$$\begin{aligned}
 F_n(0) &= 0 && (n = 1, 2, \dots, b - a - 1, b - a + 1, \dots, b) \\
 U_n(0) &= 0 && (n \leq 0, n \geq b + 1) \\
 F_n(\pm\infty) &= 0 && (\text{all } n) \\
 F_{b-a}(0) &= -1
 \end{aligned}
 \tag{3.26}$$

for loading condition (B).

The general solutions of the multi-filament failure problem have been obtained explicitly by Hikami and Chou (1990) using the Legendre polynomials and Fourier transformation. The stress concentration factors in all fibers on the crack plane are given in closed forms. First, for the loading condition (A), the stress concentration factor of the *s*th fiber ahead of the tip of a crack containing *b* broken fibers is given by

$$\begin{aligned}
 K_b^s &= (b + 2s - 1) \\
 &\times \frac{2s \cdot (2s + 2) \cdot (2s + 4) \cdots (2s + 2b - 2)}{(2s - 1) \cdot (2s + 1) \cdot (2s + 3) \cdots (2s + 2b - 3) \cdot (2s + 2b - 1)}
 \end{aligned}
 \tag{3.27}$$

As a special case of Eq. (3.27), the stress concentration factor in the first intact fiber (*s* = 1) adjacent to *b* broken fibers is

$$K_b^1 = \frac{4 \cdot 6 \cdot 8 \cdots (2b + 2)}{3 \cdot 5 \cdot 7 \cdots (2b + 1)}
 \tag{3.28}$$

Hedgepeth (1961) deduced Eq. (3.28) by inspecting the numerical results of the cases *b* = 1, 2, . . . , 6. This inspection on the general form of the stress concentration factor has been rigorously proven by Hikami and Chou. Figure 3.6 depicts the numerical results for *K<sub>b</sub><sup>s</sup>*.

Furthermore, the maximum shear stress takes place in the matrix at the tip of the crack. Thus, the dimensionless displacement at the crack tip *U<sub>b</sub>(0)* is termed the maximum shear stress concentration factor, *S<sub>max</sub>*. Hikami and Chou (1990) have obtained

$$S_{\max} = \frac{\pi(2b - 1)!}{2^{2b}[(b - 1)!]^2}
 \tag{3.29}$$

Fichter (1969) deduced the above result by calculating the cases of *b* = 1, 2, . . . , 6. The axial stress in fibers away from the crack plane has also been obtained.

In the case of loading condition (B), Fig. 3.7, Hikami and Chou

Fig. 3.6. Stresses concentration factor  $K_b^s$  in the  $(b + s)$ th fiber.  $b$  denotes the number of broken fibers;  $s = 1$  corresponds to the special case of Hedgepeth (1961). (After Hikami and Chou 1990.)

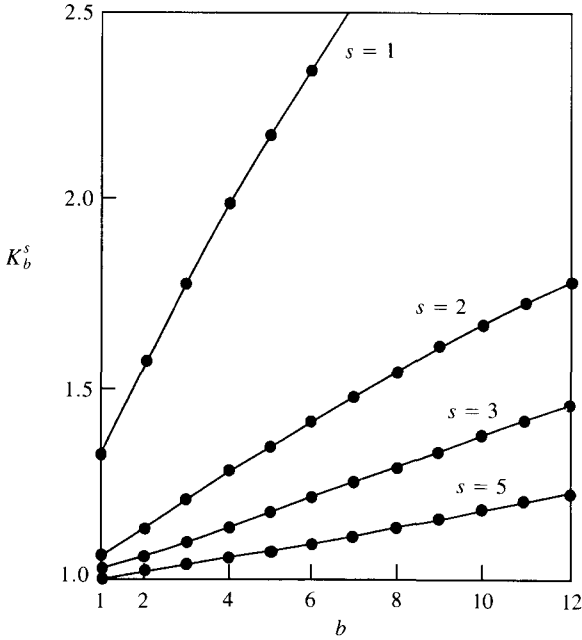
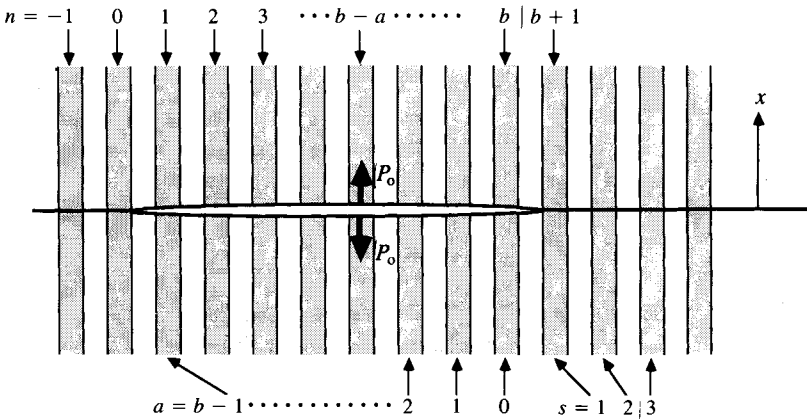


Fig. 3.7. Model of a multi-filament crack in a unidirectional composite under concentrated force dipole in the  $(b - a)$ th fiber on the crack plane. (After Hikami and Chou 1990.)



(1990) assume that a unit force dipole is applied on the  $(b - a)$ th fiber. Then the more general cases with multiple dipoles can be obtained by the linear combination of the solutions of the simple problem.

The closed form solution of the stress concentration factor at the  $s$ th fiber in front of the tip of a crack containing  $b$  fibers and a unit force dipole at the  $n (=b - a)$ th fiber is given as

$$K_b^{s,a} = \frac{1}{2} \frac{(2a + 1)!! (2b - 2a - 1)!! (2s - 3)!! (2s + 2b - 2)!!}{(2a)!! (2b - 2a - 2)!! (2s - 2)!! (2s + 2b - 1)!!} \frac{1}{(s + a)} \tag{3.30}$$

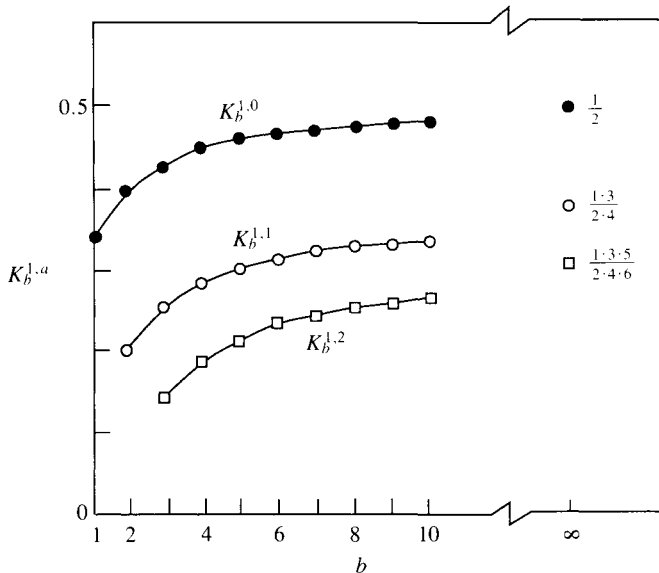
where  $!!$  denotes double factorial (i.e.  $n!! = (n!)!$ ). The highest fiber stress concentration takes place at the edge of the crack ( $s = 1$ )

$$K_b^{1,a} = \frac{(2a + 1)!! (2b - 2a - 1)!! (2b)!!}{(2a + 2)!! (2b - 2a - 2)!! (2b + 1)!!} \tag{3.31}$$

Figure 3.8 depicts the numerical results for  $K_b^{1,a}$ .

For a semi-infinite crack the stress concentration factor at the  $s$ th fiber from the crack tip due to the unit applied force dipole at the

Fig. 3.8. Stress concentration  $K_b^{1,a}$  in the  $(b + 1)$ th fiber when the unit load is applied at the  $(b - a)$ th fiber.  $b$  denotes the number of broken fibers. (After Hikami and Chou 1990.)



$a$ th fiber has the following value:

$$\lim_{b \rightarrow \infty} K_b^{s,a} = \frac{1}{2(s+a)} \cdot \frac{(2s+1)!!}{(2a)!!} \cdot \frac{(2s-3)!!}{(2s-2)!!} \quad (3.32)$$

The axial fiber stress distributions away from the fracture plane for both loading conditions (A) and (B) also have been obtained by Hikami and Chou (1990). Also Fukuda and Kawata (1980) have shown in their analysis of a finite number of fibers that the stress concentration factor tends to that of Hedgepeth as the total fiber number increases.

The static stress concentration factors in a layer of unidirectional composites containing dacron fibers imbedded in a polyurethane elastomer have been measured by Zender and Deaton (1963). The number of fiber breakages in this experiment is controlled by partially slitting the specimens in the transverse direction. The slit length determines the number of broken fibers. The results of the experiments show reasonably close agreement with the theoretical analysis. It should be noted that although the broken fibers induce the adjacent fibers to fail in the vicinity of the cut, the chances are that such a location is not the weakest location of the fiber. This has to do with the statistical nature of fiber strength distribution and will be discussed in Section 3.4.

The problem of static stress concentration factors in a three-dimensional fiber array has been examined by Van Dyke and Hedgepeth (1969). They consider square and hexagonal arrays where a specified number of fibers are broken. Other stress concentration problems including the effects of finite length of fibers (Fichter 1970), relative locations of fiber breaks (Chen 1973), holes (Kulkarni, Rosen and Zweben 1973) and notches (Zweben 1974) also have been treated.

### 3.3.2 *Dynamic case*

When fibers are suddenly broken in a composite under stress, the load in the broken fibers must be transferred through the matrix to the adjacent fibers in order to restore equilibrium. Of interest is not only the resulting static stress, but also the dynamic overshoot which occurs during the transient phase. Hedgepeth (1961) examined the dynamic aspect of stress concentration for the two-dimensional fiber array as shown in Fig. 3.5. The analytical model is also based upon the assumptions of the shear-lag analysis;

that is, it is composed of tension-carrying elements connected by purely shear-carrying material.

The formulation of boundary value problem for the evaluation of dynamic stress concentration is outlined below. The fibers are separated by a constant distance and are numbered from  $n = -\infty$  to  $n = \infty$  (Fig. 3.5). The coordinate along the fiber is denoted by  $x$  and the displacement of the  $n$ th fiber at the location  $x$  and time  $t$  is given by  $u_n(x, t)$ . Similarly, the force per unit thickness in the  $n$ th fiber is denoted by  $P_n(x, t)$  and is given in terms of  $u_n$  by

$$P_n = Ed \frac{\partial u_n}{\partial x} \quad (3.33)$$

where  $E$  and  $d$  are, respectively, the fiber Young's modulus and width. The equilibrium of an element of the  $n$ th filament then requires

$$Ed \frac{\partial^2 u_n}{\partial x^2} + \frac{G}{h} (u_{n+1} - 2u_n + u_{n-1}) = m \frac{\partial^2 u_n}{\partial t^2} \quad (3.34)$$

Here,  $G$  and  $h$  denote matrix shear modulus and width, respectively;  $m$  is the mass per unit area of the  $n$ th filament.

In general, for  $b$  broken filaments, let  $1 \leq n \leq b$  denote the broken filaments. The boundary conditions are:

$$\begin{aligned} P_n(0, t) &= 0 & (1 \leq n \leq b) \\ u_n(0, t) &= 0 & (n \leq 0 \text{ or } n \geq b + 1) \end{aligned} \quad (3.35)$$

For large  $x$ , of course, the force in each filament approaches the uniform applied force per unit thickness,  $P_o$ . Thus

$$P_n(\pm\infty, t) = P_o \quad (3.36)$$

For the time-dependent problem, the following initial conditions are required:

$$\begin{aligned} P_n(x, 0) &= P_o \\ \frac{\partial u_n}{\partial t}(x, 0) &= 0 \end{aligned} \quad (3.37)$$

Using a Laplace transform of the time-dependent differential equation and boundary conditions, the resulting equations are similar in form to those of the static problem discussed in Section 3.3.1. The variation of stress concentration factor with time is shown in Fig. 3.9 for one, two and three broken fibers. As can be seen

from Fig. 3.9, the stress concentration factor,  $K_b^1$ , varies with the dimensionless time  $\bar{t}$  ( $=t/\sqrt{(md/G)}$ ), and approaches the steady-state value. In all cases, the first peak is the largest one and the value of the stress at this peak determines the dynamic overshoot.

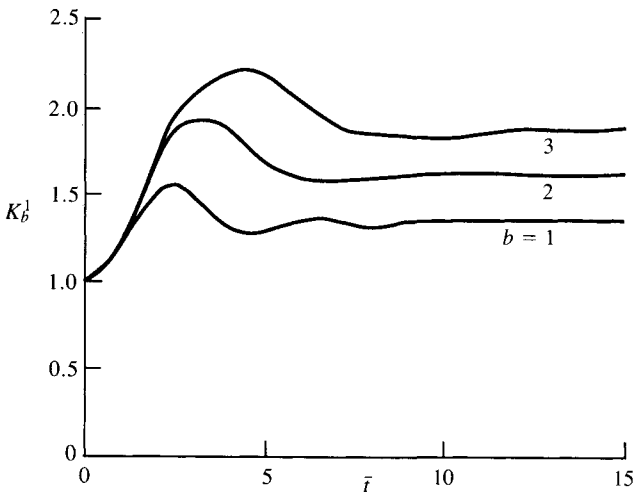
Hedgepeth (1961) defines the dynamic-response factor as the ratio between the maximum stress and the static stress. Values for one, two and three broken fibers are, respectively, 1.15, 1.19 and 1.20. It can be shown that the dynamic-response factor approaches 1.27 as the number of broken fibers tends to infinity. Further discussions of dynamic stress concentration factors are given in Section 3.4.9.

Following the approach of Hedgepeth (1961), Ji, Liu and Chou (1985) have investigated the variation of dynamic stress concentration along the length of a fiber next to a broken fiber. Define the dimensionless parameter in fiber axial location as

$$\xi = \frac{x}{\sqrt{\left(\frac{E}{G}\right) \cdot d} \tag{3.38}$$

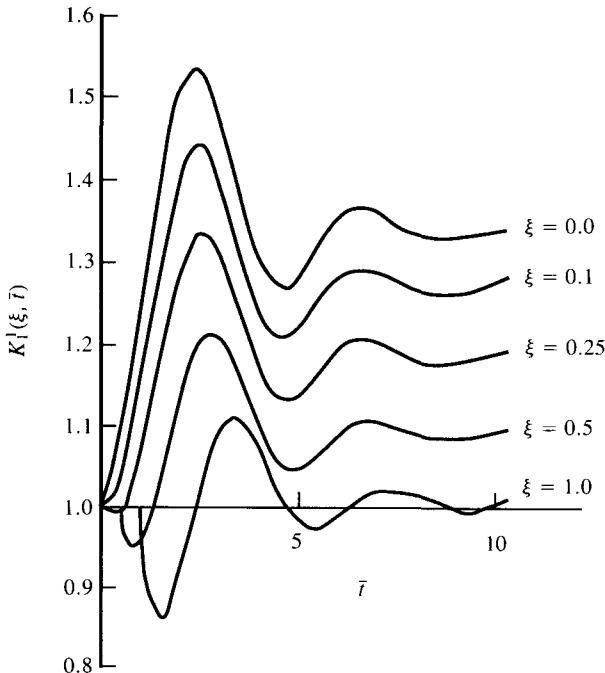
The asymptotic expressions of the stress concentration factor

Fig. 3.9. The variation of dynamic stress concentration factor  $K_b^1$  with dimensionless time  $\bar{t}$  for  $b = 1, 2$  and  $3$  (After Hedgepeth 1961.)



$K_1^1(\xi, \bar{t})$  for the fiber  $s = 1$  at  $x = 0$  due to the fracture of the fiber  $n = b = 1$  (see Fig. 3.5) has been obtained. The results are depicted in Fig. 3.10, and the following observations can be made: (a) the fiber axial stress is always tensile at  $\xi = 0$ . For  $\xi \neq 0$ , the initial stress induced by fiber fracture is compressive, and the magnitude of this initial compressive stress increases with  $\xi$ ; (b) the dynamic stress concentration factor, which is defined by the maximum initial tensile stress, decreases as  $\xi$  increases, i.e. away from the plane of fiber fracture; (c) the dynamic stress concentration factor is appreciable (say,  $K_1^1(\xi, \bar{t}) > 1.1$ ) within the range of  $0 \leq \xi \leq 1$ . When  $\bar{t} > 10$ , the dynamic stress concentration factor results for  $\xi < 1$  approach the static stress concentration values. The change of stress concentration factor with the location on a fiber needs to be taken into account when there is a scattering in fiber strength and variation of fiber strength with fiber length. The results of Ji, Liu and Chou indicate that the variation of stress concentration is significant for  $\xi \leq 1$ , namely  $x$  is of the order of fiber diameter times

Fig. 3.10. Dynamic stress concentration factor  $K_1^1$  with dimensionless time  $\bar{t}$  for  $0 \leq \xi \leq 1$ . (After Ji, Liu and Chou 1985.)



$\sqrt{(E/G)}$ . For  $\xi \geq 1.0-2.0$ , the dynamic response diminishes with increasing  $\bar{l}$  value, and the static stress concentration factor approaches 1.0; there is virtually no static stress concentration. On the other hand, dynamic response in fiber stress concentration exists at small  $\bar{l}$  even for  $\xi \geq 2$ ; this factor needs to be taken into account in the statistical composite strength models.

The variation of stress concentration along the length of a fiber has implications on the dynamic failure characteristics of fiber composites. For instance, in the experimental observation of Ji (1982), carbon composite specimens often fracture at locations near specimen end-tabs. The reflection and hence magnification of the stress waves at specimen ends could cause fiber fractures at locations away from the plane of the existing fiber breakages.

### 3.4 Statistical tensile strength theories

#### 3.4.1 Preliminary

Statistics is concerned with scientific methods for collecting and analyzing data, as well as drawing valid conclusions and making reasonable decisions on the basis of such analysis. Spiegel (1961) and Kirkpatrick (1974) provide introductions to the basics of statistics. Statistical treatment of composite strength has emerged as an important analytical tool for the obvious reason that the strengths of brittle fibers and yarns are *statistical* in nature, and not deterministic such as in metals. A concise outline of the fundamentals in statistics based upon Spiegel (1961) is given below.

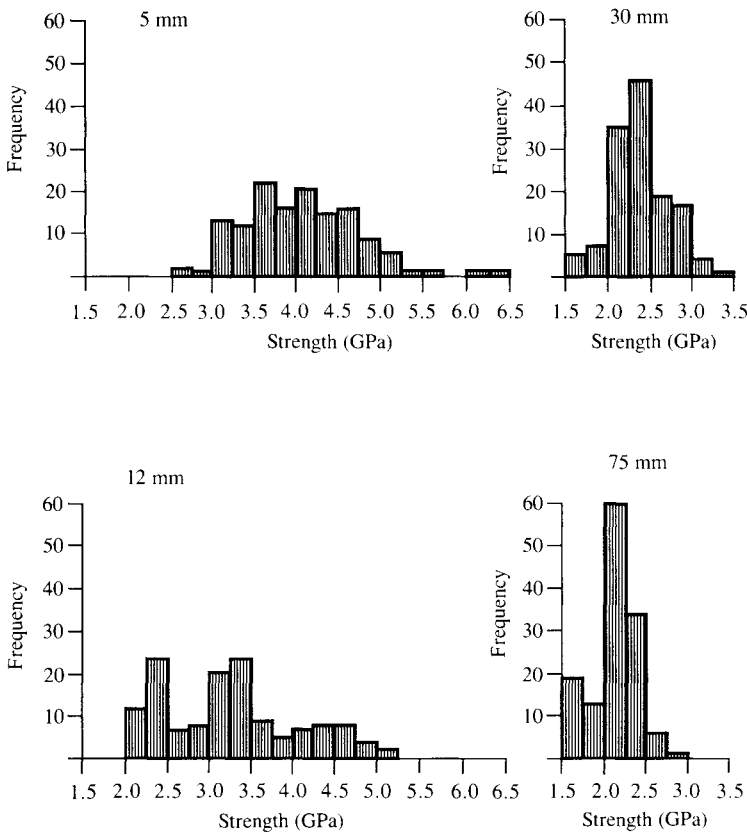
In collecting data concerning characteristics of a group of objects, it is often impractical to observe the entire group or *population* if it is large. A small part of the group examined is known as a *sample*. Valid conclusions can often be inferred from analysis of the sample. Because such inference cannot be absolutely certain, the language of *probability* is often used in stating conclusions.

When summarizing large masses of raw data, it is often useful to distribute the data into *classes* or *categories*. The number of individuals belonging to each class is called the *class frequency*. Figure 3.11 gives a graphical representation of the *frequency distribution* of the measured strength of carbon fibers (M. G. Bader and B. Gul-Mohammed, private communication, 1990; see also Dhingra 1980). The *relative frequency* of a class is the frequency of the class divided by the total frequency of all classes and is generally expressed as a percentage. A histogram can be approximated by a continuous frequency distribution curve as shown schematically in

Fig. 3.12. Also shown in Fig. 3.12 is the *cumulative frequency*, which, for a particular class or strength level, is the total frequency of all classes observed at equal to and less than this particular class. Cumulative frequency can also be presented on a relative or percentage basis.

Several types of averages can be defined for a given frequency distribution. The most commonly used ones may include the arithmetic mean, geometric mean, quadratic mean (root mean square), median and mode. The degree to which numerical data tend to spread about an average value is called the *variation* or *dispersion* of the data. The *standard deviation* is often used to measure dispersion, and is defined as the root mean square of the

Fig. 3.11. Distributions of carbon fiber tensile strength in air at gauge-lengths of 5, 12, 30 and 75 mm. (After Bader and Gul-Mohammed 1990.)



deviations from the mean. Furthermore, the *variance* is defined as the square of the standard deviation, and the *coefficient of variation* is the ratio of the standard deviation to the mean. The coefficient of variation is independent of units used and it fails to be useful when the mean is close to zero.

The probability of occurrence of an event  $e$  is denoted by

$$Pr = P\{e\} \tag{3.39}$$

The probability of non-occurrence of the event is denoted by

$$1 - Pr = P\{\text{not } e\} = 1 - P\{e\} \tag{3.40}$$

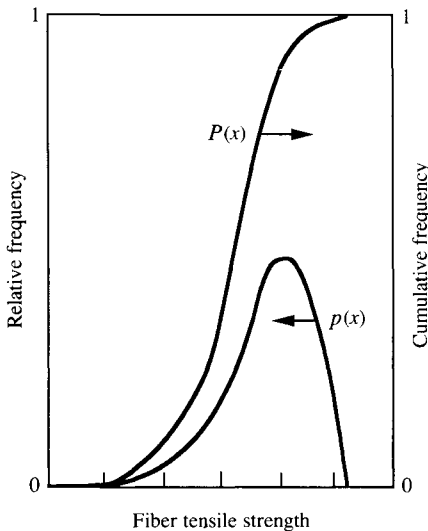
Some basic relations of probabilities of events are summarized below. Consider two events  $e_1$  and  $e_2$ . The probability that  $e_2$  occurs given that  $e_1$  has occurred is the conditional probability of  $e_2$  relative to  $e_1$ ; it is denoted by  $P\{e_2 | e_1\}$ . If  $e_1$  and  $e_2$  are *independent* events and hence the occurrence or non-occurrence of  $e_2$  is not affected by  $e_1$ , then

$$P\{e_2 | e_1\} = P\{e_2\} \tag{3.41}$$

Otherwise, they are *dependent* events. The probability that *both*  $e_1$  and  $e_2$  occur is denoted by

$$P\{e_1 e_2\} = P\{e_1\}P\{e_2 | e_1\} \tag{3.42}$$

Fig. 3.12. Relative frequency and cumulative frequency vs. fiber tensile strength.



For independent events, the above equation is simplified to

$$P\{e_1 e_2\} = P\{e_1\}P\{e_2\} \tag{3.43}$$

In the case of three events  $e_1$ ,  $e_2$  and  $e_3$ , Eq. (3.42) is modified to become

$$P\{e_1 e_2 e_3\} = P\{e_1\}P\{e_2 | e_1\}P\{e_3 | e_1 e_2\} \tag{3.44}$$

If  $e_1$  and  $e_2$  are *mutually exclusive* events, namely the occurrence of one excludes the occurrence of the other, Eq. (3.42) becomes

$$P\{e_1 e_2\} = 0 \tag{3.45}$$

Finally, the event that *either  $e_1$  or  $e_2$  or both occur* is given by

$$P\{e_1 + e_2\} = P\{e_1\} + P\{e_2\} - P\{e_1 e_2\} \tag{3.46}$$

For the special case of  $n$  mutually exclusive events  $e_1, e_2, \dots, e_n$ , the probability of occurrence of either  $e_1$  or  $e_2$  or  $\dots$  or  $e_n$  is then

$$P\{e_1 + e_2 + \dots + e_n\} = P\{e_1\} + P\{e_2\} + \dots + P\{e_n\} \tag{3.47}$$

The applications of these relations to the probabilities of various events in composite failure are given in this chapter as well as in Chapters 4 and 5.

The function representing the frequency distribution in Fig. 3.12 is also known as the *probability density function*. The knowledge of the probability density function is fundamental to any analysis based upon a statistical approach. One of the well-known probability density functions is the normal distribution given by

$$p(x) = \frac{1}{s\sqrt{2\pi}} \exp\left(-\frac{1}{2}\left(\frac{x - \bar{x}}{s}\right)^2\right) \quad s > 0 \tag{3.48}$$

where  $\bar{x}$  and  $s$  are the mean and standard deviation, respectively. It can be shown, for normal distribution, that 68.27% of the cases are included between  $(\bar{x} - s)$  and  $(\bar{x} + s)$ , and 99.73% of the cases are between  $(\bar{x} - 3s)$  and  $(\bar{x} + 3s)$ . Given a continuous probability density function  $p(x)$  the *cumulative distribution function* is defined by

$$P(x) = \int_{-\infty}^x p(x) dx \tag{3.49}$$

Other commonly used distribution functions may include the binomial distribution, Bernoulli distribution, and Poisson distribution. However, the Weibull distribution (Weibull 1939a&b, 1951) is

probably best known in composite strength theories. Weibull proposed a cumulative distribution function in the general form of

$$P(x) = \begin{cases} 0 & x \leq x_u \\ 1 - \exp\left(-\frac{(x - x_u)^m}{x_o}\right) & x > x_u \end{cases} \quad (3.50)$$

where  $m$  is a shape parameter and  $x_o$  is a scale parameter. The function  $(x - x_u)^m/x_o$  has the characteristics of being positive, non-decreasing and vanishing at constant value of  $x_u$ , which is not necessarily equal to zero.

### 3.4.2 *Strength of individual fibers*

Coleman (1958) examined the strength of long fibers from a common source (say, from the same spool) for the case that their tensile strengths are independent of the rate of loading. To obtain a form for the cumulative strength distribution function  $P(\sigma_f)$ , Coleman observed that (a) when a fiber is tested it breaks at its weakest cross-section, (b) the strength of a fiber must be positive regardless of the fiber length, and (c)  $P(\sigma_f)$  must be a monotonically increasing function of  $\sigma_f$ . Coleman postulated that a fiber may be regarded as composed of a set of  $N$  non-interacting unit lengths (or *links*). It is further assumed that all the links in a fiber have the same cumulative strength distribution function  $P(\sigma_f)$ .

The probability that a link has a strength greater than  $\sigma_f$  is  $1 - P(\sigma_f)$ , and the probability that all *links* do not fail at  $\sigma_f$  is  $[1 - P(\sigma_f)]^N$  (Eq. (3.43)). It follows then the probability that at least one link breaks at  $\sigma_f$  is

$$P_f(\sigma_f) = 1 - [1 - P(\sigma_f)]^N \quad (3.51)$$

$P_f(\sigma_f)$  can be regarded as the cumulative distribution function of the strength of fibers.

Coleman has shown that  $P(\sigma_f)$  has the form of a Weibull distribution. For long fibers ( $N \rightarrow \infty$ ), Eq. (3.51) gives the cumulative probability of failure

$$P_f(\sigma_f) = 1 - \exp\left[-L\left(\frac{\sigma_f}{\sigma_o}\right)^\beta\right] \quad (3.52)$$

$P_f(\sigma_f)$  is the probability of failure of a fiber at a stress level equal to or less than  $\sigma_f$ . Here,  $L$  is the length ratio with respect to a reference length,  $\sigma_o$  is the scale parameter for unit fiber length ratio (i.e.  $L = 1$ ), and  $\beta$  is the shape parameter. Equation (3.52) implies

a probability density function of

$$p_f(\sigma_f) = L\sigma_o^{-\beta}\beta\sigma_f^{\beta-1} \exp\left[-L\left(\frac{\sigma_f}{\sigma_o}\right)^\beta\right] \tag{3.53}$$

Following Coleman, the mean fiber strength,  $\bar{\sigma}_f$ , and standard deviation,  $s$ , are given by

$$\bar{\sigma}_f = \sigma_o L^{-1/\beta} \Gamma\left(1 + \frac{1}{\beta}\right) \tag{3.54a}$$

$$s = \sigma_o L^{-1/\beta} \sqrt{\left[\Gamma\left(1 + \frac{2}{\beta}\right) - \Gamma^2\left(1 + \frac{1}{\beta}\right)\right]} \tag{3.54b}$$

where  $\Gamma$  denotes the gamma function. An important feature of Eq. (3.54a) is that the fiber strength depends upon the fiber length. The coefficient of variation, which is a function of  $\beta$  only, is

$$\frac{s}{\bar{\sigma}_f} = \sqrt{\left[\frac{\Gamma\left(1 + \frac{2}{\beta}\right)}{\Gamma^2\left(1 + \frac{1}{\beta}\right)} - 1\right]} \tag{3.55}$$

Over the range of practical interest,  $\beta$  is approximately equal to 1.2/(coefficient of variation). Thus,  $\beta$  is an inverse measure of the dispersion of material strength. For values of  $\beta$  between 20 and 2, the coefficient of variation can be expressed approximately as  $\beta^{-0.92}$ . Values of  $\beta$  between 2 and 4 correspond to brittle fibers, whereas a value of 20 is appropriate for a ductile metal.  $\beta$  is about 4 for carbon fibers, between 2.7 and 5.8 for boron fibers and about 11 for glass fibers. The factor  $\sigma_o L^{-1/\beta}$  in Eqs. (3.54) is often referred to as a characteristic strength level of the fibers (Kelly 1973, Rosen 1964).

Manders and Chou (1983a) have shown that the scale and shape parameters of the Weibull distribution function for fiber strength can be estimated from experimental measurements in a number of ways. First, by taking logarithms of Eq. (3.54a), it is seen that a graph of  $\ln(\bar{\sigma}_f)$  against  $\ln(L)$  is linear and has gradient  $-1/\beta$ . The shape parameter can be obtained in this way by testing single fibers of a range of gauge-lengths. The second procedure is to plot the cumulative distribution on appropriate logarithmic axes as follows. The cumulative probability of survival is simply

$$P_s = 1 - P_f \tag{3.56}$$

and Eq. (3.52) can be rewritten after taking logarithms as

$$\ln(P_s) = -L \left( \frac{\sigma_f}{\sigma_o} \right)^\beta \tag{3.57}$$

Taking logarithms a second time with a change of sign

$$\ln(-\ln(P_s)) = \ln(L) + \beta \ln(\sigma_f) - \beta \ln(\sigma_o) \tag{3.58}$$

shows that a graph of  $\ln(-\ln(P_s))$  against  $\ln(\sigma_f)$  is linear with gradient  $\beta$  (at fixed gauge-length).

The procedures outlined above rely on testing many separate fibers. If a single fiber could be uniformly stressed along its length it would fracture into a series of unequal fragments of which the average length would decrease with higher applied stress. The distribution of lengths between fractures at any given stress should be exponential following Eq. (3.57), and plotting  $\ln(P_s)$  against  $L$  should give a straight line passing through the origin with gradient  $-(\sigma_f/\sigma_o)^\beta$ . Taking logarithms with a change of sign gives

$$\ln(-\text{gradient}) = \beta \ln(\sigma_f) - \beta \ln(\sigma_o) \tag{3.59}$$

so that a graph of  $\ln(-\text{gradient})$  against  $\ln(\sigma_f)$  is linear with gradient  $\beta$ .

### 3.4.3 *Strength of fiber bundles*

Having examined the strength of single fibers, the strength theory of fiber bundles can be developed (see Daniels 1945, Epstein 1948, Coleman 1958, Kelly 1973, Phoenix 1974). Following the treatment of Coleman (1958), a bundle composed of a very large number,  $M$ , of fibers of equal length is considered. The fibers are further assumed to have the same cross-sectional area and the same shape of stress-strain curves, but differ in their values of the elongation at break. It can be shown that the probability density function of bundle tensile strength  $\sigma_b$  (breaking load for the bundle/total fiber cross-sectional area) tends for large  $M$  toward a normal distribution (Eq. 3.48)

$$p_b(\sigma_b) = \frac{1}{s_b \sqrt{2\pi}} \cdot \exp \left[ \frac{-(\sigma_b - \bar{\sigma}_b)^2}{2s_b^2} \right] \tag{3.60}$$

with a mean bundle strength

$$\bar{\sigma}_b = \sigma_{fm} [1 - P_f(\sigma_{fm})] \tag{3.61}$$

and standard deviation

$$s_b = \sigma_{fm} \sqrt{\{P_f(\sigma_{fm})[1 - P_f(\sigma_{fm})]\}M^{-1/2}} \tag{3.62}$$

Here,  $P_f(\sigma_{fm})$  is the cumulative fiber strength distribution function and  $\sigma_{fm}$  is the value of fiber stress  $\sigma_f$  which gives  $\sigma_f[1 - P_f(\sigma_f)]$  its maximum value, namely

$$\frac{d}{d\sigma_f} \{ \sigma_f [1 - P_f(\sigma_f)] \}_{\sigma_f = \sigma_{fm}} = 0 \tag{3.63}$$

Equation (3.63) implies that the maximum fiber stress  $\sigma_{fm}$  is found from the condition that at failure the load borne by the bundle is a maximum.

Assuming  $P_f(\sigma_f)$  follows the Weibull distribution of Eq. (3.52) for fiber length  $L$ , Eqs. (3.61) and (3.63) give, respectively,

$$\sigma_{fm} = \sigma_o(L\beta)^{-1/\beta} \tag{3.64}$$

and

$$\bar{\sigma}_b = \sigma_o(L\beta e)^{-1/\beta} \tag{3.65}$$

where  $e = 2.71828 \dots$ . Equation (3.65) implies that the proportion of surviving fibers is  $\exp(-1/\beta)$ . The strength of loose bundles is lower than the mean strength of single fibers of the same length by the ratio of Eq. (3.65) to Eq. (3.54a), which is termed the ‘Coleman factor’

$$\frac{\bar{\sigma}_b}{\bar{\sigma}_f} = \left[ \beta^{1/\beta} \exp(\beta^{-1}) \Gamma\left(1 + \frac{1}{\beta}\right) \right]^{-1} \tag{3.66}$$

It is noticed that when there is no dispersion in the strength of the component fibers of a bundle  $\bar{\sigma}_b = \bar{\sigma}_f$ . As the coefficient of variation of the fibers increases above zero, however, the bundle strength efficiency decreases monotonically and approaches zero in the limit of infinite dispersion.  $\bar{\sigma}_b/\bar{\sigma}_f \approx 70\%$  for the coefficient of variation about 17%.

The ratio given in Eq. (3.66) is independent of the length of the fibers so that the strength of loose bundles decreases with length in the same way as the mean strength of single fibers. The Weibull

parameters can therefore be obtained by plotting  $\ln(\text{strength of loose bundle})$  against  $\ln(\text{length})$  as described above for single fibers.

The above analysis is concerned with single bundles, whereas some situations are better modeled as a chain-of-bundles, such as a moderately twisted yarn where the link length is a frictional load transfer length among fibers. A review of this problem is given by Smith and Phoenix (1981).

### 3.4.4 *Correlations between single fiber and fiber bundle strengths*

Equation (3.54a) indicates that the Weibull shape parameter of single fiber strength can be determined from the measurement of strength at several fiber gauge-lengths. There are shortcomings in such measurements. First, it is rather tedious to extract individual fibers from a bundle and to perform numerous tests on fibers with very small diameters. Second, the extraction of fibers from a bundle inevitably has 'selected' the stronger ones, since the weaker fibers are prone to damage and fracture in the process. Third, experiments based upon laser diffraction fringes have shown that the measured fiber diameters vary along the fiber length due to fiber twist and the non-circular fiber cross-section.

In this section, following the approach of Chi, Chou and Shen (1984), a theoretical expression of the load–strain relationship for a bundle of fibers under tension is derived first. Then, two methods for determining the two parameters of Weibull distribution for single fiber strength are developed. This is done by analyzing the characteristics of the load–strain curves. The open circles in Fig. 3.13 show the experimental results of a displacement-controlled test for a loose bundle of carbon fibers.

#### 3.4.4.1 *Analysis*

The correlation between single fiber and fiber bundle strengths is established based upon the following assumptions: (1) the single fiber strength under tension obeys the cumulative Weibull distribution function,  $P_f(\sigma_f)$ , of Eq. (3.52); (2) the relationship between stress,  $\sigma_f$ , and strain  $\epsilon_f$  for a single fiber obeys Hooke's law up to fracture:

$$\sigma_f = E_f \epsilon_f \quad (3.67)$$

where  $E_f$  is the fiber Young's modulus; (3) the applied load is distributed uniformly among the surviving fibers at any instant during a bundle tensile test.

To establish the tensile load–strain ( $F$ – $\epsilon$ ) relation, Eq. (3.52) is rewritten in terms of fiber strain:

$$P_f(\epsilon_f) = 1 - \exp\left[-L\left(\frac{\epsilon_f}{\epsilon_o}\right)^\beta\right] \tag{3.68}$$

Here,  $\epsilon_o$  is the scale parameter for unit fiber length ratio (i.e.  $L = 1$ ) and is given by

$$\epsilon_o = \sigma_o/E_f \tag{3.69}$$

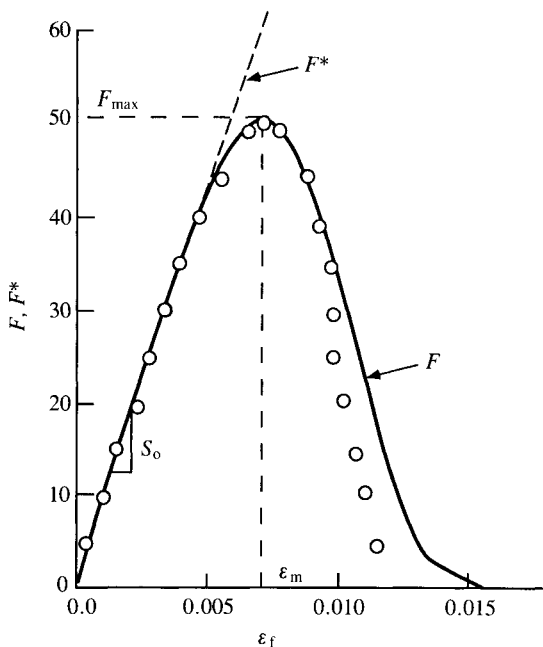
Assume iso-strain conditions for the fibers in a bundle. At an applied strain,  $\epsilon_f$ , the number of surviving fibers in a bundle, which consists of  $N_o$  fibers, is

$$N = N_o[1 - P_f(\epsilon_f)] = N_o \exp[-L(\epsilon_f/\epsilon_o)^\beta] \tag{3.70}$$

$N$  can be related to the applied tensile force,  $F$ , on the bundle by

$$F = \sigma_f AN = AE_f \epsilon_f N_o \exp[-L(\epsilon_f/\epsilon_o)^\beta] \tag{3.71}$$

Fig. 3.13. Comparison of a theoretical  $F$ – $\epsilon_f$  curve (solid line) with experimental data (open circles) for carbon fiber,  $E_f = 225$  GPa,  $d_f = 7 \mu\text{m}$ ,  $N_o = 1000$ ,  $\beta = 4.5$  and  $\epsilon_o = 0.026$ . (After Chi, Chou and Shen 1984.)



Equation (3.71) is the relationship of  $F-\varepsilon_f$  for a bundle of fibers under tension, where  $A$  is the cross-sectional area of a single fiber. If  $A$ ,  $N_o$ ,  $L$ ,  $E_f$ ,  $\varepsilon_o$  and  $\beta$  are known, the  $F-\varepsilon_f$  curve for a bundle of fibers can be drawn. The solid line in Fig. 3.13 shows the result of the theoretical prediction.

According to Eq. (3.71), the  $F-\varepsilon_f$  curve is continuous and smooth. After reaching the point of maximum load,  $F_{\max}$ , the tensile force on the bundle decreases gradually to zero. The slope of the curve,  $S_o$ , at  $\varepsilon_f = 0$  is

$$S_o = AE_f N_o \quad (3.72)$$

and the tensile load defined by the tangent line of the  $F-\varepsilon_f$  curve at  $\varepsilon_f \approx 0$  is

$$F^* = AE_f N_o \varepsilon_f \quad (3.73)$$

Based upon the  $F-\varepsilon_f$  relation, the survivability of single fibers in the bundle can be determined from Eqs. (3.71) and (3.73)

$$\frac{F}{F^*} = 1 - P_f(\varepsilon_f) = P_s \quad (3.74)$$

Next, the strain corresponding to the maximum load on the  $F-\varepsilon_f$  curve,  $\varepsilon_m$ , is obtained from  $dF/d\varepsilon_f = 0$

$$\varepsilon_m = \varepsilon_o \left( \frac{1}{L\beta} \right)^{1/\beta} \quad (3.75)$$

Thus, the maximum load is

$$F_{\max} = AN_o E_f \varepsilon_o \left( \frac{1}{L\beta e} \right)^{1/\beta} \quad (3.76)$$

From Eqs. (3.72), (3.75) and (3.76), the slope of the straight line connecting the origin and the point  $(F_{\max}, \varepsilon_m)$  in Fig. 3.13 is

$$S = F_{\max}/\varepsilon_m = S_o \left( \frac{1}{e} \right)^{1/\beta} \quad (3.77)$$

As a result,

$$\beta = 1/\ln \left( \frac{\varepsilon_m S_o}{F_{\max}} \right) \quad (3.78)$$

#### 3.4.4.2 *Single fiber strength distribution*

Based upon the analysis of the fiber and bundle strength relations, Chi, Chou and Shen (1984) proposed the following two

methods for determining single fiber strength distribution (shape parameter  $\beta$  and scale parameter  $\varepsilon_o$ ) from measurements on fiber bundles, and constructing the theoretical  $F-\varepsilon_f$  curve.

Method (A)

The method is based upon Eqs. (3.68) and (3.74) and the experimental  $F-\varepsilon_f$  curve. The procedure is outlined below:

- (1) Calculate  $S_o$  from Eq. (3.72) and the data of  $A$ ,  $E_f$  and  $N_o$  of the fiber bundle.
- (2) Calculate  $F^*$  from Eq. (3.73),  $F^* = S_o E_f$ . Measure  $F$  from the  $F-\varepsilon_f$  curve. Then determine from Eq. (3.74) the fiber survivability as a function of strain,  $P_s(\varepsilon_f) = F/F^*$ .
- (3) The shape parameter,  $\beta$ , can be obtained from the gradient of the graph of  $\ln(-\ln(P_s))$  vs.  $\ln(\varepsilon_f)$ , based upon the relation

$$\ln(-\ln(P_s)) = \ln(L) + \beta \ln(\varepsilon_f) - \beta \ln(\varepsilon_o) \quad (3.79a)$$

- (4) The scale parameter,  $\varepsilon_o$ , is determined either from Eq. (3.75) using the measured  $\varepsilon_m$  value, or from the value of  $\ln(L) - \beta \ln(\varepsilon_o)$  measured from the graph of  $\ln(-\ln(P_s))$  vs.  $\ln(\varepsilon_f)$ .

Method (B)

In this method,  $F_{max}$  and  $\varepsilon_m$  are known from experiments. The calculation steps are:

- (1) Determine  $S_o$ ,  $\beta$  and  $\varepsilon_o$  from Eqs. (3.72), (3.78) and (3.75), respectively.
- (2) From Eqs. (3.71) and (3.72), the  $F-\varepsilon_f$  relation can be written as

$$F = S_o \varepsilon_f \exp\left(-L \left(\frac{\varepsilon_f}{\varepsilon_o}\right)^\beta\right) \quad (3.79b)$$

3.4.5 Experimental measurements of Weibull shape parameter

It is understood that the shape parameter  $\beta$  gives a measurement of the scattering of the strength data. On a  $p_f(\sigma_f)$  vs.  $\sigma_f$  plot, the range of strength distribution is narrower for higher  $\beta$  values. The discussions of Sections 3.4.2–3.4.4 for the estimation of the Weibull shape parameter are summarized below (see Manders and Chou 1983a; Chi, Chou and Shen 1984).

**Single fibers**

- (i) Variation of mean strength with length: The method requires tests at different gauge-lengths. Fiber diameters are measured to obtain true stress.
- (ii) Distribution of strength at fixed gauge-length: Diameters are measured to obtain true stress. The method measures both inherent variability, and also artificial scatter introduced by experimental techniques.
- (iii) Distribution of lengths between multiple fractures of a single fiber: Estimate is based on strain, not stress. The method requires correction for non-uniformity of strain near fractures.

**Loose bundles**

- (iv) Variation of mean strength with length: The method assumes identical fiber diameters and stiffness.
- (v) Proportion of surviving fibers is obtained from the load–strain curve. Estimate is based on strain not stress. The method assumes fibers are identical.
- (vi) Determination of the initial slope of the load/strain curve and the strain corresponding to the maximum load on the bundle.

Manders and Chou (1983a) have established the Weibull shape parameter based upon the methods (i)–(v) by performing tests on a single batch of PAN-based carbon fiber (Hercules AS-4, 12 000 filament unsized tow) while the loose bundle tests (iv) and (v) are carried out with the E-glass fiber (St. Gobain, vetrotex type DCN56 filament, unsized tow). Chi and Chou (1983), and Chi, Chou, and Shen (1984) have examined methods (i), (ii), (v) and (vi) using Thornel-300 carbon fibers and bundles containing 1000 fibers.

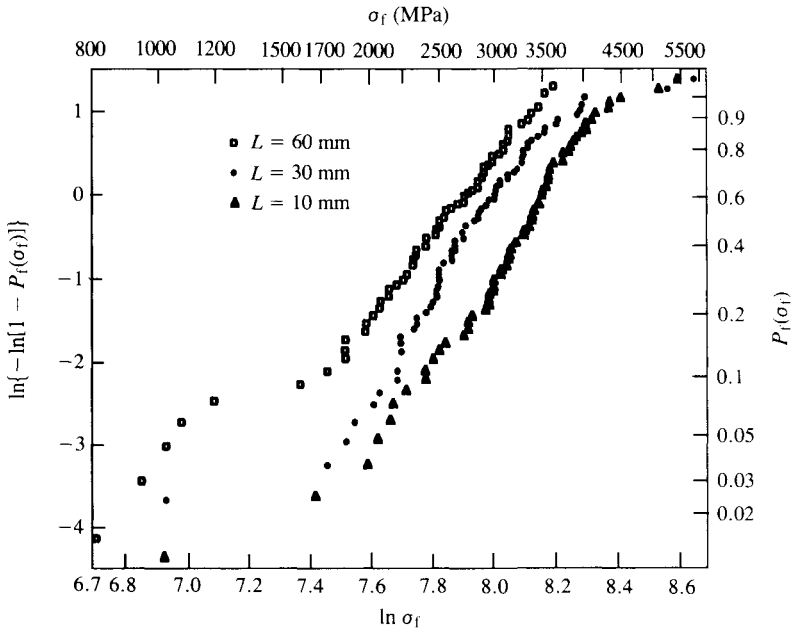
**3.4.5.1 Single fiber tests**

In order to obtain the strengths of single filaments and their distributions, it is necessary to measure the diameters and ultimate tensile load of the filaments. For the measurement of filament diameters, Chi and Chou (1983) used a helium–neon laser, and the diameters were determined from the laser diffraction fringes (see Lipson and Lipson 1981) The results indicate an average filament diameter of  $7.12 \mu\text{m}$  with the standard deviation of  $0.2 \mu\text{m}$ .

Fiber strength measurements are performed for fiber gauge-lengths of 10, 30 and 60 mm, and the number of measurements are 80, 81 and 64, respectively. The results are presented on the Weibull probability paper as shown in Fig. 3.14. Here  $\sigma_f$  denotes fiber ultimate strength;  $P_f(\sigma_f)$  is the fiber cumulative probability of failure at stresses equal to or less than  $\sigma_f$  and  $\ln\{-\ln[1 - P_f(\sigma_f)]\}$  is a representation of failure probability. The variations of fiber failure probability with strength can be approximated as linear with the exceptions of the low strength range for 60 mm length fibers, and the high strength range for 10 mm and 30 mm length fibers.

The Weibull shape parameter,  $\beta$ , can be obtained by following method (i), by plotting the mean fiber strength  $\ln(\bar{\sigma}_f)$  vs. fiber length  $\ln(L)$  (see Eq. (3.54a)) as shown in Fig. 3.15. A measurement of the slope of the straight line gives the value of  $\beta = 6.2$ . It is worth noting that because of the high scatter in strengths a large number of tests needs to be performed to determine with high accuracy whether the Weibull distribution is an accurate description of strength, and this is where the loose bundle approach is

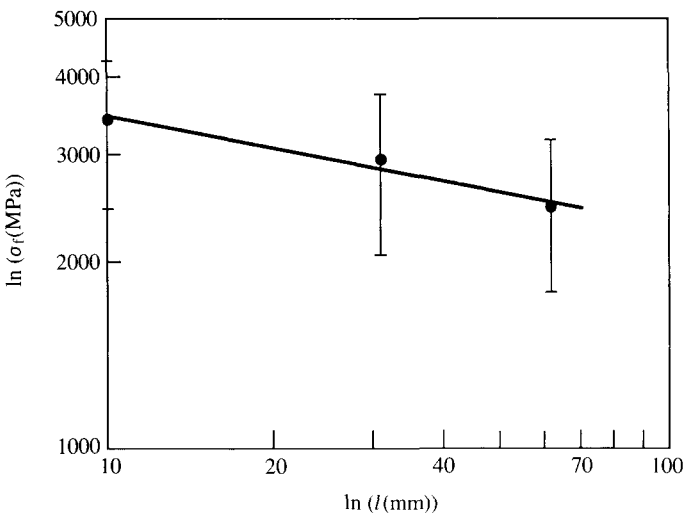
Fig. 3.14. Strength distributions of single filaments on Weibull probability paper. (After Chi and Chou 1983.)



advantageous. If method (ii) is followed, then the slope is measured from the linear portion of the data of Fig. 3.14 for  $\ln\{\ln[1 - P_f(\sigma_f)]\}$  vs.  $\ln(\sigma_f)$  (see Eq. (3.58)). The distributions of the three sets of data are reasonably linear and parallel, and an average of the approximate gradients is taken to obtain the shape parameter of 5.3.

Method (iii) requires multiple fracture tests of a single fiber. In the experiments of Manders and Chou (1983a), single carbon fibers are bonded to the surface of a 2 mm thick filled PVC carrier sheet using a film of polystyrene adhesive approximately  $50 \mu\text{m}$  thick. The fiber is strained to successively higher levels by bending the carrier strip around mandrels of decreasing radii. The strain in the fiber is virtually uniform because the ratio of the carrier thickness to fiber diameter is  $\sim 200$ . The combination of adhesive and carrier is found to be quite resistant to repeated straining, and facilitates visual location of the fiber fractures. At each strain level the lengths between fiber fractures are measured by travelling microscope and are ranked and plotted as the cumulative distribution on the logarithmic axes. According to Eq. (3.57), the distributions should be linear and pass through the origin, but, while they are relatively straight, they intersect the fracture spacing axis at some positive intercept. The minimum crack spacing given by the intercept represents the effective 'unstressed' length of fiber over which the

Fig. 3.15. Relationship between filament average strength and gauge-length. (After Chi and Chou 1983.)



load builds up. The logarithm of the gradient has been plotted against the logarithm of strain and at low strains, the curve is relatively linear with a gradient corresponding to  $\beta = 6.4$ . At high strain the curve becomes horizontal because the fiber debonds from the adhesive film and no new fractures occur. Despite this shortcoming the technique is able to measure the shape parameter for shorter fibers than the other techniques.

Henstenburg and Phoenix (1989) have considered the problem of measuring the Weibull parameters for fiber strength using data from a multiple fracture test of a single fiber. Using a Monte-Carlo approach they arrived at a simple method which applies to fibers of length equal to the mean fragmentation length.

#### 3.4.5.2 *Loose bundle tests*

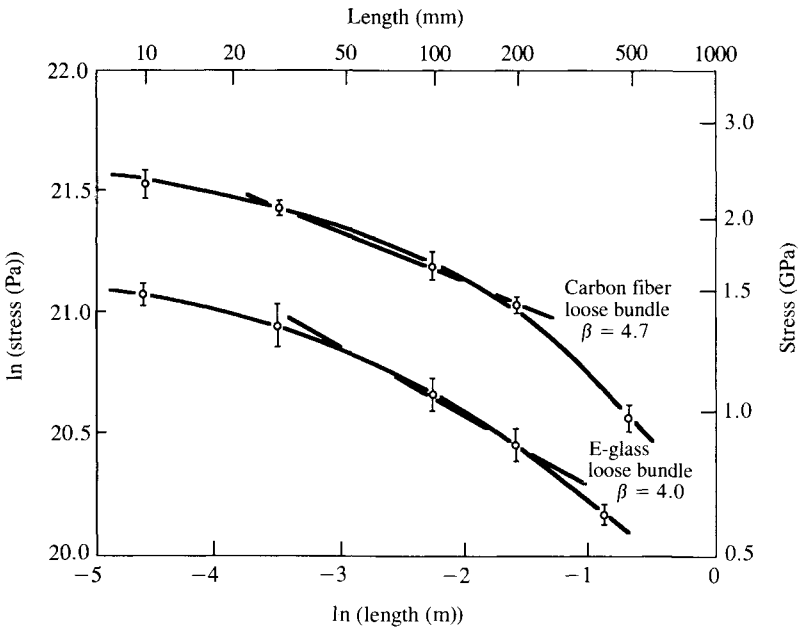
In the loose bundle tests of Manders and Chou (1983a), based on method (iv), tows of different lengths are cemented into grooved end-tabs while particular care is taken to ensure that none of the fibers are slack. Manders and Chou obtained between five and ten results for each gauge-length, and they are plotted in the same way as for the single fiber tests in Fig. 3.16. The cross-sectional area of the tow is calculated from the manufacturer's value of its density and weight per length. Because each failure of a loose bundle involves the independent fracture of many fibers, there is much less scatter than for the single fibers. According to Manders and Chou, the mean strength ratios of loose bundles and single carbon fibers of the same length range from 0.67 to 0.85 for fibers with lengths between 10 and 200 mm, and this compares quite well with the theoretical Coleman factor which ranges from 0.65 to 0.76 for fibers with  $\beta$  equal to 5 and 10, respectively (Coleman 1958). The discrepancy may be due to the fact that the strengths are not perfectly Weibull distributed, and that the optical technique for measuring fiber diameter overestimates the cross-sectional area of non-circular crenelated fibers. Also, fiber breaks may be pre-existing in the bundle, becoming more noticeable at longer bundle lengths.

It has been noticed that both single fibers and loose bundles show an increase in strength variability at longer gauge-lengths. This could be interpreted as the influence of a relatively small population of severe and broadly distributed flaws. The majority of short gauge-lengths would not contain one of these severe flaws and the population would have little influence on the mean strength, but longer fibers would be more likely to contain one or more such

flaws and their mean strength would be significantly lowered. The observation of similar behavior in glass fiber suggests that a ‘double’ Weibull distribution with two shape and scale parameters may be more appropriate (Metcalf and Schmitz 1964; Harlow and Phoenix 1981a & b). It is also noticed, in the case of loose bundles, that the recoil and entanglement of failed fiber causes neighboring fibers to fail, thereby weakening the bundle.

In the loose bundle tests of Chi, Chou and Shen (1984), the shape parameter and scale parameter were determined based upon methods (v) and (vi), which correspond to methods (A) and (B) of Section 3.4.4.2. The relevant data are:  $N_o = 1000$ , fiber diameter =  $7 \mu\text{m}$ ,  $E_f = 255 \text{ GPa}$  and gauge-length = 60 mm. The shape parameters obtained from methods (v) and (vi) are 4.6 and 4.5, respectively. The scale parameter,  $\epsilon_o$ , corresponding to a fiber of unit length (1 mm in this case), is 0.026 for both methods. The experimental data points indicating the load–strain ( $F-\epsilon_f$ ) relationship are shown in Fig. 3.13. The consistency between the theory and experiment is rather satisfactory in the range of bundle strain not much greater than  $\epsilon_m$ .

Fig. 3.16. Variation of mean strength with length for loose bundles of carbon and E-glass fibers. (After Manders and Chou 1983a.)



### 3.4.6 Strength of unidirectional fiber composites

This section deals with statistical strength theories of unidirectional fiber composites. Upon the fracture of a fiber, the load originally carried by the fiber needs to be transferred to its neighboring fibers. A simple approximation of the load redistribution is to assume that the load is shared equally by all the unbroken fibers. A more precise treatment takes into account the local concentration of load on neighboring fibers. A Monte-Carlo simulation is also presented to illustrate the statistical nature of composite failure.

#### 3.4.6.1 Equal load sharing

In general, the high-strength high-stiffness fibers used in composites are brittle and their tensile strength should be characterized statistically. Parratt (1960) notes that the tensile failure of composites reinforced with brittle fibers occurs when the fibers have been broken up into lengths so short that any increase in applied load cannot be transmitted to the fibers because the limit of interface or matrix shear has been reached. Rosen (1964), following Gucer and Gurland (1962), considers fibers as having a statistical distribution of flaws or imperfections that result in individual fiber breaks at various stress levels. The fracture initiated in a fiber is contained by the matrix material. Composite failure occurs when the remaining unbroken fibers, at the weakest cross-section, are unable to resist the applied load. Then composite failure results from tensile fracture of the fibers. In Rosen's failure model, the composite is assumed to be strained uniformly and the load in a broken fiber is distributed equally among the remaining unbroken fibers in a cross-section. Harlow and Phoenix (1978a) have labelled such a model as *equal load sharing*. Scop and Argon (1967) also have dealt with the problem of equal load sharing in their treatment of the strength of laminated composites.

Figure 3.17 depicts Rosen's failure model. In the vicinity of an internal fiber end in such a composite, the axial load carried by the fiber is transmitted by shear through the matrix to adjacent fibers (see Section 3.3.1). A portion of the fiber at each end is, therefore, not fully effective in resisting the applied stress. At some distance from an internal break, the fiber stress will reach a given fraction of the undisturbed fiber stress. Rosen considers that the fiber length  $\delta$ , measured from the fiber end, over which the stress is less than a given fraction (i.e. 90%) of the uniform stress that would exist in infinite fibers, as ineffective.  $\delta$  is thus known as the ineffective

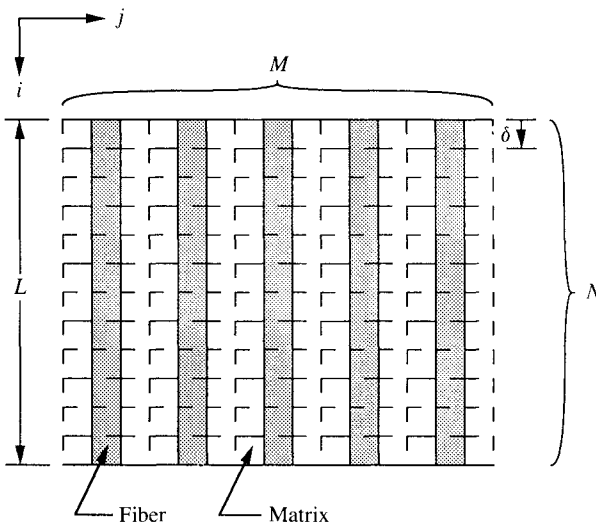
length. The model composite in Fig. 3.17 is assumed to be composed of a series of layers of height  $\delta$ . The segment of a fiber within a layer may be considered as a link in the chain that constitutes the fiber. Each layer is then a bundle of such links and the composite is a series of such bundles.

The treatment of a fiber as a chain of links is appropriate to the hypothesis that fracture is a result of local imperfections in the fibers. The links may be considered to have a statistical strength distribution that is equivalent to the statistical flaw distribution along the fibers. Rosen defines the link dimension by a shear-lag analysis of the stress distribution in the vicinity of a fiber end (see Section 3.3.1). The length of the composite specimen is designated by  $L$  and the number of links is given by  $N = L/\delta$ .

The relationship between fiber strength and the strength of links has been briefly discussed in the formulation of Eq. (3.51). Obviously, the probability density function  $p_1(\sigma_1)$  for fiber links can be characterized if the experimental data on fiber strength distribution  $p_f(\sigma_f)$  are known. Suppose that the fibers are characterized by a strength distribution of the Weibull type (Eq. (3.53)), the link strength density function can be readily written as

$$p_1(\sigma_1) = \delta \sigma_0^{-\beta} \beta \sigma_1^{\beta-1} \exp\left[-\delta \left(\frac{\sigma_1}{\sigma_0}\right)^\beta\right] \quad (3.80)$$

Fig. 3.17. Chain-of-links model for a unidirectional fiber composite.



For a bundle of links and a large number,  $M$ , of fibers, the distribution of bundle strength  $p_b(\sigma_b)$  and the mean bundle strength  $\bar{\sigma}_b$  are given by Eqs. (3.60) and (3.61), respectively.

The bundles may be treated as links in a chain, which now represents the whole composite of Fig. 3.17. The weakest link theorem can again be applied to define the failure of the composite. For  $N$  bundles forming a chain (composite) the probability density function  $p_c(\sigma_c)$  for the average fiber stress at composite failure,  $\sigma_c$ , is given by

$$p_c(\sigma_c) = Np_b(\sigma_c)[1 - P_b(\sigma_c)]^{N-1} \tag{3.81}$$

where

$$P_b(\sigma_c) = \int_0^{\sigma_c} p_b(\sigma) d\sigma \tag{3.82}$$

The notations of  $p_c(\sigma_c)$ ,  $p_b(\sigma_b)$ ,  $p_f(\sigma_f)$  and  $p_l(\sigma_l)$  have been used to denote the strength density functions of the fibers at the level of composite, bundle, fiber and link, respectively. Thus, it is understood that  $\sigma_c$ ,  $\sigma_b$ ,  $\sigma_f$  and  $\sigma_l$  all refer to stresses in the reinforcements; the contribution of matrix to composite strength is not considered.

The most probable composite failure stress  $\sigma_c^*$  is obtained by setting

$$\frac{d}{d\sigma_c} [p_c(\sigma_c)]_{\sigma_c = \sigma_c^*} = 0 \tag{3.83}$$

Following Rosen (1964), the substitution of Eq. (3.81) into Eq. (3.83) yields

$$\sigma_c^* = \bar{\sigma}_b - s_b \sqrt{2 \cdot \log N} + s_b \frac{\log \log N + \log 4\pi}{2\sqrt{2 \cdot \log N}} \tag{3.84}$$

It can be seen from Eq. (3.62) that, for composite dimensions large relative to fiber cross-section ( $M \gg 1$ ),  $s_b \rightarrow 0$  and Eq. (3.84) is reduced to the mean bundle strength expression of Eq. (3.65)

$$\sigma_c^* = \sigma_0(\delta\beta e)^{-1/\beta} \tag{3.85}$$

When the fiber volume content is considered, the tensile strength of the composite is given by  $V_f \sigma_c^*$ . In Eq. (3.85), the ineffective length  $\delta$  can be determined from the stress analyses discussed in Section 3.3.1. It is obvious that the composite strength is enhanced due to a reduction in fiber ineffective length and fiber strength dispersion. The statistical nature of fiber fracture and the resulting weakest link mode of failure have been demonstrated experimentally in a

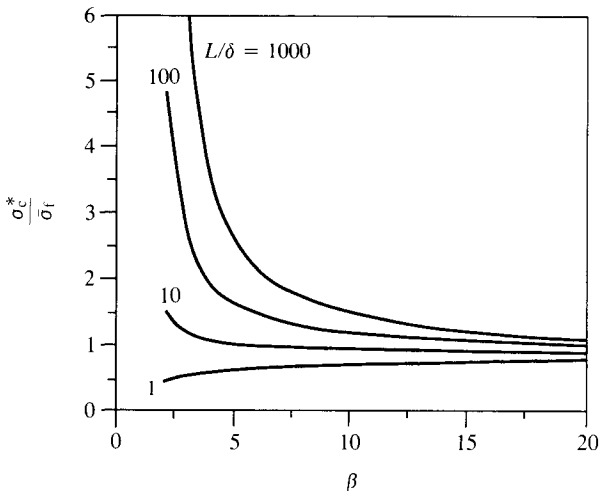
glass/epoxy system by Rosen (1964). This experiment also points out the very significant phenomenon in brittle fiber composites: fiber breakages may exist in a composite of continuous fibers at stress levels well below the maximum load.

If the composite strength (Eq. (3.85)) is compared with the mean strength of the tested fibers of length  $L$  (Eq. (3.54)), some interesting conclusions can be drawn (Rosen 1970). Figure 3.18 shows that for reference fibers of ineffective length  $\delta$ , the strength of the composite is less than the mean fiber strength. When the fiber length is greater than  $\delta$ , the composite strength is larger than the mean fiber strength of a fiber bundle of length  $L > 7\delta$ . Also for a fiber strength coefficient of variation ( $s/\sigma$ ) less than 15% (or the shape parameter  $\beta > 8$ ), the composite strength is close to the mean fiber strength, as shown in Fig. 3.18.

#### 3.4.6.2 *Idealized local load sharing*

When a fiber breaks in a composite there is inevitably a redistribution of load in the vicinity of the fiber breakage. Thus, local load sharing takes place (see Zweben 1968; Scop and Argon 1969; Zweben and Rosen 1970; Fukuda and Kawata 1976b; Harlow and Phoenix, 1978a&b; Harlow 1979; Phoenix 1979). The localized nature of stress redistribution around a random fiber break has been discussed in Section 3.3. Zweben (1968) first considered the

Fig. 3.18. Composite strength/mean fiber strength vs.  $\beta$  at various  $L/\delta$  values.



micromechanical stress transfer process and the probabilistic aspects of the generation of clusters of breaks to form catastrophic breaks. Fukuda and Kawata (1976b) generalized the original concept of Zweben and derived the cumulative strength distribution for the composite.

In the following, an analysis is presented under the Weibull distribution for fiber strength, and somewhat simplified assumptions on local fiber load sharing but with the advantage that various quantities can be worked out either exactly or asymptotically. The result is that insight can be gained on the *approximate* Weibull behavior for composite strength where the Weibull parameters for the composite will be connected to various fiber and matrix properties, and in particular to the composite volume. The size effect law for the composite will also be discussed. Most of the features have been experimentally observed but have been difficult to explain. The ideas for this section are taken from Harlow and Phoenix (1978a&b, 1979, 1981a&b); Smith (1980, 1982); Phoenix and Smith (1983); Smith *et al.* (1983); and Phoenix, Schwartz and Robinson (1988).

The model considered is the planar, chain-of-bundles model of Fig. 3.17 where  $M$  is the number of fibers and  $N$  is the number of bundles each with fiber elements of length  $\delta$ , which might better be termed 'the effective load transfer length'. Following the notation of Phoenix, the cumulative distribution function for the failure of a single fiber element of length  $\delta$  is taken as the Weibull distribution and expressed as

$$F(\sigma) = 1 - \exp\{- (\sigma/\sigma_\delta)^\beta\} \quad \sigma \geq 0 \tag{3.86}$$

where  $\sigma$  is the fiber stress, and  $\beta$  and  $\sigma_\delta$  are the Weibull shape and scale parameters, respectively. (At this point it should be mentioned that  $\delta$  should take into account certain statistical aspects of fiber strength which modify its magnitude somewhat as described by Harlow and Phoenix (1979), and Phoenix, Schwartz and Robinson (1988). Roughly,  $\delta$  varies inversely as the shape parameter  $\beta$ .) According to principles discussed earlier, the strength of a fiber element of length  $\delta$  can be expressed in terms of those for a longer reference length  $L$  (used, say, for tension tests) according to

$$\sigma_\delta = \sigma_L \left( \frac{\delta}{L} \right)^{-1/\beta} \tag{3.87}$$

where  $\sigma_L$  is the Weibull scale parameter for fiber strength at the reference length. Often  $\sigma_\delta$  will be about double  $\sigma_L$  in magnitude.

The local load-sharing rule is 'idealized' as follows: In a bundle, if the stress is nominally  $\sigma$  (ignoring the matrix), a surviving fiber element carries load  $K_r\sigma$ , where

$$K_r = 1 + r/2, \quad r = 0, 1, 2, 3, \dots \quad (3.88)$$

and  $r$  is the number of consecutive failed elements immediately adjacent to the surviving element (counting on both sides). At the same time a failed fiber element carries no stress over length  $\delta$ . Essentially the load of a failed fiber is shifted equally onto its two nearest surviving neighbors, one on each side. This rule is more severe than the true situation where the stress redistribution is somewhat more diffuse, as described say by Hedgepeth (1961), but it captures the essential features and has the advantages of simplicity and being fully described for all configurations.

Before proceeding with an approximate analysis of this model, it is useful to review an extensive numerical analysis performed by Harlow and Phoenix (1978a&b), where the basic insight into its behavior was uncovered. To eliminate boundary effects, they considered circular bundles (composite tubes), and studied the behavior of the cumulative strength distribution as the bundle size  $M$  increases. They defined  $G_M(\sigma)$  as the cumulative distribution function for failure of a bundle with  $M$  fibers under the stress  $\sigma$ , and worked out exact formulas for  $G_M(\sigma)$  for  $M$  up to 5 by considering all configurations of failed and surviving fibers and all ways that failure could proceed through these configurations and then summing all probabilities for these ways. For example, for  $M = 2$ ,

$$\begin{aligned} G_2(\sigma) &= F(\sigma)^2 + 2F(\sigma)[F(2\sigma) - F(\sigma)] \\ &= 2F(\sigma)F(2\sigma) - F(\sigma)^2 \end{aligned} \quad (3.89)$$

where in the intermediate step the first term represents direct failure under the applied stress of both fiber elements, and the second term represents the two ways one element can fail under the direct stress and the other under the overstress, which is naturally taken as  $2\sigma$  in this situation (rather than  $3\sigma/2$ ). For  $M = 4$ , they obtained by a tedious calculation

$$\begin{aligned} G_4(\sigma) &= 16F(4\sigma)F(2\sigma)F(3\sigma/2)F(\sigma) - 4F(4\sigma)F(2\sigma)F(\sigma)^2 \\ &\quad - 4F(4\sigma)F(3\sigma/2)^2F(\sigma) + 4F(4\sigma)F(\sigma)^3 \\ &\quad - 8F(2\sigma)^2F(3\sigma/2)F(\sigma) \\ &\quad + 2F(2\sigma)^2F(\sigma)^2 - 8F(4\sigma)F(3\sigma/2)F(\sigma)^2 \\ &\quad + 4F(3\sigma/2)^2F(\sigma)^2 - F(\sigma)^4 \end{aligned} \quad (3.90)$$

Generally no simple pattern emerged except that each term involved a product of  $M$  quantities in  $F$ . The evaluation procedure was automated on a computer, but results were only obtained at that time for  $M$  up to 9 because of the tremendous increase in computational complexity resulting from the increasing number of ways the bundle can fail as the bundle size increases. (Even with present supercomputer capability the limit is still about  $M = 14$ .) At the same time we desire results for  $M$  orders of magnitude larger.

Suspecting an eventual weakest-link type relationship, Harlow and Phoenix (1978b) considered plotting the ‘renormalization’

$$W_M(\sigma) = 1 - [1 - G_M(\sigma)]^{1/M} \tag{3.91}$$

since in reverse this yields the weakest-link relation

$$G_M(\sigma) = 1 - [1 - W_M(\sigma)]^M \tag{3.92}$$

They discovered an extremely rapid numerical convergence

$$W_M(\sigma) \rightarrow W(\sigma) \quad \text{as } M \rightarrow \infty \tag{3.93}$$

where  $W(\sigma)$  was called the *characteristic distribution function* for failure. This convergence is shown in Fig. 3.19 for the Weibull shape parameter  $\beta = 5$ , which is typical of brittle fibers. The coordinates are Weibull coordinates ( $\ln\{-\ln(1 - W)\}$  vs.  $\ln(\sigma/\sigma_\delta)$ ) wherein a Weibull distribution always plots as a straight line. For each value of  $\sigma$  the convergence is abrupt at some value of  $M$ , which increases slowly with decreasing values of  $\sigma$ . Also the convergence becomes complete far into the lower tail of  $W(\sigma)$  (probabilities below  $10^{-10}$ ) for  $M = 9$ . In an extremely complex calculation, Harlow and Phoenix (1981a&b) uncovered the analytical character of  $W(\sigma)$  in terms of the largest eigenvalue of a Markov recursion matrix. It suffices to say here that  $W(\sigma)$  has no simple analytical form, though shortly we will develop an approximation which will give us considerable insight.

The importance of  $W(\sigma)$  is that, from Eq. (3.92), the distribution function for bundle failure can be given extremely accurately by the approximation

$$G_M(\sigma) \approx 1 - [1 - W(\sigma)]^M \tag{3.94}$$

and this works for  $M$  many orders of magnitude larger than the values used in the calculation of  $W(\sigma)$  on the computer. Perhaps one should note that any boundary effects, which may come into play for small bundles, are being ignored.

Because the composite is seen as a weakest-link arrangement of its  $N$  bundles (Fig. 3.17), and the bundles are treated as statistically independent, the cumulative distribution function for the failure of the composite, denoted as  $H_{M,N}(\sigma)$ , is given as

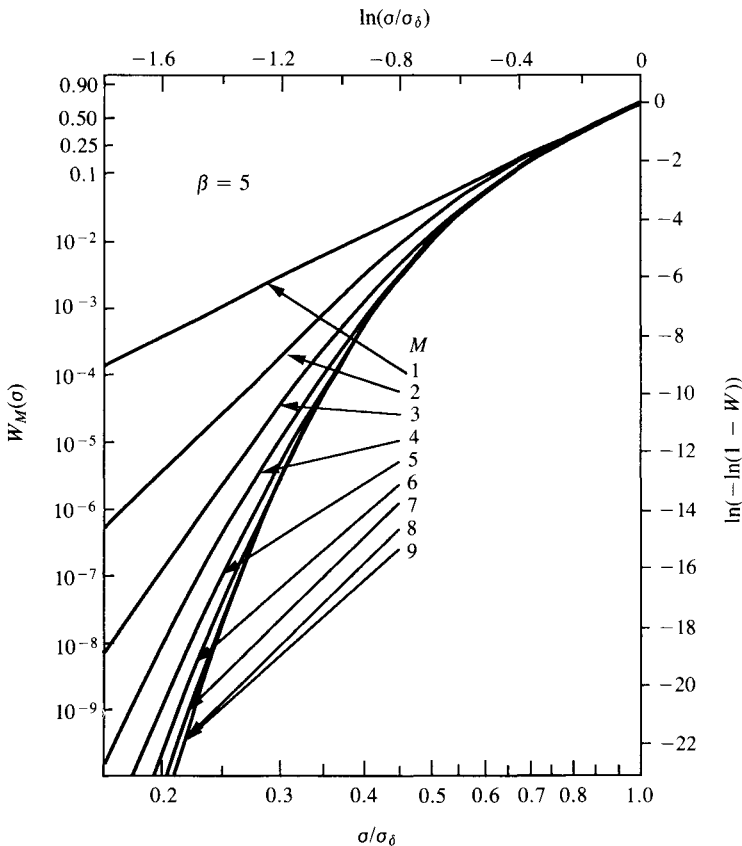
$$H_{M,N}(\sigma) = 1 - [1 - G_M(\sigma)]^N \tag{3.95}$$

Combining Eqs. (3.94) and (3.95) and writing  $V = MN$  yields the accurate approximation

$$H_{M,N}(\sigma) \approx 1 - [1 - W(\sigma)]^V \tag{3.96}$$

which surprisingly, perhaps, is a result which is symmetric in  $M$  and

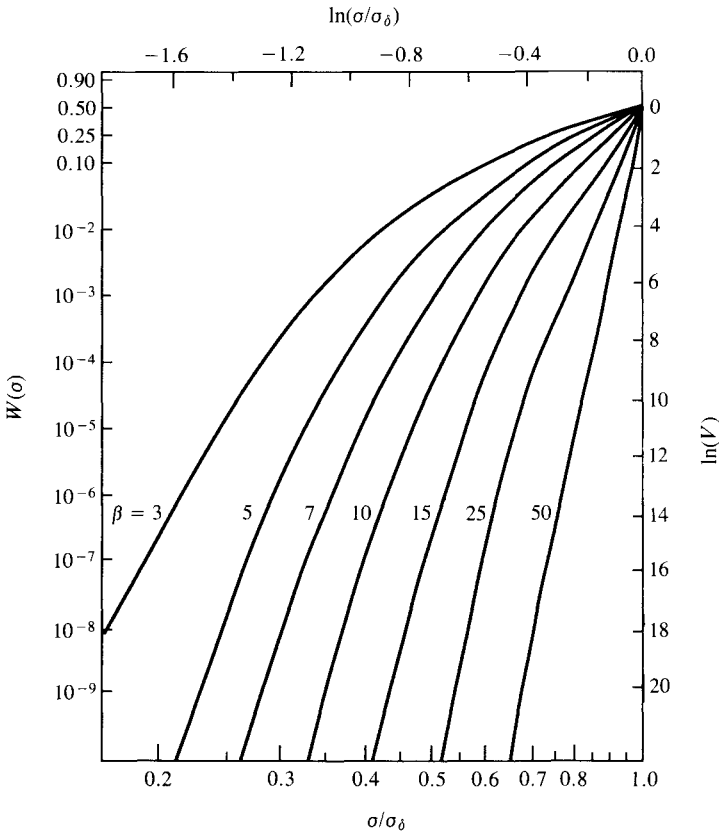
Fig. 3.19. Convergence of the renormalized distribution functions  $W_M(\sigma)$  to the characteristic distribution function  $W(\sigma)$  as  $M$  increases. (After Harlow and Phoenix 1978b.)



$N$ . Note that by the binomial expansion  $H_{M,N}(\sigma) \approx VW(\sigma)$ . Thus if  $V$  is large, say  $10^6$  elements, it is necessary to know  $W(\sigma)$  where its value is much less than  $10^{-6}$ . As mentioned, this is provided for in Fig. 3.19. Note that despite the fact that Eq. (3.96) is a ‘weakest-link’ relation, in terms of  $V = MN$  elements, there is no identifiable and independent material element to which one can attach  $W(\sigma)$ . At best,  $W(\sigma)$  characterizes the effects of local failure events which are actually statistically dependent.

Figure 3.20 displays  $W(\sigma)$  for values of  $\beta$  from 3 to 50. Now Fig. 3.20 can be used to construct a figure for  $H_{M,N}(\sigma)$  upon noting that  $\ln\{-\ln(1 - H)\} = \ln\{-\ln(1 - W)\} + \ln V$ , which on Weibull prob-

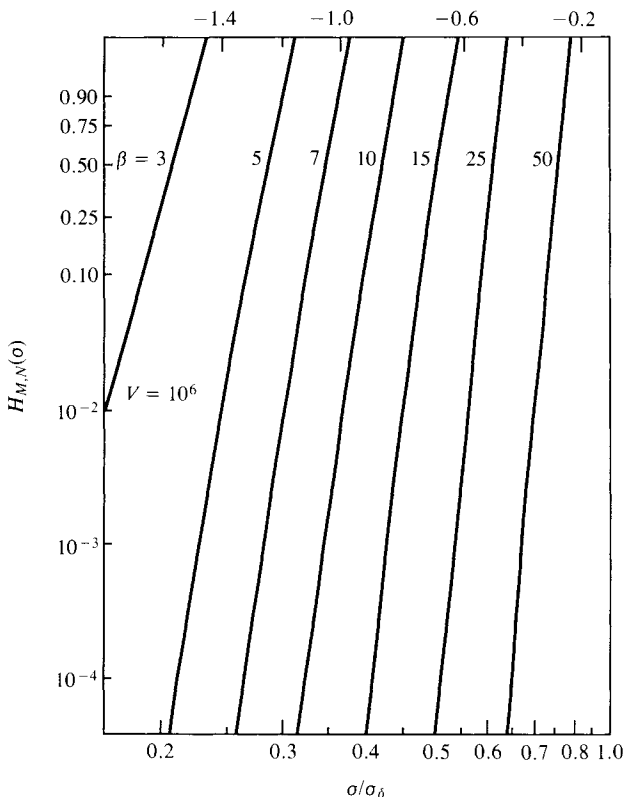
Fig. 3.20. Characteristic distribution function  $W(\sigma)$  for various values of the Weibull shape parameter  $\beta$  for fiber strength. (After Harlow and Phoenix 1978b.)



ability paper amounts to a simple translation of each curve upward (or the left-hand scale downward) the amount  $\ln(V)$  on the right-hand scale provided for this purpose. Figure 3.21 shows the result of such a translation for  $V = 10^6$  elements, which amounts to a display of the original region on Fig. 3.20 below  $10^{-5}$ . This yields plots of the cumulative distribution function of composite failure,  $H_{M,N}(\sigma)$ , for various  $\beta$  for a relatively small composite specimen.

Several features of Fig. 3.21 warrant discussion. First, all the lines are approximately straight over a very wide probability range, which suggests that the strength of a composite approximately (but not exactly) follows a Weibull distribution. In fact, an empirical plot to cover the probability range shown would require testing about

Fig. 3.21 Cumulative distribution function  $H_{M,N}(\sigma)$  for composite strength for volume  $MN = 10^6$  and various values of the fiber shape parameter  $\beta$ . (After Harlow and Phoenix 1978b.)



20 000 specimens, and using standard statistical techniques it is probable that a Monte-Carlo simulation would *not* lead to rejection of the hypothesis that the Weibull distribution is actually the correct distribution! Second, the lines show only a modest change in slope, by a factor of less than three, as the original Weibull shape parameter for the fiber  $\beta$  decreases from 50 to 3, which is a factor of more than ten. Since the slope is directly proportional to the Weibull shape parameter, this indicates that the *effective* Weibull shape parameter for the composite decreases modestly, from about 50 to 20 as that for the fiber decreases drastically, from about 50 to 3. On the other hand, the horizontal location of the plots is quite strongly influenced by the value of  $\beta$ , which suggests that an increase in variability in fiber strength substantially decreases composite strength. It is seen, for example, that the median strength drops from about  $0.75\sigma_\delta$ , to about  $0.2\sigma_\delta$  as  $\beta$  drops from 50 to 3. Note also that the median strength of the composite is much less than that for a fiber element of length  $\delta$ , being only about  $\frac{1}{3}$  for the typical case  $\beta = 7$ . On the other hand, standard tension tests on fibers are performed at gauge-lengths  $L$  about two orders of magnitude larger than  $\delta$ , and by Eq. (3.87) their strengths are about one-half of  $\sigma_\delta$ . Fortuitously then, the strength of the composite will be little different from the strength of the fiber from typical laboratory tension tests as is often observed. Finally, the method of constructing Fig. 3.21 indicates that there is a mild size effect in composite strength and a mild shift in the effective Weibull shape parameter for the composite. Had a larger volume  $V = 10^9$  been chosen rather than  $10^6$ , the curved nature of the graphs on Fig. 3.20, from which Fig. 3.21 was derived, would produce a slightly lower strength and a slightly higher effective shape parameter for the composite depending on  $\beta$ .

Attention is now turned toward a simple but approximate theoretical explanation based on some key ideas motivated by the above numerical analysis and results. First, the range for the composite failure stress lies  $\ll \sigma_\delta$ , as we saw from Fig. 3.21. (Note that both the median and the stress at 0.99 probability of failure lie well below  $\sigma_\delta$  for typical values of  $\beta$  below 15.) Second, the 'initial' failures, that is fiber elements which fail directly under the applied stress  $\sigma$ , are viewed as 'seeds' for the growth of failure clusters, which are lateral strings of adjacent fiber breaks contained within bundles. Third, the *number* of such seeds is easily seen to follow the binomial distribution with parameters  $MN$  and  $F(\sigma)$  (the number depends, of course, on  $\sigma$ ) with the mean number being  $MNF(\sigma)$ .

Fourth, cluster growth from a seed is viewed for calculation purposes in terms of the sequential failure of adjacent fibers in a bundle, with growth in either direction to form a string. Fifth, instability occurs when a string of  $k$  breaks occurs such that  $F(K_{k-1}\sigma) < \frac{1}{2}$ , say, but  $F(K_k\sigma) \approx 1$ ; thus, subsequent fiber failures become almost certain leading to catastrophic growth of a transverse 'crack' and failure of the composite. This value of  $k$ , which depends on the stress level  $\sigma$ , is called the *critical crack size*, and in view of Eq. (3.88) is better defined as the  $k$  value for which

$$K_{k-1}\sigma \leq \sigma_\delta < K_k\sigma \quad (3.97)$$

Sixth, the following analysis is based on the Weibull shape parameter  $\beta$  for fiber strength being 'large', but fortunately the results work quite well for  $\beta$  down to about 4.

Proceeding with the analysis, it is first important to realize that the initial breaks or 'seeds' are actually quite far apart. For example, from Fig. 3.21 we recall that the median composite strength was about  $0.27\sigma_\delta$  for  $\beta = 5$ , and  $F(0.27\sigma_\delta) = 0.0014$ . This means that the average spacing of seeds along a fiber is the inverse of this value times  $\delta$ , or about  $700\delta$ , and laterally in a bundle is about 700 fiber diameters. Moreover this spacing grows larger as the composite volume increases due to the size effect. To see why, we note that the size effect means that the median strength will decrease as the volume increases. As an example, repeat the process used to develop Fig. 3.21 from Fig. 3.20 but for a volume  $MN = 10^9$  instead of  $10^6$ . One can see that the median strength will now be only  $0.22\sigma_\delta$  instead of  $0.27\sigma_\delta$  and since  $F(0.22\sigma_\delta) = 0.00052$ , the average spacing is almost  $2000\delta$ . Note that although the seeds are now farther apart (fewer per unit volume), there are more of them in the composite because the volume grew by a factor of  $10^3$ . (It may come as a surprise to the reader that a small composite will show lots of single breaks per unit volume just before failure, but a large composite will show relatively few!) Thus, as a first approximation we can ignore the possible interactions of two clusters growing near each other since the critical  $k$  will turn out to be quite small.

The probability of a given fiber element becoming a seed *and* its immediate neighbors developing further into a failure string of size  $k$  is approximately

$$P\{\text{seed and string}\} \approx F(\sigma)2F(K_1\sigma)2F(K_2\sigma) \cdots 2F(K_{k-1}\sigma) \quad (3.98)$$

where the factors '2' appear because, at each step of the growth

beyond the seed, there are two choices for the next failure (one on each side) which approximately doubles the probability for that step. Thus, such a string can stretch out variously to the left, or to the right, or be centered relative to the original break. Clearly Eq. (3.98) ignores considerable detail about the events of cluster growth, as discussed more fully in Phoenix and Smith (1983), but it works mainly because  $F(K_j\sigma) \gg F(K_{j-1}\sigma)$  when  $\beta$  is large. (The nature of the simplification can be appreciated upon studying Eqs. (3.89) and (3.90) for small bundles where in each case the first term will dominate all the others when  $\beta$  is large.) Using a Taylor series expansion in  $(\sigma/\sigma_\delta)^\beta$  it can be seen that

$$F(\sigma) \approx (\sigma/\sigma_\delta)^\beta \tag{3.99}$$

This is especially true when  $\sigma \ll \sigma_\delta$ , but it turns out that for present purposes we can take this as a good approximation for  $0 \leq \sigma \leq \sigma_\delta$ , particularly in Eq. (3.98). Substituting Eq. (3.99) in Eq. (3.98), we have

$$\begin{aligned} P\{\text{seed and string}\} &\approx 2^{k-1}(\sigma/\sigma_\delta)^\beta (K_1\sigma/\sigma_\delta)^\beta \cdots (K_{k-1}\sigma/\sigma_\delta)^\beta \\ &= 2^{k-1}(K_1K_2 \cdots K_{k-1})^\beta (\sigma/\sigma_\delta)^{k\beta} \end{aligned} \tag{3.100}$$

This factorization and collapse of terms, to yield an exponent of  $k\beta$  instead of  $\beta$ , is an important feature which follows from the use of the Weibull distribution. It is the point at which the effect of micromechanical ‘redundancy’ in the composite emerges as a reduction in variability.

In the composite there are  $MN$  potential seed fibers, each of which may produce a string, and the composite will fail if at least one such event occurs. Treating the  $MN$  seed and string events as statistically independent (which works because of the wide spacing mentioned above), we actually have a weakest-link situation so that the probability of composite failure is

$$\begin{aligned} H_{M,N}(\sigma) &\approx 1 - [1 - P\{\text{seed and string}\}]^{MN} \\ &\approx 1 - [1 - 2^{k-1}(K_1K_2 \cdots K_{k-1})^\beta (\sigma/\sigma_\delta)^{k\beta}]^{MN} \end{aligned} \tag{3.101}$$

From the calculus,  $(1 - a\sigma^b)^n \rightarrow \exp\{-na\sigma^b\}$  as  $n \rightarrow \infty$  so that

$$H_{M,N}(\sigma) \approx 1 - \exp\{-MN2^{k-1}(K_1K_2 \cdots K_{k-1})^\beta (\sigma/\sigma_\delta)^{k\beta}\} \tag{3.102}$$

which is of the Weibull form, though  $k$  depends on the stress  $\sigma$  following Eq. (3.97).

Before discussing several important features of Eq. (3.102), it is useful to develop a connection to the characteristic distribution function  $W(\sigma)$ . For  $k = 1, 2, 3, \dots$ , let

$$\mathbf{F}^{[k]}(\sigma) = 1 - \exp\{-d_k(\sigma/\sigma_\delta)^{k\beta}\} \tag{3.103}$$

where

$$d_k = 2^{k-1}(K_1 K_2 \cdots K_{k-1})^\beta \tag{3.104}$$

Equation (3.103) gives us a family of Weibull distributions with increasing shape parameter  $k\beta$  in  $k$ . Furthermore, following Eq. (3.97) we can partition the important stress range  $0 \leq \sigma \leq \sigma_\delta$  into the segments

$$\sigma_\delta/K_k < \sigma \leq \sigma_\delta/K_{k-1} \quad k = 1, 2, 3, \dots \tag{3.105}$$

and for each  $k$  restrict the corresponding distribution to its appropriate stress range. Then Eq. (3.102) becomes

$$H_{M,N}(\sigma) \approx 1 - [1 - \mathbf{F}^{[k]}(\sigma)]^{MN} \tag{3.106}$$

where  $k$  and  $\sigma$  are chosen to follow Eq. (3.105). An approximation to  $W(\sigma)$  then follows from a comparison of Eqs. (3.96) and (3.106) yielding

$$W(\sigma) \approx \mathbf{F}^{[k]}(\sigma) \tag{3.107}$$

where again  $k$  and  $\sigma$  satisfy Eq. (3.105).

Figure 3.22 shows a plot of  $W(\sigma)$  for  $\beta = 5$  together with the family of Weibull distributions  $\mathbf{F}^{[k]}(\sigma)$  for  $k = 1, 2, 3, \dots$ , where each is extended over the whole stress range  $0 \leq \sigma \leq \sigma_\delta$ . For each stress level  $\sigma$  one of these Weibull distributions comes very close to  $W(\sigma)$ , and indeed it is normally the one whose  $k$  value satisfies Eq. (3.105). Unfortunately, Eq. (3.107) has a jagged appearance when plotted because of small ‘jumps’ occurring as  $k$  changes at the transition stresses of the boundaries of Eq. (3.105). A graphically pleasant ‘repair’ with a smooth appearance is to work with the inner ‘envelope’ of the family of Weibull distributions, that is

$$W(\sigma) \approx \min\{\mathbf{F}^{[1]}(\sigma), \mathbf{F}^{[2]}(\sigma), \mathbf{F}^{[3]}(\sigma), \dots\} \tag{3.108}$$

Figure 3.22 indicates that this approximation works extremely well.

In principle we could develop similar graphs to Fig. 3.22 for the other cases  $\beta = 3, 7, 10, \dots, 50$  in Fig. 3.20. In developing Fig. 3.21 from Fig. 3.20 for a given volume  $V$ , it is quickly seen that one of the Weibull cases, that is one value of  $k$ , would ‘dominate’ for each value of  $\beta$ , which is why each line in Fig. 3.21 is approximately straight. For each plot, the appropriate  $k$  and Weibull shape

parameter  $k\beta$  would be determined through Eq. (3.105) from the relevant stress range in Fig. 3.21, especially near the median. For example, for  $\beta = 10$ , the case  $k = 3$  is appropriate in developing Fig. 3.21, as the *effective* Weibull shape parameter for composite strength is about  $3 \times 10 = 30$  (as determined from the slope of the  $\beta = 10$  line in Fig. 3.21).

It is now possible to determine the appropriate Weibull distribution for each plot in Fig. 3.21. Substituting the appropriate Weibull distribution  $F^{[k]}(\sigma)$  into Eq. (3.106) (which actually returns us to Eq. (3.102)) yields the following Weibull approximation for composite strength:

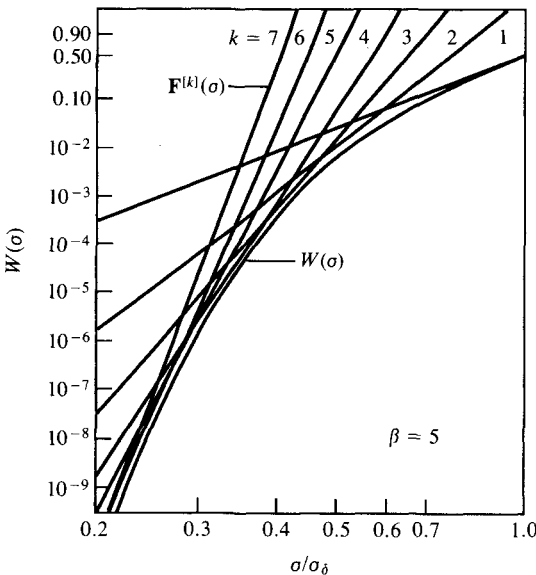
$$H_{M,N}(\sigma) \approx 1 - \exp\{- (\sigma/\sigma_{k,MN})^{k\beta}\} \tag{3.109}$$

where

$$\sigma_{k,MN} = \sigma_\delta (MNd_k)^{-1/(k\beta)} \tag{3.110}$$

For each value of  $\beta$ , this Weibull approximation closely fits the plot on Fig. 3.21, provided  $k$  is chosen by the above graphical scheme.

Fig. 3.22. Envelope construction from Weibull family  $F^{[k]}(\sigma)$  to approximate the characteristic distribution function  $W(\sigma)$  for composite strength. Reprinted with permission from *International Journal of Solids and Structures*, **19**, Phoenix and Smith, Copyright © (1983), Pergamon Press, plc.



Of course  $k$  will change if the volume  $V = MN$  is changed significantly.

At this stage it is important to recall the interpretation of  $k$  as the 'critical crack size'. It is now appreciated that given the composite volume  $MN$  and the Weibull shape parameter  $\beta$  for the fiber strength, a special value of  $k$  emerges which is the size of the longest crack or string of fiber breaks when such a composite fractures. This value of  $k$  also determines the effective Weibull shape parameter for composite strength,  $k\beta$ . Thus far, the calculation of the appropriate  $k$  value has been performed graphically, but it is possible to estimate  $k$  explicitly. The method is given in Phoenix and Smith (1983), and begins by the study of

$$\sigma_\delta / K_k < \sigma_{k,MN} < \sigma_\delta / K_{k-1} \tag{3.111}$$

For large  $MN$ , this leads to the appropriate  $k$  being the value which satisfies

$$\gamma(k) > \ln(MN)/\beta > \gamma(k-1) \tag{3.112}$$

where

$$\gamma(r) = r \ln(K_r) - \{\ln(K_1) + \ln(K_2) + \dots + \ln(K_{r-1})\} \tag{3.113}$$

for  $r = 1, 2, 3, \dots$  and  $\gamma(0) = 0$ . For  $K_j = 1 + j/2$ , we obtain the values given in Table 3.1. According to Eq. (3.112) the critical value of  $k$  depends on the ratio  $\ln(MN)/\beta$ , and thus it increases slowly as the composite volume is increased but decreases more rapidly as the variability in fiber strength is decreased ( $\beta$  is increased).

As an example, for the case  $\beta = 5$  on Fig. 3.21, the graphical procedure puts the stress range near  $0.27\sigma_\delta$  which by Fig. 3.22 or Eq. (3.105) puts  $k = 5$ . On the other hand,  $\ln(10^6)/5 = 2.76$ , and by Eqs. (3.112) and (3.113) and Table 3.1 one also obtains  $k = 5$ . Thus the effective Weibull shape parameter for the composite being represented is  $k\beta = 25$ .

Table 3.1.

$r$	$\gamma(r)$	$r$	$\gamma(r)$
0	0	5	3.15
1	0.405	6	3.95
2	0.981	7	4.78
3	1.65	8	5.62
4	2.38	9	6.48

Finally, it is interesting to consider the ultimate size effect for the composite. In the case of a Weibull distribution, we recall that the strength decreases as the volume  $V$  in proportion to  $V^{-1/\beta}$ . On the other hand, the curvatures of the lines on Figs. 3.20 and 3.21, together with our finding that  $k$  slowly increases as the volume  $V = MN$  increases suggest that the strength of the composite will not ultimately have a Weibull size effect, but one which is increasingly milder as  $V$  increases. Smith (1980, 1982) considered this question and concluded that

$$\text{composite strength} \approx \beta 2^{1-1/\beta} \sigma_\delta / \ln(V) \tag{3.114}$$

which indicates that the strength decreases as the inverse of the log of the volume. It turns out that Eq. (3.114) tends to be an overestimate and a composite must be astronomically huge ( $V > 10^{20}$ ) for this result to be accurate.

In conclusion, a few extensions and limitations of the above analysis should be mentioned. As stated earlier, the results given are based on  $\beta$  being ‘large’. This allowed us to write the approximation Eq. (3.98), which led us to Eq. (3.100) and then to the definition of  $d_k$  in Eq. (3.104). As mentioned earlier, the calculation of the event implied in Eq. (3.98) is more complex if ‘double counting’ of certain failure possibilities is to be avoided. For example, for  $k = 2$ , a more accurate rendition is

$$\begin{aligned} P\{\text{seed and string}\} &\approx 2F(\sigma)[F(K_1\sigma) - F(\sigma)] + F(\sigma)^2 \\ &= 2F(\sigma)F(K_1\sigma) - F(\sigma)^2 \\ &\approx [2(K_1)^\beta - 1](\sigma/\sigma_\delta)^{2\beta} \end{aligned} \tag{3.115}$$

so  $d_2$  should be  $[2(K_1)^\beta - 1]$  rather than just  $2(K_1)^\beta$ . The same sort of analysis shows that  $d_3$  should actually be  $4(K_1K_2)^\beta - (K_1)^{2\beta} - (K_2)^\beta - 2(K_1)^\beta + 1$  and so on for higher  $k$ . But it turns out that these refinements make very little difference, especially when calculating the scale parameter values  $\sigma_{k,MN}$  in Eq. (3.110) where the error is typically one or two per cent.

The above results were developed for the idealized case of local load sharing defined by Eq. (3.88), but appear also to work for more realistic cases provided one chooses  $K_r$  to be the largest load sharing constant at the edge of a failure configuration. Generally such values of  $K_r$  tend to be smaller than  $1 + r/2$  (see, for example, Hedgepeth 1961). Following through the above analysis, the main effects are not only to increase the scale parameters for strength, thus increasing the composite strength itself, but also to increase the

critical  $k$  values thus reducing the composite variability. Second, an analysis has been carried out by Smith *et al.* (1983), for three-dimensional composites, with the parallel fibers forming a two-dimensional hexagonal array. Here the clusters of broken fibers can take on many different geometric configurations other than a linear string, but for large  $\beta$  one still comes up with a form for  $d_k$  that is similar in structure to Eq. (3.104) except that  $2^{k-1}$  is replaced by a much more complex configurational constant. Many of the ideas carry through except that one no longer finds quite the same simple relationship between the critical cluster size  $k$  and the effective Weibull shape parameter for composite strength. The strength of such a three-dimensional composite is typically larger than in the two-dimensional planar case described above. The reason is that while there are many more failure configurations, the load sharing occurs over many more fibers at the boundary of a failure cluster so that the reduction in the  $K_r$  values more than compensates for the increased number of failure possibilities, especially for larger  $\beta$ .

Finally, experimental data to illustrate the above features have been presented by Phoenix, Schwartz and Robinson (1988), who also extend the ideas, through viscoelasticity of the matrix, to explain creep rupture phenomena under constant stress.

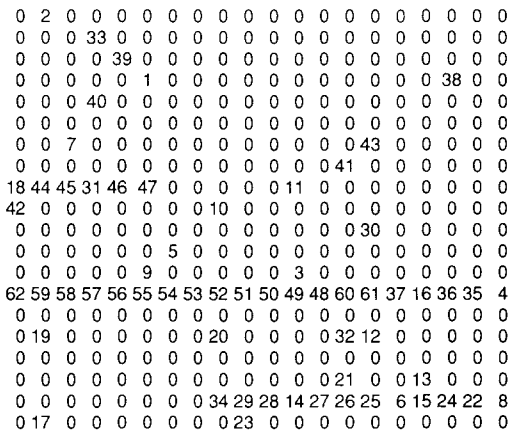
### 3.4.6.3 *Monte-Carlo simulation*

The Monte-Carlo method is a numerical technique suitable for simulating complicated stochastic processes, and it has been employed to analyze a wide range of physical processes of a statistical nature (Oh 1979). The Monte-Carlo simulation of composite strength can be regarded as testing the composite materials 'analytically' in an automated fashion. In each Monte-Carlo experiment, random numbers are generated and assigned to the underlying random variables and the outcome of the process of interest can be observed. When the number of such independent experiments is sufficiently high, the observations will yield a good assessment of the statistical characteristics of the process. In dealing with the strength of fibers as well as composites, the Monte-Carlo experiment involves the partitioning of fiber or a composite into elements, then random numbers are assigned to the strength of the elements. For a given applied load, the stress in the elements of a fiber or a composite can be determined as described in Section 3.3. From the assigned strength value and the arrangement of breaks of elements the failure load is then obtained. In the following, fractures of fibers as well as composites based upon the Monte-Carlo simulation

(Fukuda and Kawata 1977; Oh 1979; Manders, Bader and Chou 1982) are considered. Several common procedures for generating the normal random numbers are available.

Fukuda and Kawata studied the fracture of a two-dimensional fiber composite based upon the Monte-Carlo method by choosing a mean strength of 100 and a standard deviation of 10. A simulation of the fracture process is shown in Fig. 3.23 for  $E_t/E_m = 20$ , and  $M = N = 20$ , where  $M$  and  $N$  are defined in Fig. 3.17. The elements or links in the partitioned composite specimen are specified by the position  $(i, j)$ . Here, 0 indicates that the link is not broken and the other numerals indicate the sequence of link breakage. As the initial condition, each link  $(i, j)$  is assumed to have a stochastic strength,  $STR(i, j)$ , which is the normal random number with a specific value of mean and standard deviation. Both the Weibull distribution and normal distribution have been used for expressing the link strength distributions. Stress concentration factors of all links,  $SCF(i, j)$ , are initially assigned as 1. A link with the least value of  $STR(i, j)/SCF(i, j)$  is sought, and let this link be  $(i_o, j_o)$ . The link breaks first at the tensile stress of  $STR(i_o, j_o)$ . When this link breaks, stress concentration occurs in the two adjacent links  $(i_o, j_o \pm 1)$ . The values of  $STR(i, j)/SCF(i, j)$  are again calculated for the remaining  $M \times N - 1$  links. A link which has the least of this value breaks second. This procedure is repeated until all the links in a plane transverse to the loading direction ( $j = 1, 2, \dots, M$ ) are broken.

Fig. 3.23. Monte-Carlo simulation of fiber link fractures. (After Fukuda and Kawata 1977.)



The result given in Fig. 3.17 resembles the sequence of fiber failure observed in the experimental work of Rosen (1964). The predictions of composite strength are shown in Fig. 3.24. It should be noted that the Monte-Carlo approaches are generally limited to  $MN < 50\,000$  under current supercomputer power which may not be enough for a realistic composite. Also the Monte-Carlo approach is inherently poor at handling the lower tails of the distributions.

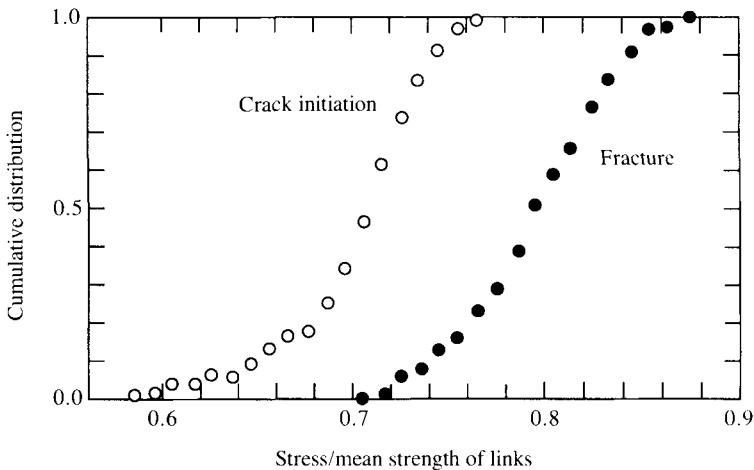
### 3.4.7 *Strength of cross-ply composites*

Cross-ply construction is the simplest form of lamination of unidirectional laminae. This simple geometric configuration facilitates the understanding of the fundamental problems concerning laminate strength. It provides a model system for investigating the matrix cracking of laminates under tensile loading. This section analyzes the problem from both deterministic and statistical viewpoints. The treatment of Aveston, Cooper and Kelly (1971) of multiple fracture, although it deals with unidirectional composites, is basic to matrix cracking of laminated composites in general. Hence, it is outlined first.

#### 3.4.7.1 *Energy absorption during multiple fracture*

Section 3.2 discusses the mode of fracture of unidirectional composites as affected by the ultimate failure strains of the fiber and

Fig. 3.24. Numerical results of Monte-Carlo simulation. (After Fukuda and Kawata 1976b.)



matrix materials as well as the fiber volume fraction. The energy absorption of composites during the failure process was first investigated by Aveston, Cooper and Kelly (1971). Contributions to the fracture surface energy during single fracture may be derived from deformation of the fiber or matrix, the work done in fracturing the fiber–matrix interfacial bond, and work done in pulling the fibers out of the matrix against frictional forces. It is found that the work of fracture increases with increasing fiber diameter and decreasing fiber–matrix interfacial strength.

Multiple fracture of fibers occurs in ductile matrix composites at low fiber volume fraction. Multiple fracture of matrix, on the other hand, takes place in brittle matrix composites at high fiber volume fraction, as a result of applied tensile loads or thermal stresses induced by cooling from the stress-free temperature. The energy consideration for the development of multiple matrix cracking in a unidirectional lamina subject to axial tensile loading is introduced below (see Aveston, Copper and Kelly 1971; Aveston and Kelly 1973, 1980; Kelly 1976).

Consider the formation of a single matrix crack normal to the fiber direction, at the strain  $\varepsilon_{mu}$  under conditions of fixed load. It is assumed that the stress in the matrix is equal to the matrix fracture stress and there is a decrease in the combined energy of the specimen and the loading system. The energy changes due to the formation of a crack at a fixed load include  $\Delta W$  = the work done by the applied load per unit area of the composite,  $\gamma_{db}$  = energy absorbed per unit area of debonded fiber,  $U_s$  = the work done per unit area of the composite against the frictional force between the fiber and matrix,  $\Delta U_m$  = the elastic strain energy lost due to the relaxation of the strain in the matrix, and  $\Delta U_f$  = the increase in strain-energy of the fibers per unit area of the composite. If the surface energy in forming a matrix crack is  $\gamma_m$ , a crack will occur provided

$$2\gamma_m(1 - V_f) + \gamma_{db} + U_s + \Delta U_f \leq \Delta W + \Delta U_m \quad (3.116)$$

The terms in Eq. (3.116) have been evaluated by Aveston, Cooper and Kelly under the assumption that the changes in stress (strain) in the matrix and fiber due to the formation of the crack vary linearly with distance from the crack surface. By further assuming purely frictional bond between the fiber and matrix, Eq. (3.116) yields the

following expression for the failure strain of the matrix:

$$\epsilon_{\text{mu}} = \left\{ \frac{12\tau\gamma_m E_f V_f^2}{E_c E_m^2 r(1 - V_f)} \right\}^{1/3} \quad (3.117)$$

where  $\tau$  = fiber–matrix interfacial shear strength (See Eq. (3.2)),  $r$  = fiber radius, and  $E$  = Young’s modulus with the subscripts f, m and c indicating fiber, matrix and composite, respectively. Equation (3.117) indicates that the composite strain at the formation of the transverse matrix crack can be enhanced by suitable control of the elastic moduli of the fiber and matrix, fiber volume fraction and diameter, matrix surface energy, and the fiber–matrix interfacial strength.

Budiansky, Hutchinson and Evans (1986) have generalized the results of Aveston, Cooper and Kelly for unbonded, frictionally constrained slipping fibers initially held in the matrix by thermal or other strain mismatches. The other case considered by Budiansky *et al.* for the onset of matrix cracking involves fibers that initially are weakly bonded to the matrix, but may be debonded by the stresses near the tip of an advancing matrix crack. McCartney (1987) has used an energy-balance calculation for a continuum model of brittle matrix cracking in a uniaxially fiber-reinforced composite and confirmed that the Griffith fracture criterion is valid for matrix cracking.

### 3.4.7.2 *Transverse cracking of cross-ply laminates*

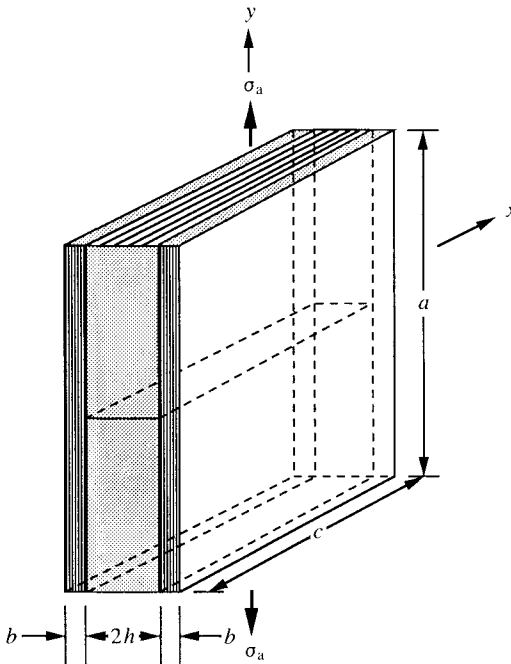
Multiple transverse cracks in the matrix of unidirectional fiber composites have been observed in a number of systems, for example, glass-reinforced cement, and gypsum reinforced with polyvinyl chloride or glass, where the failure strains of the fibers are greater than those of the matrices. Transverse cracking also occurs in the 90° plies of cross-ply laminates. Experimental observations and analytical modeling of this behavior have been made by Bailey, Garrett, Parvizi, Bader and Curtis (see Garrett and Bailey 1977a&b; Parvizi and Bailey 1978; Parvizi, Garrett and Bailey 1978; Bader, Bailey, Curtis and Parvizi 1979; Bailey, Curtis and Parvizi 1979; Parvizi 1979; Bailey and Parvizi 1981 who followed Aveston and Kelly’s shear-lag approach and interpreted this phenomenon by the concept of constrained cracking). Manders, Chou, Jones and Rock (1983) proposed a statistical treatment of multiple cracks. Wang, Crossman, Warren and Law (see Wang and Crossman 1980; Crossman, Warren, Wang and Law 1980; Crossman and Wang 1982; Wang 1984), on the other hand, theorized it based

based upon the strain-energy release rate of crack extension. The theory of Bailey *et al.* is introduced in this section. The work of Manders *et al.* is discussed in Section 3.4.7.3 and that of Wang *et al.* is introduced in Section 3.4.7.4.

(A) Cross-ply laminate

The cross-ply construction of  $[0^\circ/90^\circ/0^\circ]$  is shown in Fig. 3.25. For the cases of glass/epoxy and carbon/epoxy systems, the mechanical properties of unidirectional laminates are shown in Table 3.2. The glass/epoxy  $0^\circ$  test curves are essentially linearly elastic to fracture but the  $90^\circ$  specimens show a pronounced *knee* at a strain of about 0.3%, after which a whitening effect can be observed. The  $0^\circ$  carbon/epoxy test curves are elastic to failure but they are not linear, there being an increase in the modulus with increasing strain. The  $90^\circ$  carbon/epoxy is linear to failure with no knee or acoustic emission prior to failure. The failure strains of the  $90^\circ$  specimens in both systems are characteristically low due to strain concentrations in the matrix (see Kies 1962).

Fig. 3.25. Illustration of a  $[0^\circ/90^\circ/0^\circ]$  specimen.



When extended in tension, initial failure of the cross-ply laminate is usually in the central  $90^\circ$  ply, which cracks in a direction normal to the applied tension and parallel to the fibers in that layer (Fig. 3.26). The failure sequence in both laminates follows a similar pattern. Two knees appear on the stress-strain curve of glass/epoxy, first at 0.3% strain, associated with the visual whitening effect and at 0.5% strain due to transverse cracking, but this is not apparent in the carbon/epoxy laminate. On further extension, more cracks are formed until the whole gauge portion of the test-piece is filled with a regular array of cracks. The strain at which the first crack occurs increases as the thickness ( $2h$ ) of the  $90^\circ$  layer is reduced and at the same time the crack spacing tends to become smaller. In the case of the thinnest transverse layers, transverse cracking is not observed at all before the final catastrophic failure of the test-piece. Microscopy has shown that the earliest indications of failure are debonds at or near the fiber/matrix interface. These occur at strains even lower than those at which the whitening is observed in the glass/epoxy systems. The next stage is a coalescence of a number of debonds to form a microcrack, which grows rapidly when it reaches a critical size, about three to four fiber diameters.

Longitudinal splitting is observed to occur in the  $0^\circ$  plies of the cross-ply laminate at strains intermediate between the transverse

Table 3.2. *Mechanical properties of unidirectional laminates (after Bader et al. 1979), Reprinted with permission from Mechanical Behaviour of Materials-Copyright © 1979, Pergamon Press, plc.).*

Property	$0^\circ$ CFRP*	$0^\circ$ GRP**	$90^\circ$ CFRP	$90^\circ$ GRP	Units
Low-strain Young's modulus	127	42	8.3	14	GPA
Fracture stress	1.7	0.92	0.039	0.056	GPa
Fracture strain	1.2	2.2	0.48	0.50	%
Poisson's ratio	0.29	0.27	0.02	0.09	-

\* CFRP: carbon fiber-reinforced plastic

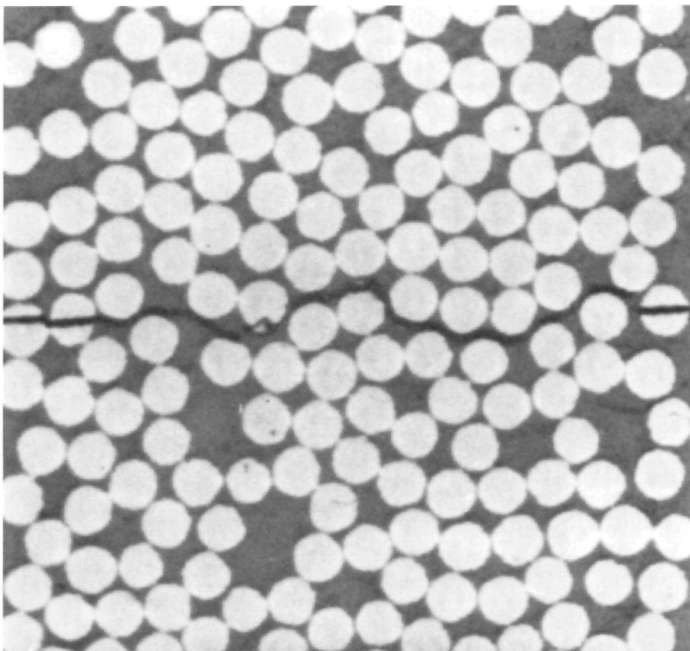
\*\*GRP: glass fiber-reinforced plastic

cracking strain for the  $90^\circ$  plies and final failure (Fig. 3.27). Longitudinal splitting is due to mismatches in the Poisson's ratios and the coefficients of thermal expansion of the  $0^\circ$  and  $90^\circ$  plies. The strain to initiate splitting increases as the thickness of the longitudinal plies is reduced. Splitting has not been observed in the carbon/epoxy cross-ply laminates.

(B) Transverse crack spacing

The low strain failure behavior was first explained by Kies (1962), who predicts the magnification of strain in the matrix when a unidirectional composite is stressed in the transverse direction. In the limit when the fibers are almost touching one another, the strain magnification factor approaches the value  $E_f/E_m$ . It should be noted that even at comparatively low fiber volume fractions there are invariably regions in the lamina where fibers almost touch one another. The glass fibers are nearly

Fig. 3.26. Transverse-ply crack in a  $[0^\circ/90^\circ/0^\circ]$  carbon fiber-reinforced cross-ply laminate with an inner-ply thickness of  $2h = 0.125$  mm. (After Bailey, Curtis and Parvizi 1979.)



isotropic, but the transverse Young's modulus of carbon is much lower than its longitudinal modulus and it is this modulus which should be used for calculating the strain magnification factor. The first matrix crack usually forms between fibers which are touching or nearly touching along a direction perpendicular to the loading axis.

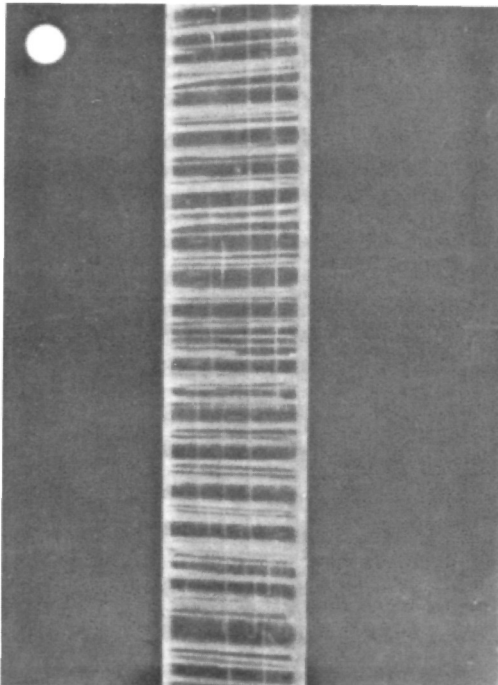
The crack density, and hence the crack spacing, is related to the geometry of the laminate. These can be explained by the cross-ply laminate shown in Fig. 3.25. When the strain has reached the fracture strain,  $\epsilon_{tu}$ , of the  $90^\circ$  ply, the first crack occurs in the transverse ply, and an additional stress  $\Delta\sigma$  is placed on the longitudinal plies. From a shear-lag analysis similar to that given in Section 3.3.1,

$$\Delta\sigma = \Delta\sigma_0 \exp(-\sqrt{(\phi)y}) \quad (3.118)$$

where

$$\phi = \frac{E_c G_{12}}{E_{11} E_{22}} \left( \frac{b+h}{bh^2} \right)$$

Fig. 3.27. Longitudinal-ply splitting in a  $[0^\circ/90^\circ/0^\circ]$  glass fiber-reinforced cross-ply specimen. (After Bailey, Curtis and Parvizi 1979.)



$E_c$  is the laminate Young's modulus in the  $y$  direction,  $E_{11}$  and  $E_{22}$  are the Young's moduli of a unidirectional ply in the fiber and transverse directions, respectively, and  $G_{12}$  is the shear modulus of a unidirectional ply. This additional stress has its maximum value  $\Delta\sigma_o$  in the plane of the crack ( $y = 0$ ) and decays with distance  $y$  from the crack plane as some load is transferred back into the transverse ply through interlaminar shear stress

$$\tau_i = -b \frac{d\Delta\sigma}{dy} \tag{3.119}$$

The tensile load in the transverse ply is zero at the crack plane but builds up by shear transfer from the longitudinal plies. At a given distance  $y$  from the crack, the load  $F$  in the inner ply is given by

$$F = \int_0^y 2c\tau_1 dy \tag{3.120a}$$

where  $c$  is defined in Fig. 3.25. The first crack in the transverse ply occurs when the load carried by it is equal to  $2ch\sigma_{tu}$  where  $\sigma_{tu}$  denotes the ultimate tensile strength of the  $90^\circ$  ply in the cross-ply laminate, which may be different from the transverse tensile strength of a unidirectional ply. This load is then transferred onto the longitudinal plies. Another crack can only occur when the transverse ply is again loaded to  $2ch\sigma_{tu}$ . The transverse ply will not be loaded to this value except at infinity and  $\Delta\sigma_o = \sigma_{tu}h/b$ , if the applied stress on the laminate is maintained at  $\sigma_a = E_c\varepsilon_{tu}$  after the first cracking. For another crack to occur,  $\sigma_a$  and hence  $\Delta\sigma_o$  must be increased to such a value that  $F = 2ch\sigma_{tu}$ .

If the first crack is assumed to take place in the middle of the specimen ( $y = 0$ ) of length  $a$ , the following cracking sequence will occur:

- (1) Initial crack at  $\sigma_a = E_c\varepsilon_{tu}$ , and

$$F = 2bc \Delta\sigma_o [1 - \exp(-\sqrt{(\phi)y})] \tag{3.120b}$$

- (2) Second and third cracks occur simultaneously at the ends of the specimen when the applied load increases to such a value that

$$\Delta\sigma_o = \sigma_{tu} \frac{h}{b} [1 - \exp(-\sqrt{(\phi)a/2})]^{-1} \tag{3.121}$$

The crack spacing is  $a/2$ .

- (3) The next series of cracks will occur midway between the present cracks. The total shear stress between two existing cracks is

$$\tau_i = b \Delta\sigma_o \sqrt{(\phi)} \{ \exp(-\sqrt{(\phi)}y) - \exp[\sqrt{(\phi)}(y - a/2)] \} \quad (3.122)$$

and from Eq. (3.120a)

$$F = 2bc \Delta\sigma_o [1 + \exp(-\sqrt{(\phi)}a/2) - 2 \exp(-\sqrt{(\phi)}a/4)] \quad (3.123)$$

The value of  $\Delta\sigma_o$  when the cracks occur now at intervals of  $a/4$  is

$$\Delta\sigma_o = \sigma_{tw} \frac{h}{b} [1 + \exp(-\sqrt{(\phi)}a/2) - 2 \exp(-\sqrt{(\phi)}a/4)]^{-1} \quad (3.124)$$

- (4) For crack spacing of  $a/8$

$$\Delta\sigma_o = \sigma_{tw} \frac{h}{b} [1 + \exp(-\sqrt{(\phi)}a/4) - 2 \exp(-\sqrt{(\phi)}a/8)]^{-1} \quad (3.125)$$

This crack sequence will continue until the strength of the longitudinal plies is exceeded or the spacing between neighboring cracks is so small that the normal stress in the  $90^\circ$  ply cannot be built up to  $\sigma_{tw}$ .

### (C) Transverse cracking constraint

The strain required to initiate transverse cracks is greater when the transverse lamina is thinner, and in some cases cracking is constrained completely up to the strain at which the longitudinal laminae fail catastrophically. This phenomenon of constrained cracking is attributed to the fact that in order for a crack to form it must be both mechanistically possible and energetically favorable. The former requirement is satisfied for cross-ply laminates from the viewpoint of strain magnification as discussed in (B). The effect of lamina thickness on the transverse failure strain can be understood from the viewpoint of energetics.

For a specimen under constant load, a crack initiates if the following condition is satisfied:

$$\Delta W > \Delta U + U_D + 2\gamma A \quad (3.126)$$

where  $\Delta W$  is the work done by the applied stress per unit area of the specimen,  $\Delta U$  is the increase in stored energy per unit area of the specimen,  $U_D$  is the energy loss per unit area due to any dissipative processes present (e.g. sliding friction between debonded fiber and matrix),  $\gamma$  is the fracture surface energy per unit fracture surface area, and  $A$  denotes the fracture surface area. It has been found that for practical ply thicknesses the interface between the longitudinal and transverse plies remains bonded during the cracking of the transverse ply and the laminate behaves in a fully elastic manner, thus Eq. (3.126) becomes

$$\Delta W > \Delta U + 2 \frac{h}{h+b} \gamma_t \tag{3.127}$$

Here,  $\gamma_t$  is the fracture surface energy of the transverse ply in a direction parallel to the fibers. Since half of the work done by the applied stress is stored as elastic energy of the specimen, it follows that

$$\frac{1}{2} \Delta W > 2\gamma_t \frac{h}{h+b} \tag{3.128}$$

When the first crack occurs in the transverse ply at a strain of  $\epsilon_{tu}$  an additional stress  $\Delta\sigma$ , Eq. (3.118), is thrown onto the outer plies and the laminate increases in length by  $\delta a$ , given by

$$\delta a = 2 \int_0^{a/2} \frac{\Delta\sigma}{E_{11}} dy \tag{3.129}$$

For  $a/h \gg 1$ , Eq. (3.129) becomes

$$\delta a = \frac{2hE_{22}\epsilon_{tu}}{bE_{11}\sqrt{(\phi)}} \tag{3.130}$$

The work done by the applied stress  $\sigma_a$  at the strain of first transverse failure is

$$\Delta W = \delta a \sigma_a \tag{3.131}$$

Hence

$$\Delta W = \frac{2hE_cE_{22}\epsilon_{tu}^2}{bE_{11}\sqrt{(\phi)}} \tag{3.132}$$

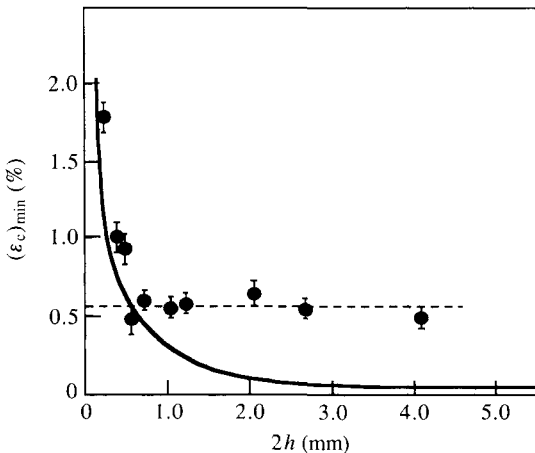
The substitution of Eq. (3.132) into Eq. (3.128) yields the minimum value of the transverse failure strain

$$(\epsilon_{tu})_{\min} = (\epsilon_c)_{\min} = \sqrt{\left[ \frac{2bE_{11}\gamma_t\sqrt{(\phi)}}{(h+b)E_{22}E_c} \right]} \tag{3.133}$$

The theoretical values of the minimum cracking strain have been calculated from Eq. (3.133) as a function of  $h$  and are compared with the experimental results in Fig. 3.28 for glass/epoxy laminates. Close agreement is observed between theory and experiment in the region where  $h < 0.25$  mm, indicating an energy controlled crack propagation. For the thicker laminates, however, this theory does not apply and cracking occurs at a constant strain of 0.5% which is close to the cracking strain of the unidirectional  $90^\circ$  lamina.

According to Bader *et al.* (1979), microscopic cracks usually develop in glass- and carbon-reinforced plastic laminates in regions where fibers lie normal to the principal tension axis, at strains which are, at the most, only 30% of the final failure strain. Thus designers are faced with a dilemma: whether to base the design on strains below the cracking threshold (typically 0.5% for glass-reinforced plastics) or the ultimate failure strain, which might be 1.5% or more. Microcracks which do not appear to be detrimental to the short-term mechanical properties of laminates may act as nuclei for further local damage leading to ultimate failure under cyclic loading and a hostile environment. Experimental evidence suggests that the formation of transverse cracks and longitudinal splitting can be constrained or inhibited by constructing the laminate from thinner individual plies.

Fig. 3.28. Plot of the theoretical and experimental transverse cracking strain,  $(\epsilon_c)_{\min}$ , as a function of the inner-ply thickness,  $2h$ , for glass-reinforced sandwich laminates. The outer ply thickness is 0.5 mm. — Eq. (3.133); --- cracking strain of the unidirectional  $90^\circ$  lamina;  $\bullet$  experiment. Reprinted with permission from Bader *et al.* in *Mechanical Behaviour of Materials*, Copyright © (1979), Pergamon Press plc.

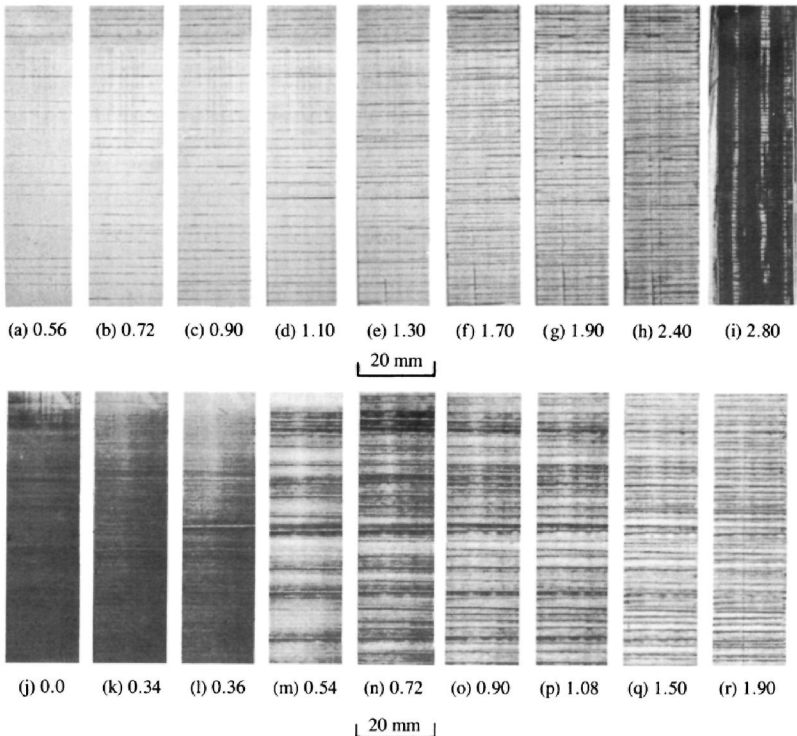


3.4.7.3 Statistical analysis

The deterministic multiple cracking theory of Garrett, Bailey and Parvizi attempts to account for the measured distribution of crack spacing in  $[0^\circ/90^\circ/0^\circ]$  glass fiber/resin matrix laminates. Manders *et al.* (1983) have proposed a statistical model which fits the experimental data and predicts a dependence of strength on size. The origins and implications of this variability of strength are discussed below after descriptions of the experimental observations.

The three-ply  $[0^\circ/90^\circ/0^\circ]$  laminates of Manders *et al.* are composed of Silenka E-glass fibers in an Epikote epoxy resin. The central  $90^\circ$  ply is 1.1 mm thick and is sandwiched between two 0.55 mm plies. A close match between the refractive indices of the fiber and matrix makes the laminate virtually transparent so that cracking and microscopic damage in the  $90^\circ$  can be closely observed (Fig. 3.29).

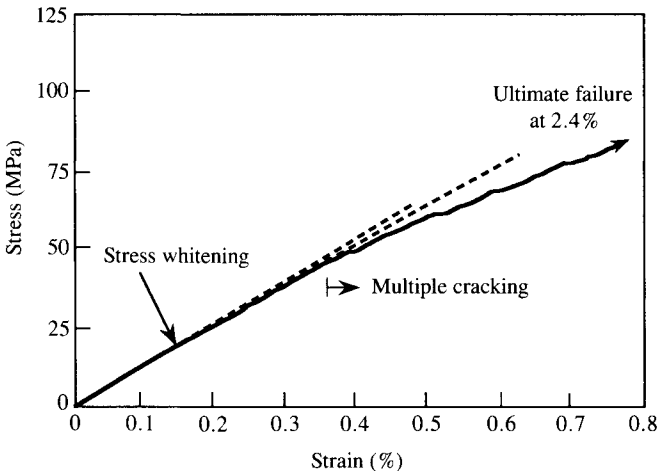
Fig. 3.29. Photographs of specimens at the indicated strain levels (%) under bright-field ((a) to (i)) and dark-field ((j) to (r)) illumination, showing multiple transverse cracks in the  $90^\circ$  ply, stress 'whitening' and longitudinal splitting in the  $0^\circ$  plies. (After Manders *et al.* 1983.)



The pattern of cracks is photographed at regular intervals of applied load using either bright- or dark-field illumination. The dark-field illumination shows fiber–matrix debonding (‘stress whitening’ which scatters light) with good contrast, whereas bright-field illumination gives better definition of the cracks, although in this case the fiber–matrix debonding appears dark with relatively poor contrast. The thermal residual tensile strain of the 90° ply is estimated to be about 0.22% due to cooling from the postcure temperature of 150° to ambient.

As the specimens are loaded the initial whitening progressively increases, most noticeably at about 0.34% strain (Fig. 3.29k). A knee is visible in the stress–strain curve of Fig. 3.30 at about 0.1% which is attributed to the onset of fiber–matrix debonding. Cracks appear instantaneously at about 0.4% strain, often in the bands of more pronounced whitening (Fig. 3.29l and m). It is concluded from this observation that a crack forms by the joining up of the fiber–matrix debonds. The beginning of multiple cracking is reflected on the stress–strain curve by a second knee. The rate of crack formation with applied strain decreases throughout the loading. At higher strains the crack spacing becomes more uniform. At a strain of about 0.7% stress whitening appears in the longitudinal 0° ply (Fig. 3.29n–r); this is seen as darkening in Figs.

Fig. 3.30. Low-strain portion of a stress–strain curve. Changes of gradient are associated with a rapid increase in stress whitening and with the beginning of multiple cracking. (After Manders *et al.* 1983.)



3.29(b)–(i), and it develops into longitudinal cracks at about 1.8% strain.

Manders *et al.* have measured the positions of every crack in a photograph by traveling microscope and calculated the spacings between cracks and their cumulative distribution functions for each load. These distributions illustrate the overall trend towards closer spacing at higher strains. In their study of the variation of crack spacing with stress, Manders *et al.* assume that the 90° ply is an ideal homogeneous brittle material with an inherent distribution of strength which is described by a cumulative distribution function termed  $S_0$  for failure of a unit volume. It is also expected that the strength of the 90° ply will be statistically the same throughout its volume; i.e. the constituent volumes which are substantially larger than the microstructure should have strengths which are independent of each other and which are identically distributed.

Thus, the cumulative distribution function of strength  $S_V$  for a volume  $V$  can be written as

$$1 - S_V = (1 - S_0)^V \tag{3.134}$$

Then the ‘risk of rupture’,  $R_V$ , proposed by Weibull (1939a and b) is given by

$$\ln(1 - S_V) = V \ln(1 - S_0) = -R_V \tag{3.135}$$

Let

$$\ln(1 - S_0) = -\phi(\sigma) \tag{3.136}$$

then the risk of rupture  $dR$  for a volume element  $dV$  is

$$dR = -\ln(1 - S_0) dV = \phi(\sigma) dV \tag{3.137}$$

For a non-uniform state of stress

$$R_V = \int_V \phi(\sigma) dV \tag{3.138}$$

and

$$S_V = 1 - \exp(-R_V) = 1 - \exp\left[-\int_V \phi(\sigma) dV\right] \tag{3.139}$$

Assuming that the stress is uniform in the cross-sectional area,  $A$ , the volume integral may be replaced by an integration over the length  $L$ . Then Eq. (3.135) becomes

$$\ln(1 - S_V) \cong -A\phi(\sigma)L \tag{3.140}$$

The quantity  $A\phi$  is found from the gradient when  $\ln(1 - S_V)$  is plotted against  $L$ .

Manders *et al.* adopted a two-parameter Weibull distribution for the strength of the 90° ply in which

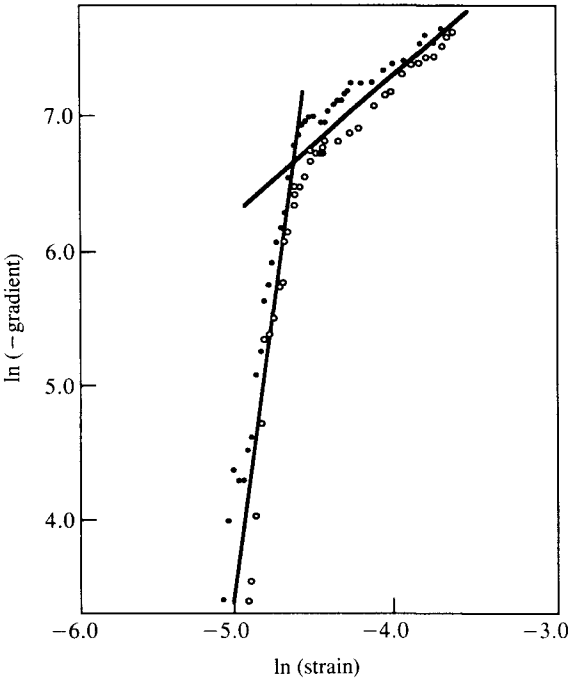
$$A\phi = A\left(\frac{\sigma}{\sigma_o}\right)^\beta = A\left(\frac{\varepsilon}{\varepsilon_o}\right)^\beta \tag{3.141}$$

The constants  $\sigma_o$  and  $\varepsilon_o$  are the scale parameters in terms of stress and strain, respectively, and  $\beta$  is the shape parameter. Taking logarithms of Eq. (3.141) gives

$$\ln(A\phi) = \beta \ln \varepsilon - \beta \ln \varepsilon_o + \ln A \tag{3.142}$$

It is seen from Eq. (3.142) that a graph of the gradients obtained from  $\ln(1 - S_V)$  vs.  $L$  and applied strain is linear with gradient  $\beta$  if the Weibull distribution is valid. This is demonstrated in Fig. 3.31, which shows two linear regions intersecting at a strain of about 0.4% (corrected for thermal residual strain), or 0.6% of applied strain. The values of  $\beta$  are about 8.5 and 1.0, respectively, for low

Fig. 3.31. Variation of gradients with 90° ply strain, corrected for residual thermal strain. Solid and open circles correspond to two nominally identical specimens. (After Manders *et al.* 1983.)

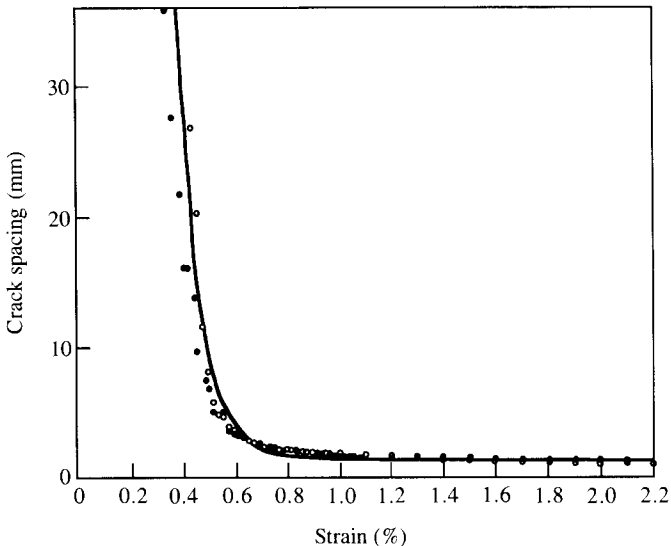


strain and high strain. The two intercepts ( $\ln A - \beta \ln \varepsilon_0$ ) for the two linear segments are 47 and 11.

Finally, Eq. (3.140) can be evaluated after substitution of Eq. (3.142) using the fitted values of  $\beta = 8.5$  and intercept = 47 to obtain median crack spacings ( $S_V = 0.5$ ) as a function of strain. The results of the theoretical correlations are shown by the solid curve in Fig. 3.32.

It is suggested by Manders *et al.* that the deterministic model of Garrett, Bailey and Parvizi and the probabilistic models are complementary. At low strains, the crack spacing is large and the length necessary to build up stress in the  $90^\circ$  ply on either side of a crack is relatively small. Therefore, most of the region between cracks is fairly uniformly stressed and the positions of new cracks are determined by the distribution of flaws in the matrix; a new crack rarely forms exactly midway between two existing cracks. Consequently, the distribution of crack spacings covers a wider range than the factor of two predicted by Garrett, Bailey and Parvizi. At high strains the opposite is true. The region between cracks is non-uniformly stressed. Since the highest stress is found midway between two existing cracks, this is where the new crack forms as described by the deterministic model. When the crack

Fig. 3.32. Crack spacing vs. strain. Solid curve is based upon the statistical model predictions. (After Manders *et al.* 1983.)



spacing is significantly higher than the 'unstressed length' (approximately equal to the 90° ply thickness) the probabilistic model is appropriate, and when it is of similar magnitude the deterministic model is more appropriate.

Further analytical treatments of the statistical strength of cross-ply laminates can be found in the work of Fukunaga, Peters, Schulte and Chou (1984) and Peters and Chou (1987).

#### 3.4.7.4 *Transverse cracking and Monte-Carlo simulation*

The occurrence of transverse cracks in cross-ply laminates under ascending tension can be regarded as a kind of stochastic process due to the presence of randomly distributed microflaws. As discussed in Section 3.4.6.3, a stochastic process can be simulated by the Monte-Carlo procedure. In this case, it is postulated that 'intralaminar flaws' exist randomly in the unidirectional ply, which lie in the ply thickness direction and align with the fibers, Fig. 3.33(a). When the transverse ply in the cross-ply laminate is subjected to tension, these flaws effect the observed transverse cracking. For purpose of simulation, the identity of the intralaminar flaws is represented by randomly generated 'effective flaws'. The effective flaws are not, of course, the real flaws. However, if chosen properly, they represent an inherent property of the ply system and effect the essential characteristics of the transverse cracking process in the simulation model.

Wang and Crossman (1980) first conducted an energy analysis to predict the onset of a single transverse crack based on the classical fracture mechanics concept, in conjunction with the effective flaw postulation. Their analysis was validated by a series of experiments (see Crossman, Warren, Wang and Law 1980; Crossman and Wang 1982). Later, Wang, Chou and Lei (1984) and Wang (1984, 1987) incorporated the energy method into a Monte-Carlo procedure to simulate the stochastic nature of multiple cracking. In this section, the work of Wang *et al.* is discussed in some detail.

#### (A) Ply-elasticity and three-dimensional stress states

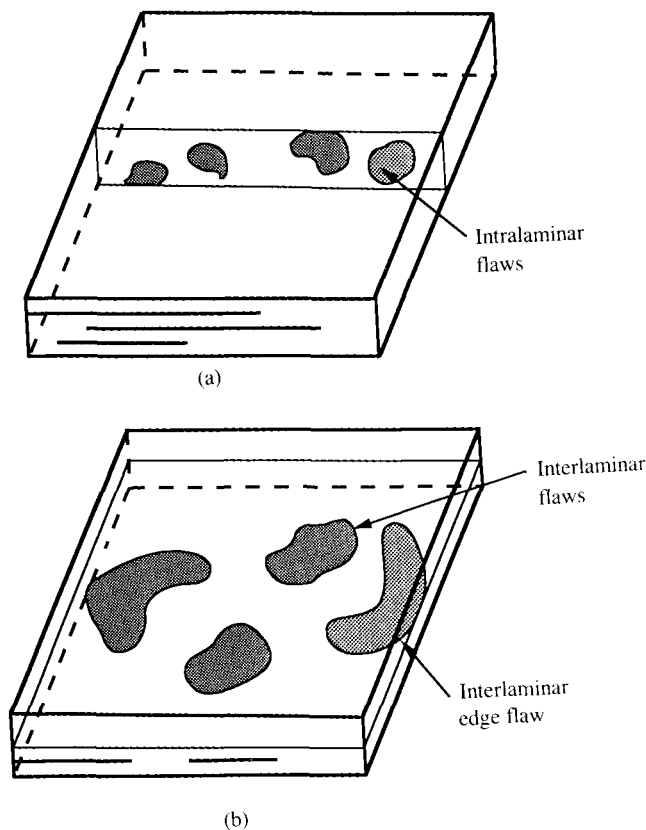
At the outset, it is useful to describe briefly the basis of the energy method. The method is simply derived within the confines of ply elasticity and the classical theory of fracture mechanics. The theory of ply elasticity regards each unidirectional ply as a three-dimensional, elastic, homogeneous and anisotropic solid; and the laminate is modeled as a three-dimensional layered medium containing flaws. An individual effective flaw is handled as a small

crack; hence the elastic stress field surrounding the flaw is almost always three-dimensional. Under certain simplifying assumptions, however, some three-dimensional fields may be reduced to generalized plane-strain fields. Even then, numerical techniques are usually required for solutions (see Pipes and Pagano 1970; Wang and Crossman 1977).

(B) Effective flaw distribution

The exact mechanism of transverse cracking is rather complicated when viewed at the fiber–matrix scale. It is usually postulated that the crack is caused initially by the coalescence of material microflaws which lie aligned with the fibers in the transverse ply. When viewed at the ply scale, however, a transverse

Fig. 3.33. Schematic view of (a) effective intralaminar flaws, and (b) effective interlaminar flaws. (After Wang 1987.)



crack represents a separation of the transverse ply along the fiber–matrix interface (see Fig. 3.29). To facilitate a mathematical description of the event at the ply level, the concept of effective flaws is now introduced. Assume that in each unidirectional ply there exists a characteristic probability density distribution of effective flaw sizes as shown in Fig. 3.34. The linear size of the flaws is denoted by  $2a$  and the location by  $x$ . Then, the discrete random variables  $\{a_i, i = 1, 2, \dots, M\}$  and  $\{x_i, i = 1, 2, \dots, M\}$  characterize the size and the location distributions of the flaws. When two or more plies are grouped together, such as in the  $[0^\circ/90^\circ_n/0^\circ]$  laminate (with  $n > 1$ ), the flaw size distribution in the grouped  $90^\circ$  plies is represented by the volumetric rule (see Lei 1986):

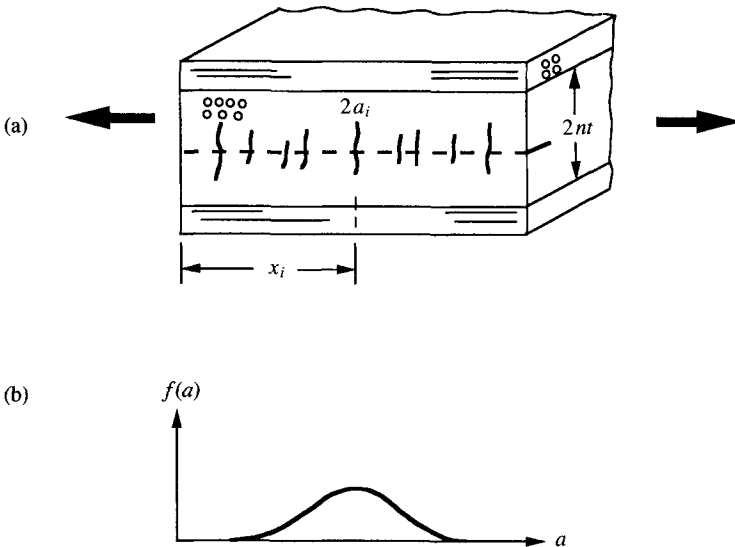
$$a_{i,n} = a_i(n)^{2/\lambda} \tag{3.143}$$

where  $i = 1, 2, \dots, M$  and  $\lambda$  is a constant related to the distributional characteristics of  $\{a_i\}$ .

For simplicity, the flaw location distribution in the grouped  $90^\circ$  plies is assumed to be independent of  $n$

$$x_{i,n} = x_i \quad i = 1, 2, \dots, M \tag{3.144}$$

Fig. 3.34. (a) The size ( $2a_i$ ) and location ( $x_i$ ) of an intralaminar flaw. (b) The probability density distribution of effective intralaminar flaw size in transverse plies. (After Wang 1987.)



(C) Onset of the first transverse crack

The  $[0^\circ/90^\circ_n/0^\circ]$  laminate shown in Fig. 3.34a is now used to illustrate the energy method. Consider that the laminate is under both the applied tensile strain  $\epsilon_{xx}$  and the temperature change  $\Delta T$  ( $\Delta T$  is positive for a temperature drop). Let the distribution of the flaws be characterized by Eqs. (3.143) and (3.144), Fig. 3.34b. With the size and the location of a particular flaw known, an elastic stress analysis can be performed; and by treating the flaw as a small crack, one can also calculate the crack-tip strain-energy release rate  $G(a_{i,n}, \epsilon_{xx}, \Delta T)$  (see Wang 1987). The condition governing the propagation of the small crack into a full transverse crack is then given by

$$G(a_{i,n}, \epsilon_{xx}, \Delta T) = G_{Ic} \tag{3.145}$$

where  $G_{Ic}$  is the material fracture toughness for mode I matrix crack propagation.

Now, for the first crack to form, it is assumed that the crack is caused by the largest of  $\{a_{i,n}\}$ , denoted by  $a_{max}$ . The critical laminate strain  $(\epsilon_{xx})_{cr}$  for the onset of the first crack is then determined from Eq. (3.145) by setting  $a_{i,n} = a_{max}$ . Now, this first crack is physically detectable.

(D) Shear-lag effect

When the first transverse crack is formed, the local tensile stress  $\sigma_{xx}$  formerly existing in the unbroken  $90^\circ$  plies is now zero. If the  $0^\circ/90^\circ$  interface bonding is strong, a localized interlaminar shear stress  $\tau_{xz}$  is then developed in the vicinity of the transverse crack, as shown in Fig. 3.35. This interlaminar shear stress decays exponentially a small distance away from the transverse crack; while within the same distance, the tensile stress  $\sigma_{xx}$  in the  $90^\circ$  plies regains its original magnitude. This local stress-transfer zone, or the shear-lag zone, is proportional to the thickness of the grouped  $90^\circ$  plies,  $2nt$ .

When there is an effective flaw located near a transverse crack, Fig. 3.36, the flaw may be under the shear-lag zone of the transverse crack. The degree of the shielding effect depends on the relative spacing,  $s/nt$ . Specifically, if the size of this flaw is  $2a$  and the associated strain-energy release rate at the flaw tip is  $G(a, \epsilon_{xx}, \Delta T, s)$ , then the shear-lag effect on the strain-energy release rate can be expressed by the factor,  $R(s)$ , defined by

$$R(s) = G(a, \epsilon_{xx}, \Delta T, s)/G(a, \epsilon_{xx}, \Delta T) \tag{3.146}$$

where  $G(a, \epsilon_{xx}, \Delta T)$  is calculated without the influence of shear-lag. It may be noted that the range of the retention factor  $R(s)$  is between zero and unity over the range of the shear-lag zone, as shown in Fig. 3.36, for a carbon/epoxy composite.

When a flaw is situated between two consecutive transverse cracks, then it is under the shear-lag effect from both cracks. The associated strain-energy release rate,  $G^*$ , is given by

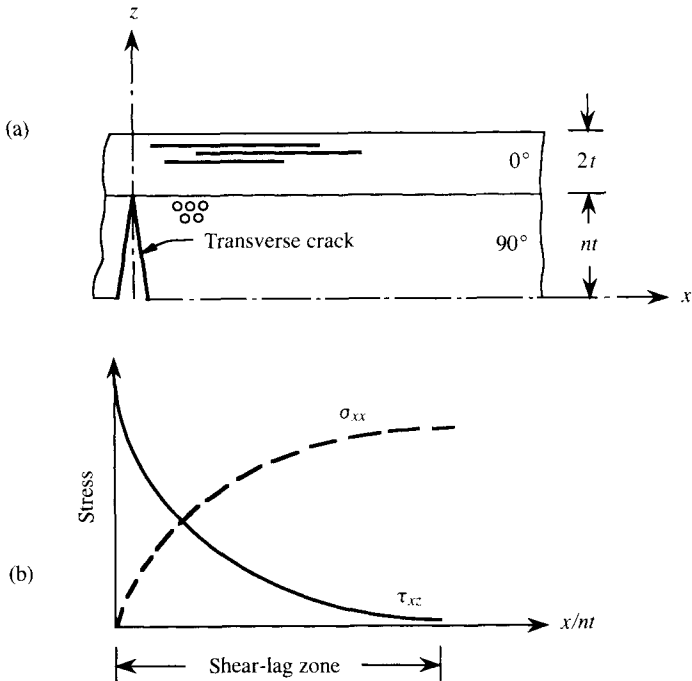
$$G^*(a, \epsilon_{xx}, \Delta T) = R(s_L)G(a, \epsilon_{xx}, \Delta T)R(s_R) \quad (3.147)$$

where  $s_L$  and  $s_R$  are the distances from the flaw to the left crack and to the right crack, respectively.

(E) Multiple cracks as a function of loading

After the formation of the first crack from the largest flaw in  $\{a_{i,n}\}$ , subsequent cracks can form from the remaining flaws at laminate strains appropriately higher than  $(\epsilon_{xx})_{cr}$ . A search is then

Fig. 3.35. (a) A transverse crack in a cross-ply laminate. (b) Local stress transfer caused by transverse cracking and the shear-lag zone. (After Wang 1987.)



commenced to determine the next flaw that yields the highest strain-energy release rate  $G^*$  (with due regard to the shear-lag effect cast by the existing cracks). The applied laminate strain corresponding to the next crack, which should be higher than  $(\epsilon_{xx})_{cr}$ , is determined by using  $G^*$  in Eq. (3.145).

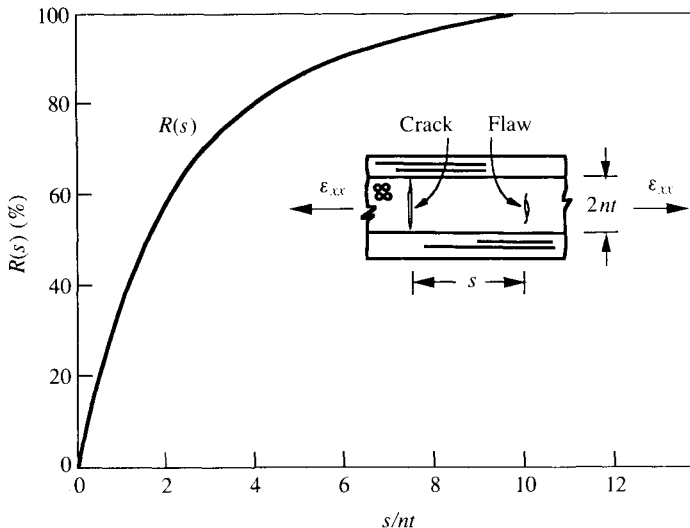
Successive searches for the next most energetic flaw follow, and the entire load sequence of transverse cracks is simulated until it is no longer energetically possible to produce any more transverse cracks, or until some other failure modes (e.g. delamination, fiber break, etc.) set in during the loading process.

(F) Determining the effective flaw distribution

One difficulty in the above simulation procedure lies in the fact that the effective flaws are hypothetical quantities, and that they must be chosen properly to yield the essential features of transverse cracking. Appropriate experiments are required to determine the effective flaw distribution.

In the work of Lei (1986), the effective intralaminar flaw distribution in the AS4-3501-06 carbon–epoxy unidirectional ply was determined by testing  $[0^\circ_2/90^\circ_2]_s$  tensile coupons. In the test, transverse cracks were detected by X-radiography and were recorded as a function of the laminate tensile stress. The shaded band

Fig. 3.36. The energy retention factor,  $R(s)$ , vs.  $s/nt$  due to the shear-lag effect (after Wang 1987.)

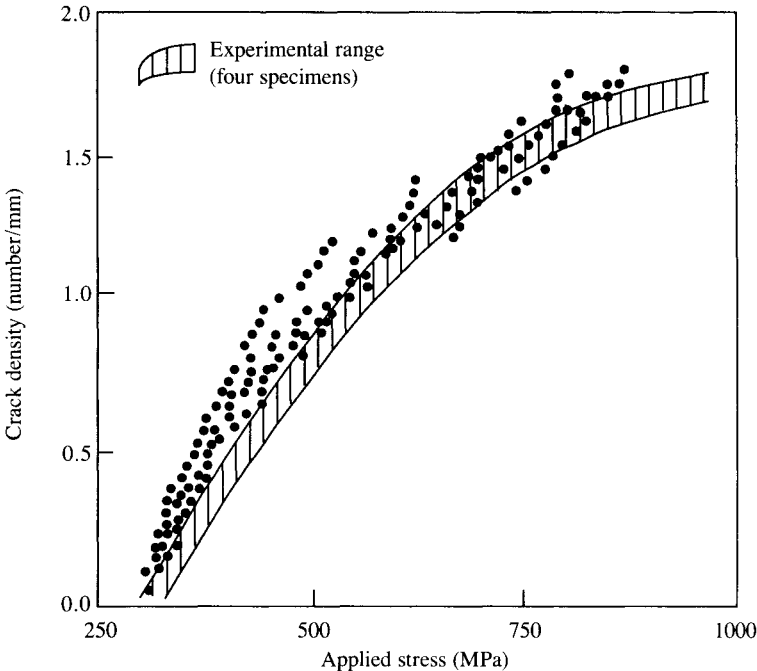


in Fig. 3.37 is formed by plotting data obtained from four specimens, in terms of crack density (cracks per unit length of specimen) versus the applied laminate stress. This band, representing a cumulative formation of the transverse cracks during loading, resembles a form of the output from a certain stochastic process.

It is noted that the experimental band possesses a certain position on the stress scale, a certain characteristic curvature in the coordinate plane and an asymptotic value on the crack density scale. These features will now be used to determine the effective flaw distribution in the  $[90^{\circ}_4]$  layer. To do so, a random number generator is used to form a set of  $M$  random values in the interval of  $(0, 1)$ . These  $M$  values are assigned to be  $\{x_i\}$ , the locations of  $M$  flaws along the unit length of the  $[90^{\circ}_4]$  layer. The sizes of the  $M$  flaws  $\{a_{i,4}\}$  are assumed to fit a Weibull cumulative function,

$$F(a) = 1 - \exp[-(a/\alpha)^\beta] \tag{3.148}$$

Fig. 3.37. Cumulative crack density (number of cracks per millimeter specimen length) vs. applied laminate stress for  $[0^{\circ}_2/90^{\circ}_2]_s$  laminates. The shaded data band indicates experimental range of four specimens. The dots represent results of Monte-Carlo simulations. (After Wang 1987.)



At this point, the parameters  $M$ ,  $\alpha$  and  $\beta$  are assumed known. And a new set of  $M$  random values is again generated in the interval  $(0, 1)$ . These values are assigned to  $\{F_i\}$ , corresponding to the values of  $F(a)$  at  $a = a_{i,4}$ . The flaw size  $\{a_{i,4}\}$  is then determined using Eq. (3.148).

With the assumed values of  $\alpha$ ,  $\beta$  and  $M$ , a simulation of the transverse cracking process as described earlier can now be performed. An appropriate choice of  $\alpha$ ,  $\beta$  and  $M$  is one that simulates closely the experimental data band shown in Fig. 3.37. Generally,  $\alpha$  affects primarily the curvature of the band,  $\beta$  shifts the band along the stress scale, and  $M$  determines the asymptotic value of the band on the crack density scale (see Lei 1986). Figure 3.37 shows also the simulated crack density vs. laminate stress data from five simulation specimens. Properly selected values of  $\alpha$ ,  $\beta$  and  $M$  can fit the experimental data band very well.

Once the values  $\alpha$ ,  $\beta$  and  $M$  are chosen, the effective flaw size distribution in any number of grouped  $90^\circ$  plies can be found using Eq. (3.143); and then the transverse cracking in the grouped  $90^\circ$  plies in laminates can be simulated. Figure 3.38 shows the simulated results for four  $[0_2^{\circ}/90^\circ]_s$  coupons along with the experimental data band from four test specimens. Figure 3.39 shows a similar comparison between experiment and simulation for four  $[0_2^{\circ}/90^\circ_4]_s$  coupons. In both Figs. 3.38 and 3.39, the simulated data were based on the flaw distribution found from the  $[0_2^{\circ}/90^\circ_2]_s$  coupons in conjunction with Eq. (3.143).

As was mentioned in Section 3.4.6.3, the Monte-Carlo method depends on the nature of the input random variables; and in this case, the input is the distribution of the assumed effective flaws. In the examples discussed above, the values of  $\alpha$ ,  $\beta$  and  $M$  determined by fitting the experiment could not be proved unique. Nevertheless, the simulation, which is performed in conjunction with fracture mechanics analysis, provides not only a quantitative description of the mechanisms but also an assessment of the statistical characteristics of the transverse cracking process.

### 3.4.8 *Delamination in laminates of multi-directional plies*

Delamination is another mode of failure in multi-directional laminated plates and shells. At the ply level, delamination may be viewed as a plane crack propagating in the interface between two adjacent plies, Fig. 3.40. Cracking of this kind is peculiar because the crack plane is parallel rather than perpendicular to the applied tension; the driving force stems from the interlaminar stresses. As most

laminates are designed to carry in-plane loading, interlaminar stresses are generally absent throughout the laminate except near free edges, cut-outs, large defects and other such locations where local interactions from mismatched ply properties cause stress concentrations. Again, these local stress fields are almost always three-dimensional in character.

The three-dimensional stress analysis model and the energy method discussed in Section 3.4.7.4 can be applied to describe the initiation and propagation of delamination. Crossman *et al.* (1980) and Wang and Crossman (1980) followed this approach and investigated free-edge delamination in laminates loaded in uniaxial tension; Wang, Slomiana and Bucinell (1985) considered free-edge delamination in compressively loaded laminates; and Wang, Kishore and Li (1985) examined delamination near interacting laminate defects. In all cases, experimental correlation was performed to validate the analysis.

Fig. 3.38. Cumulative crack density (number of cracks per millimeter specimen length) vs. applied laminate stress for  $[0_2^{\circ}/90_2^{\circ}]_k$  laminates. The shaded data band indicates experimental range of four specimens. The dots represent results of Monte-Carlo simulations. (After Wang 1987.)

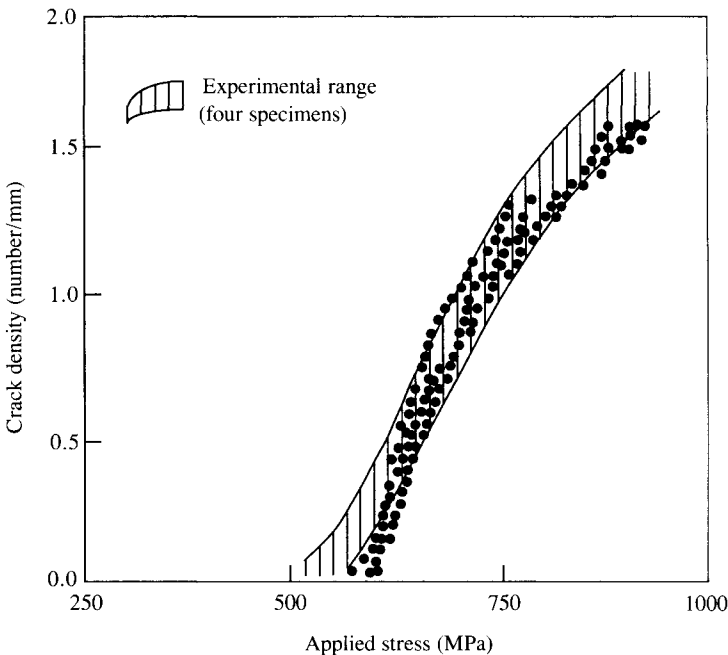


Fig. 3.39. Cumulative crack density (number of cracks per millimeter specimen length) vs. applied laminate stress for  $[0_2/90_4]_s$  laminates. The shaded data band indicates experimental range of four specimens. The dots represent results of Monte-Carlo simulations. (After Wang 1987.)

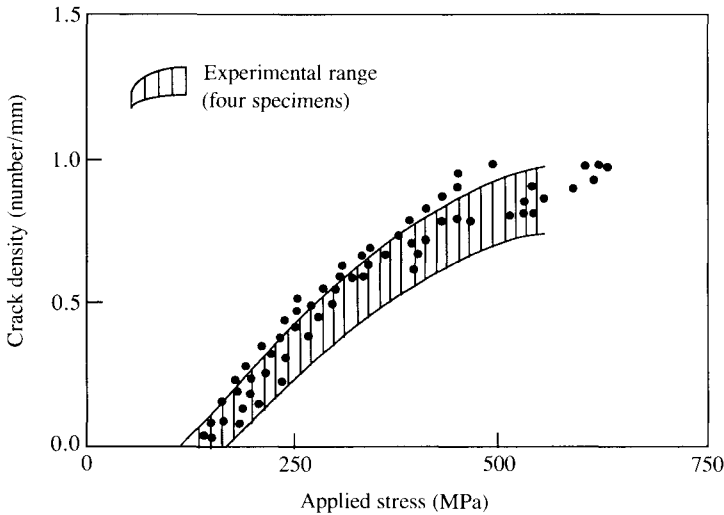
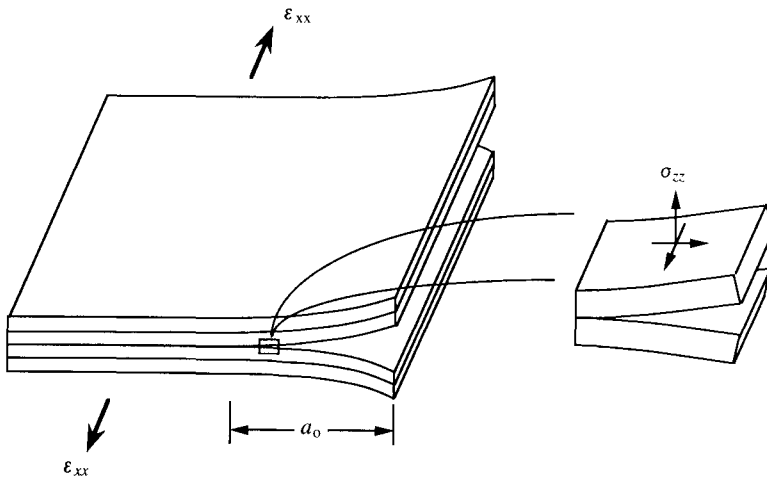


Fig. 3.40. Inter-ply cracking (edge delamination) in a multi-ply laminate. (After Wang 1987.)



For conciseness, the problem of free-edge delamination in laminates loaded in uniaxial tension is discussed in this section, and only the logic underlying the formulation of the analytical method is presented.

#### 3.4.8.1 *Free-edge delamination*

The free-edge delamination problem has attracted considerable interest for both its scientific challenge and engineering importance. Early laboratory tests have shown that laminate tensile strength can be greatly reduced if free-edge delamination occurs during the course of loading (Pagano and Pipes 1971; Bjeletich, Crossman and Warren 1979). A similar effect on laminate compressive strength has also been confirmed (Wang, Slomiana and Bucinell 1985). Further analyses of the delamination mechanisms have established that the physical behavior of delamination is profoundly influenced by ply stacking sequence, ply fiber orientation, individual ply thickness and laminate width to thickness ratio (Crossman and Wang 1982).

While there have been many predictive models describing delamination growth, the energy method developed by Wang and Crossman (1980) accounts for all these intrinsic and extrinsic factors operating in a severely concentrated three-dimensional stress field near the free edges.

To illustrate this method, the symmetric laminate having straight edges shown in Fig. 3.40 is considered as an example. Assume that the laminate under the applied laminate tensile strain  $\epsilon_{xx}$  is such that free-edge delamination is induced in one of its ply interfaces. The problem is then to determine which interface is most likely to delaminate and at what load.

For long, symmetrically stacked and finite-width laminates, it may be assumed that the laminate stress field is independent of the loading axis,  $x$ . Hence, it can be described by ply elasticity formulation under the generalized plane strain condition (Pipes and Pagano 1970). The induced free-edge delamination would then extend uniformly along the length of the laminate and advance from the free edges toward the center of the laminate piece, as shown in Fig. 3.40; and the delamination crack can be considered as a self-similar line crack with a linear size,  $a$ , propagating in the preferred ply interface.

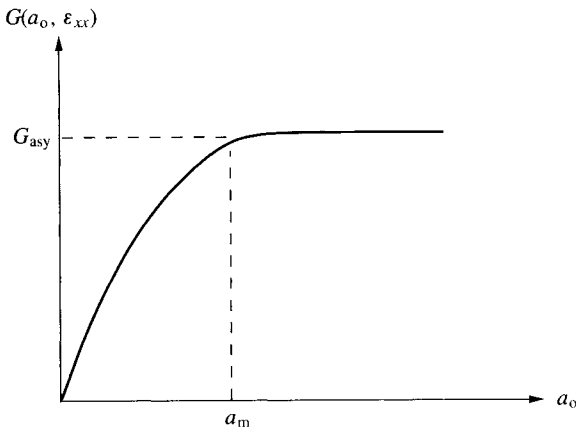
- (A) Effective interlaminar flaws and conditions for propagation  
To render a prediction for delamination initiation, the

assumption of effective flaws (Section 3.4.7.4) will again be invoked here. In this case, random interfacial flaws are assumed to exist in each ply interface of the laminate as illustrated in Fig. 3.33(b). In particular, along the laminate free edges there is a dominant interlaminar edge flaw. It is further assumed that this flaw is located in a known interface and has a linear size,  $a_o$ , in the sense depicted in Fig. 3.40. This flaw is treated as a starter delamination crack, with its size  $a_o$  still a random variable. Thus, one can proceed to calculate the crack-tip strain-energy release rate  $G(a_o, \epsilon_{xx})$  if the elastic constants of the unidirectional plies, the ply stacking sequence, the ply fiber orientations and the ply interface in which  $a_o$  is residing are known.

The general character of  $G(a_o, \epsilon_{xx})$  as a function of  $a_o$  is shown in Fig. 3.41 (for a unit of the applied laminate strain  $\epsilon_{xx}$ ).  $G$  rises sharply from zero at  $a_o = 0$ , and reaches an asymptotic value,  $G_{asy}$ , as  $a_o$  becomes greater than  $a_m$ . It should be noted that in Fig. 3.41,  $G_{asy}$  can be expressed in terms of  $\epsilon_{xx}^2$ . The physical meaning of  $a_m$  is that, at this size, the delamination no longer interacts with the free-edge boundary. Generally, this boundary effect extends roughly to a distance of about one-half the thickness of the laminate. Beyond this distance, the delamination problem merely involves the extension of cracks between two anisotropic elastic media and the free-edge effect vanishes.

The calculated strain-energy release rate  $G$  may be expressed

Fig. 3.41. Variation of the strain-energy release rate  $G$  with delamination crack size  $a_o$  for a given  $\epsilon_{xx}$  value. (After Wang 1984). Copyright ASTM, reprinted with permission.)



explicitly in terms of the applied laminate strain  $\epsilon_{xx}$ :

$$G(a_o, \epsilon_{xx}) = C_e(a_o)2t\epsilon_{xx}^2 \quad (3.149)$$

with  $C_e(a_o)$  an exclusive function of delamination size  $a_o$ . In the above,  $2t$  is this thickness of the ply.

Effects of thermal residual stresses due to cooling in fabrication can be readily included in the calculation of  $G$ . If the laminate stress-free temperature is  $T_0$  and the ambient temperature is  $T$ , then the laminate is exposed to a temperature drop of  $\Delta T = T_0 - T$ . The calculated strain-energy release rate  $G$  can be expressed in explicit terms of  $\epsilon_{xx}$  and  $\Delta T$  as

$$G(a_o, \epsilon_{xx}, \Delta T) = [\sqrt{(C_e)\epsilon_{xx}} + \sqrt{(C_T)\Delta T}]^2 2t \quad (3.150)$$

where  $C_T$  is also an exclusive function of  $a_o$ .

From fracture mechanics, the condition governing the onset of delamination is given by:

$$G(a_o, \epsilon_{xx}, \Delta T) = G_c \quad (3.151)$$

where  $G_c$  is the fracture toughness of the laminate under delamination.

Equation (3.151) provides a prediction for the critical laminate strain  $\epsilon_{xx}$  at the onset of delamination when the delaminating interface, the values of  $a_o$  and  $G_c$  are given. These values, however, are not readily available; a further analysis of the problem is still needed.

#### (B) The effective edge flaw size

Given the functional character of  $G(a_o, \epsilon_{xx})$  shown in Fig. 3.41, a one-to-one relationship between the critical  $\epsilon_{xx}$  and  $a_o$  can be obtained from Eq. (3.151) assuming the delaminating interface and the associated  $G_c$  are known. If  $a_o$  is represented by some probability density function,  $f(a_o)$ , then there is a corresponding range of  $\epsilon_{xx}$  for which Eq. (3.151) is satisfied (see Fig. 3.42). The limiting value of  $\epsilon_{xx}$  as  $a_o$  becomes equal to or greater than  $a_m$  is determined by setting  $G_{asy}/G_c = 1$ . This serves as the lower-bound of the critical strain,  $\epsilon_{xx}$ . Since  $a_m$  is about one-half the thickness of the laminate, it is small compared to the observable delamination size in relatively thin laminates. In effect, the lower-bound value for  $\epsilon_{xx}$  is usually regarded as the critical strain at the onset of delamination.

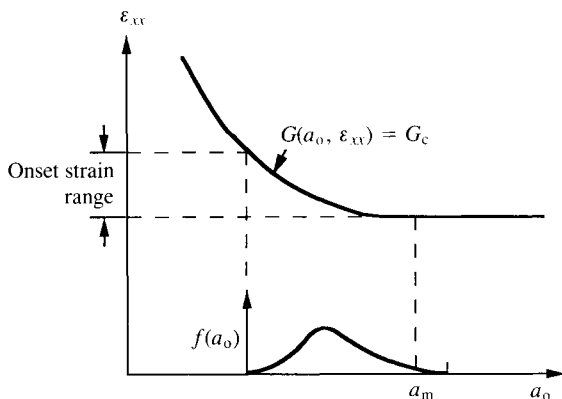
## (C) The critical delaminating ply interface

Given a specific laminate, the most probable delaminating interface cannot be presupposed from experience. It requires an analysis in which the values of  $G_{asy}/G_c$  on all possible interfaces can be compared. According to Eq. (3.151), delamination shall occur on the interface which yields the largest value of  $G_{asy}/G_c$  (for the same  $\epsilon_{xx}$ ).

While  $G_{asy}$  at each interface can be calculated readily, the  $G_c$  associated with each interface may differ from one interface to another. To elucidate this fact, consider a specific example: the  $[\pm 25^\circ/90^\circ]_s$  laminate made of the AS4-3501-06 carbon–epoxy system. Based on the generalized plane strain model mentioned earlier, the entire laminate stress field is calculated first. Of interest are the interlaminar stresses near the free edges before delamination. Figure 3.43 shows near the free edge, the through thickness distribution of the interlaminar normal stress  $\sigma_{zz}$ . Note that  $\sigma_{zz}$  is tensile and unbounded approaching the  $-25^\circ/90^\circ$  interface; and is tensile but bounded on the laminate mid-plane ( $90^\circ/90^\circ$  interface). Figure 3.44 shows the interlaminar shear stress  $\tau_{xz}$  near the free edge. Here, an unbounded  $\tau_{xz}$  exists on both the  $25^\circ/-25^\circ$  and the  $-25^\circ/90^\circ$  interfaces. These results suggest only qualitatively that free edge delamination may occur either in the  $90^\circ/90^\circ$  interface as a mode I crack, or in the  $-25^\circ/90^\circ$  interface as a mixed-mode (mode I and mode III) crack.

Further energy analysis provides  $(G_I)_{asy}$  for mode I cracks in the

Fig. 3.42. Relation between applied strain  $\epsilon_{xx}$  and flaw size  $a_o$ . Flaw size distribution  $f(a_o)$  is shown schematically. (After Wang 1987.)



mid-plane, and  $(G_I + G_{III})_{asy}$  for the mixed-mode crack in the  $-25^\circ/90^\circ$  interface. In the latter, the mixed-mode ratio for  $G_{III}/G_I$  is also obtained.

Fracture toughness for mode I delamination may actually be different from that for mixed-mode delamination. Indeed, interfacial fracture of various mixed modes often manifest themselves

Fig. 3.43. The distribution of normal stress  $\sigma_{zz}$  through the laminate thickness. (After Wang 1987.)

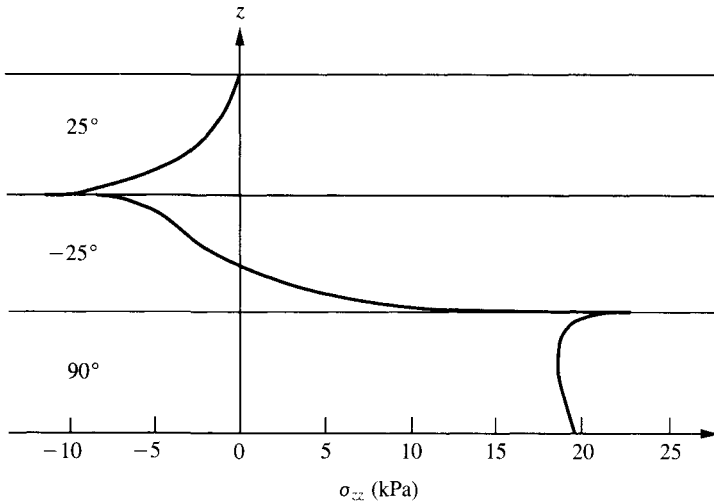
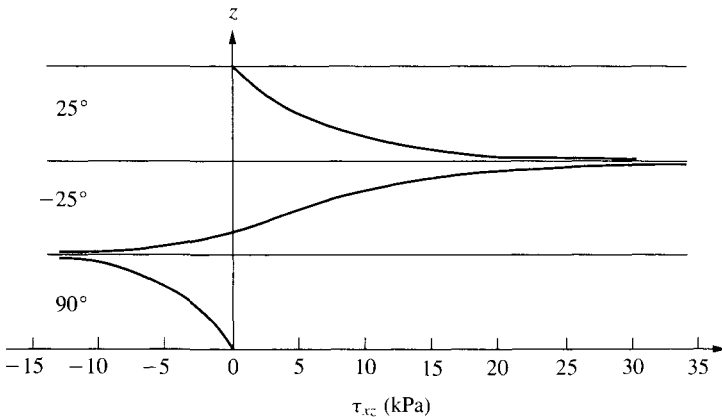


Fig. 3.44. The distribution of shear stress  $\tau_{xz}$  through the laminate thickness. (After Wang 1987.)



through differences in the fractured surface morphology, which in turn implies differences in the  $G_c$  value measured on the ply scale (Bradley and Cohen 1985). Laboratory tests using carbon–epoxy specimens have shown that  $G_c$  for mode I delamination is generally lower than  $G_c$  for mixed-mode delamination. And, the latter often increases with the amount of the shearing mode. The cause for variable  $G_c$  in mixed-mode delamination is complex; several recent studies cited local crack-tip matrix yielding and fiber bridging across the crack surfaces possibly due to shear deformation (see Russell and Street 1985). To use Eq. (3.151) for mixed-mode delamination,  $G_c$  must be first obtained as a function of mixed-mode ratio.

For the example problem, as it turned out, mid-plane delamination was predicted because it yielded a larger  $G_{asy}/G_c$  than the  $-25^\circ/90^\circ$  interface. The prediction agreed with the experiment (see Wang, Slomiana and Bucinell 1985). It should be noted that besides Eq. (3.151) many other fracture criteria for mixed-mode cracks have been suggested in the literature.

### 3.4.8.2 General delamination problems

The free-edge delamination problem discussed above serves to illustrate the basic rationale in the formulation of the energy method. The assumption of effective interfacial flaws allows a fracture analysis from which the onset of delamination could be determined. The assumption may seem awkward at first glance; but it is no more inconvenient than to assume the existence of a stress-based interlaminar strength that is used to determine delamination onset in the highly concentrated free-edge stress fields.

It should also be remarked that delamination problems encountered in practice are very complicated. Frequently, the delamination plane has a two-dimensional contour. To describe the growth of a contoured delamination may require a criterion which is directionally dependent, due to different material characteristics along the contoured crack front. In addition, delamination growth in practical laminates is almost always accompanied and/or preceded by other types of damages such as transverse cracks. Interactions amongst the various local cracks with delamination can be both deterministic and probabilistic in nature. The energy method discussed in this section appears to have sufficient generality for application to the more complex delamination problems. Generic extension of the method could conceivably be developed which can provide quan-

titiative, if approximate, predictions for a wide class of delamination problems.

### 3.4.9 *Enhancement of composite strength through fiber prestressing*

The scattering in fiber strength has been attributed to the existence of surface and bulk defects (See Section 3.4.2). Owing to the statistical strength distribution of fibers, it is necessary to design fiber composite structural components based upon a high level of survivability. The enhancement of composite strength can be achieved by eliminating some of the weak spots or defects in the fibers. One way of attaining this goal is to stress the fibers and to induce fracture at the defect sites before they are incorporated into the matrix.

Mills and Dauksys (1973) were the first to adopt the concept of fiber prestressing. In their work, carbon fiber prepregs are prestressed at temperatures as low as  $-18^{\circ}\text{C}$ . The prestress of prepregs by bending induces non-uniform tensile stress which reaches maximum values at the outer surfaces with fibers near the center of the prepreg stressed the least.

Manders and Chou (1983b) provide a theoretical analysis of enhancement of strength in composites reinforced with previously stressed fibers. The basis of their reasoning is as follows. The failure of a fiber in an aligned composite causes a stress wave to propagate outwards placing a dynamic overstress on the neighboring fibers (see Section 3.3.2). The resulting dynamic stress concentration is generally greater than the static stress concentration which prevails after the system has settled, and increases the probability that adjacent fibers also fail, weakening the composite. This analysis shows how weak fibers may be prefractured to eliminate the dynamic overstress, thereby increasing the strength of the composite. Manders and Chou discussed this strength enhancement with reference to the level of prestress, fiber variability, stress concentrations, and size of the composite.

Chi and Chou (1983) have measured in a systematic fashion the effect of fiber prestressing on the mean strength of composites as well as the dispersion of composite strength. Thornel-300 carbon fibers are used as the reinforcement materials for composites. A loose bundle contains 1000 fibers with a fiber diameter of  $7\ \mu\text{m}$ . In order to obtain consistent results in composite strength enhancement, it is essential that all the defect sites of the fibers with strength less than a certain value should be broken when they are

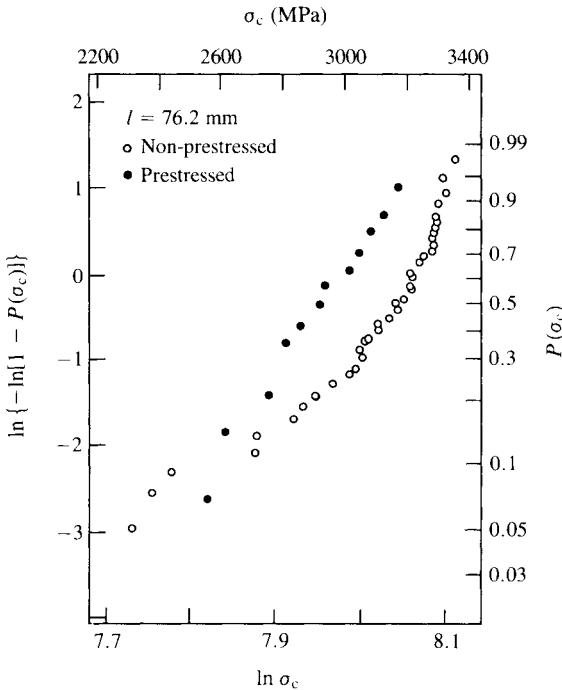
subject to prestressing at a given level. It would be most ideal if a uniform tensile stress could be applied uniformly to each small segment of a fiber with length comparable to the ineffective length of the fiber. However, this is impractical in real experiments, where the gauge-length for fiber testing is much larger than the ineffective length. Thus, a fiber already broken at its weakest site can no longer be stressed under tensile loading.

The prestressing of carbon fibers is achieved by pulling the bundle through a pair of circular bars of the same diameter at a tensile force of 30 g. The relationship among the maximum prestress in fibers,  $\sigma_p$ , the bar diameter,  $D$ , and the fiber diameter,  $d$ , is

$$\sigma_p = E_f d / D \tag{3.152}$$

where  $E_f$  denotes the fiber axial Young's modulus. The stress in the fiber caused by the applied tensile force is much smaller than  $\sigma_p$  and hence it is neglected. Composite specimens are fabricated by impregnating prestressed and non-prestressed fiber bundles in

Fig. 3.45. Negative strength enhancement in composites reinforced with prestressed loose carbon fiber bundle. (After Chi and Chou 1983.)



epoxy resin. The strength data obtained for prestressed fiber composites with gauge-length of 76.2 mm are shown in Figs. 3.45 and 3.46, using Weibull probability paper. Here,  $\sigma_c$  denotes composite strength,  $P(\sigma_c)$  is the cumulative strength distribution and  $\ln\{-\ln[1 - P(\sigma_c)]\}$  indicates the failure probability. The  $D$  values for specimens presented in Figs. 3.45 and 3.46 are 0.711 mm and 1.168 mm, respectively; the resulting  $\sigma_p$  values are 2.21 GPa and 1.35 GPa. The mean strength of the composites with non-prestressed fiber bundles is 3.01 GPa. The strength data of Fig. 3.45 show negative enhancement while significant strength enhancement can be seen in Fig. 3.46. It is noted that the strength data of prestressed composites can be fitted approximately by straight lines. Chi and Chou (1983) have concluded that the composite strength for high survivability (low failure probability) is low. These low strength tails can be eliminated by stressing the loose fiber bundles. Enhancement in strength as high as 25% for survivability of 99.9% has been achieved.

Fig. 3.46. Positive strength enhancement in composites reinforced with prestressed loose carbon fiber bundle. (After Chi and Chou 1983.)

